

**CROSSLINKABLE MIXED MATRIX MEMBRANES FOR THE
PURIFICATION OF NATURAL GAS**

A Dissertation
Presented to
The Academic Faculty

By

Jason K. Ward

In Partial Fulfillment
Of the Requirements for the Degree
Doctor of Philosophy in the
School of Chemical & Biomolecular Engineering

Georgia Institute of Technology

May 2010

Copyright © 2010 Jason K. Ward

CROSSLINKABLE MIXED MATRIX MEMBRANES FOR THE PURIFICATION OF NATURAL GAS

Approved by:

Dr. William Koros, Advisor
School of Chemical & Biomolecular
Engineering
Georgia Institute of Technology

Dr. Christopher Jones
School of Chemical & Biomolecular
Engineering
Georgia Institute of Technology

Dr. Sankar Nair
School of Chemical & Biomolecular
Engineering
Georgia Institute of Technology

Dr. Haskell Beckham
School of Polymer, Textile & Fiber
Engineering
Georgia Institute of Technology

Dr. Stephen Miller
Chevron Fellow
Chevron Energy Technology Company

Date Approved: December 18, 2009

ACKNOWLEDGEMENTS

I would like to first express my most earnest appreciation to my advisor, Dr. Bill Koros. His unwavering support and relentless drive will remain a source of inspiration in all of my future endeavors. I consider myself particularly fortunate to have been able to work with Prof. Koros over the past several years.

The whole of the Koros group has been a pleasure to work with, and friendships forged will remain with me for life. I would especially like to express thanks to JR Johnson for providing so many feasting opportunities and to Ryan Adams for pushing my buttons and humoring me during rants and wandering thoughts-out-loud. I would also like to acknowledge Ryan Lively and Dr. Oguz Karvan for their assistance, conversation, and general camaraderie.

Perhaps most influential in my graduate school success has been my best friend, my most trusted confidant, and my girlfriend, Jennifer. I am incredibly thankful for her endless patience and support through countless late-night lab visits and disrupted weekends, all in the name of science. I cannot imagine my time at Georgia Tech without her, nor can I thank her enough.

TABLE OF CONTENTS

ACKNOWLEDGEMENTS.....	iii
LIST OF TABLES.....	ix
LIST OF FIGURES.....	xi
SUMMARY.....	xv
CHAPTER 1: INTRODUCTION.....	1
1.1 NATURAL GAS OVERVIEW.....	1
1.2 NATURAL GAS PURIFICATION.....	2
1.3 MEMBRANE TECHNOLOGY FOR NATURAL GAS PURIFICATION.....	3
1.4 RESEARCH OBJECTIVES.....	6
1.5 DISSERTATION ORGANIZATION.....	7
1.6 REFERENCES.....	7
CHAPTER 2: THEORY AND BACKGROUND.....	9
2.1 POLYMER MEMBRANES FOR GAS SEPARATIONS.....	9
2.1.1 GENERAL TRANSPORT THEORY.....	9
2.1.2 MODELING POLYMER MEMBRANE TRANSPORT PROPERTIES.....	14
2.1.3 NON-IDEAL POLYMERIC MEMBRANE TRANSPORT PHENOMENA.....	17
2.2 REVIEW OF CROSSLINKABLE POLYMER MEMBRANES FOR GAS SEPARATIONS.....	20
2.3 MIXED MATRIX MEMBRANES FOR GAS SEPARATIONS.....	24
2.3.1 GAS TRANSPORT IN MOLECULAR SIEVES.....	24
2.3.2 MODELING MIXED MATRIX MEMBRANE PERFORMANCE.....	25
2.3.3 NON-IDEAL INTERFACIAL MORPHOLOGIES.....	27

2.3.4 REVIEW OF MIXED MATRIX MEMBRANES FOR GAS SEPARATIONS	29
2.4 REFERENCES	32
CHAPTER 3: MATERIALS AND METHODS	39
3.1 MATERIALS	39
3.1.1 POLYMERS	39
3.1.2 MOLECULAR SIEVES	42
3.1.3 GASES	43
3.2 MEMBRANE FORMATION	44
3.2.1 NEAT POLYMER MEMBRANES	44
3.2.2 MIXED MATRIX MEMBRANES	46
3.3 MOLECULAR SIEVE MODIFICATION	47
3.3.1 GRIGNARD PROCEDURE	47
3.3.2 REACTIVE SIZING	49
3.4 CHARACTERIZATION TECHNIQUES	51
3.4.1 GAS PERMEATION ANALYSIS	51
3.4.2 CRYOGENIC NITROGEN PHYSISORPTION (BET)	57
3.4.3 SCANNING ELECTRON MICROSCOPY (SEM)	58
3.4.4 THERMOGRAVIMETRIC ANALYSIS (TGA)	58
3.4.5 X-RAY PHOTOELECTRON SPECTROSCOPY (XPS)	58
3.4.6 GEL PERMEATION CHROMATOGRAPHY (GPC)	59
3.5 REFERENCES	59
CHAPTER 4: CROSSLINKABLE MIXED MATRIX MEMBRANES FOR NATURAL GAS PURIFICATION	61
4.1 INTRODUCTION	61
4.2 POLYMER AND MOLECULAR SIEVE TRANSPORT PROPERTIES	61

4.2.1 PDMC CHARACTERIZATION	61
4.2.2 SSZ-13 CHARACTERIZATION	63
4.2.3 MAXWELL MODEL PERMEABILITY PREDICTIONS	64
4.2.4 PERMEATION ANALYSIS.....	65
4.3 CHARACTERIZATION OF APPARENT MIXED MATRIX MEMBRANE DEFECTS	67
4.3.1 SIEVE-IN-A-CAGE DEFECTS	67
4.3.2 LEAKY INTERFACE DEFECTS	69
4.4 INVESTIGATION OF POTENTIAL FOR CROSSLINKING-INDUCED VOID FORMATION.....	71
4.5 SUMMARY AND CONCLUSIONS	73
4.6 REFERENCES	73
CHAPTER 5: CROSSLINKABLE MIXED MATRIX MEMBRANES WITH MODIFIED MOLECULAR SIEVES	75
5.1 INTRODUCTION	75
5.2 GRIGNARD-TREATED SSZ-13/PDMC MIXED MATRIX MEMBRANES..	75
5.2.1 CHARACTERIZATION OF GRIGNARD-TREATED SSZ-13.....	76
5.2.2 MIXED MATRIX MEMBRANES WITH GRIGNARD-TREATED SIEVES.....	78
5.3 REACTIVE-SIZED, GRIGNARD-TREATED SSZ-13/PDMC MIXED MATRIX MEMBRANES	83
5.4 REACTIVE-SIZED, AS-RECEIVED SSZ-13/PDMC MIXED MATRIX MEMBRANES	88
5.4.1 MIXED MATRIX MEMBRANES WITH REACTIVE-SIZED, UNCALCINED SSZ-13	93
5.5 ANALYSIS OF A NON-IDEAL MIXED MATRIX MEMBRANE TRANSPORT MECHANISM.....	95
5.5.1 BACKGROUND AND MECHANISM DEVELOPMENT	95
5.5.2 APPLICATION TO PRESENT RESEARCH	99

5.5.3 PREDICTION OF INTERPHASE PARAMETERS	102
5.6 SUMMARY AND CONCLUSIONS	103
5.7 REFERENCES	103
CHAPTER 6: MEMBRANE PERFORMANCE IN THE PRESENCE OF TOLUENE- CONTAMINATED FEEDS	106
6.1 INTRODUCTION	106
6.2 NEAT PDMC DENSE FILM MEMBRANES.....	107
6.2.1 COMPARISON OF DENSE FILM AND HOLLOW FIBER MEMBRANE PERFORMANCE	109
6.2.2 PHYSICAL AGING IN PDMC DENSE FILM MEMBRANES	115
6.3 AS-RECEIVED SSZ-13/PDMC MIXED MATRIX MEMBRANES	118
6.4 GRIGNARD-TREATED SSZ-13/PDMC MIXED MATRIX MEMBRANES	120
6.5 REACTIVE-SIZED SSZ-13/PDMC MIXED MATRIX MEMBRANES	123
6.5.1 REACTIVE-SIZED, GRIGNARD-TREATED SSZ-13/PDMC MIXED MATRIX MEMBRANES	123
6.5.2 REACTIVE-SIZED, AS-RECEIVED SSZ-13/PDMC MIXED MATRIX MEMBRANES.....	126
6.6 SUMMARY AND CONCLUSIONS	128
6.7 REFERENCES	129
CHAPTER 7: CONCLUSIONS AND RECOMMENDATIONS	133
7.1 SUMMARY AND CONCLUSIONS	133
7.2 RECOMMENDATIONS FOR ADDITIONAL RESEARCH	135
7.2.1 IN-DEPTH INVESTIGATION OF THE PROPOSED TRANSPORT MECHANISM.....	135
7.2.2 SURFACE MATERIAL IDENTIFICATION AND ATTACHMENT MECHANISM.....	136
7.2.3 FEASIBILITY OF REACTIVE-SIZED SSZ-13 IN HOLLOW FIBER MIXED MATRIX MEMBRANES	137

7.2.4 APPLICABILITY OF THE REACTIVE SIZING PROCEDURE TO OTHER MATERIALS	138
7.2.5 MIXED MATRIX MEMBRANE AGING STUDIES	138
APPENDIX A: POSSIBLE ATTACHMENT MECHANISMS OF MATERIAL ON REACTIVE-SIZED SIEVES.....	140
APPENDIX B: ESTIMATION OF INTERPHASE PROPERTIES USING THE 3-PHASE MAXWELL MODEL	143

LIST OF TABLES

Table 1.1: Typical natural gas components and pipeline sales specifications. Adapted from [3].	2
Table 2.1: Kinetic diameters [10] and critical temperatures [11] for selected gases.	10
Table 4.1: Comparison of neat PDMC and Maxwell-predicted pure gas carbon dioxide permeabilities and ideal carbon dioxide/methane selectivities. Numbers in parentheses are total membranes tested; errors represent one standard deviation.	65
Table 4.2: Comparison of measured and Maxwell-predicted pure gas carbon dioxide permeabilities and ideal carbon dioxide/methane selectivities for 15% and 25% as-received SSZ-13/PDMC membranes. Numbers in parentheses are total membranes tested; errors represent one standard deviation. Tested at 35 °C and ~65 psia.	66
Table 4.3: Comparison of measured and 3-phase Maxwell model-estimated pure gas transport properties for 15% and 25% AR-SSZ-13/PDMC hybrid membranes.	67
Table 4.4: Comparison of measured and 3-phase Maxwell model-predicted pure gas transport properties for 25% UNC-SSZ-13/PDMC hybrid membranes. Tested at 35 °C and ~65 psia.	70
Table 4.5: Comparison of measured uncrosslinked neat PDMC and 25% uncalcined (UNC) SSZ-13/PDMC pure gas transport properties to Maxwell model-predicted values. Numbers in parentheses are total membranes tested; errors represent one standard deviation. Tested at 35 °C and ~65 psia.	72
Table 5.1: Typical nitrogen physisorption results for as-received (AR) and Grignard-treated (GT) SSZ-13. Pore volume determined using the Horvath-Kawazoe method (cylindrical pores).	78
Table 5.2: Measured and Maxwell-predicted pure gas carbon dioxide permeabilities and ideal carbon dioxide/methane selectivities for 15% and 25% Grignard-treated (GT) SSZ-13/PDMC membranes. Numbers in parentheses are total membranes tested; errors represent one standard deviation. All membranes tested at 35 °C and ~65 psia.	78
Table 5.3: Measured and Maxwell-predicted pure gas carbon dioxide permeabilities and ideal carbon dioxide/methane selectivities for 15% and 25% reactive-sized, Grignard-treated (RS-GT) SSZ-13/PDMC membranes. Numbers in parentheses are total membranes tested; errors represent one standard deviation. All membranes tested at 35 °C and ~65 psia.	83

Table 5.4: Nitrogen physisorption data for as-received (AR), Grignard-treated (GT), and reactive-sized, Grignard-treated (RS-GT) SSZ-13. Pore volume determined using the Horvath-Kawazoe method (cylindrical pores)..... 85

Table 5.5: Measured and Maxwell-predicted pure gas carbon dioxide permeabilities and ideal carbon dioxide/methane selectivities for 25% reactive-sized, Grignard-treated (RS-GT) and 25% reactive-sized, as-received (RS-AR) SSZ-13/PDMC membranes. Numbers in parentheses are total membranes tested; errors represent one standard deviation. All membranes tested at 35 °C and ~65 psia. 89

Table 5.6: Surface elemental atomic percentages for as-received (AR) and reactive-sized, as-received (RS-AR) SSZ-13..... 91

LIST OF FIGURES

Figure 1.1: Robeson's 1991 permeability/selectivity tradeoff "upper bound" curve for selected high-performance polymer membranes. Adapted from [7, 8].	5
Figure 2.1: Illustration of gas molecule transport through a polymer via transient gap formation.	10
Figure 2.2: Qualitative representation of the permeability increase and selectivity decrease observed due to membrane plasticization.	18
Figure 2.3: Common interfacial morphologies and their respective effects on membrane transport properties.	27
Figure 3.1: Reaction scheme for 6FDA-DAM:DABA (3:2). Adapted from [7].	40
Figure 3.2: Reaction scheme for esterification of 6FDA-DAM:DABA (3:2) with 1,3-propane diol to form PDMC. Adapted from [7].	41
Figure 3.3: Reaction scheme for transesterification crosslinking between adjacent esters. Adapted from [7].	42
Figure 3.4: Illustration of an individual chabazite cage structure (left) and the assembly of cages into the chabazite framework (right). Adapted from [9].	43
Figure 3.5: Schematic of masked membrane placed in an assembled permeation cell. Adapted from [14].	52
Figure 3.6: Schematic of an isochoric permeation analysis system used throughout this work. Essential components are as follows: (1) permeate pressure transducer; (2) permeate reservoir; (3) circulation fan; (4) heater, controlled by PID temperature controller; (5) feed pressure transducer; (6) feed reservoir; and (7) permeation cell. Important valves are as follows: (A) permeate transducer isolation valve; (B) GC feed valve; (C) permeate vacuum valve; (D) feed valve; (E) feed vacuum valve; (F) feed isolation valve; (G) vent valve; (H) retentate metering valve; and (I) retentate shutoff valve.	54
Figure 4.1: Comparison of pure carbon dioxide isotherms for uncrosslinked and crosslinked PDMC dense film membranes.	63
Figure 4.2: Representative SEM image of as-received SSZ-13/PDMC mixed matrix membranes.	68
Figure 4.3: 3-Phase Maxwell model predictions of carbon dioxide permeability and carbon dioxide/methane selectivity for 25% uncalcined SSZ-13/PDMC membranes.	71

Figure 5.1: Typical TGA analyses of as-received (AR) and Grignard-treated (GT) SSZ-13.....	76
Figure 5.2: Pore size distributions (BJH model applied to both adsorption and desorption isotherm branches) for as-received (AR) and Grignard-treated (GT) SSZ-13.	80
Figure 5.3: Representative SEM image of Grignard-treated and as-received SSZ-13 (inset).	81
Figure 5.4: Hypothesized structure of interconnected voids within the Grignard-deposited magnesium hydroxide surface layer on modified sieves.	81
Figure 5.5: Pore size distributions (BJH model applied to both adsorption and desorption isotherm branches) for Grignard-treated (GT) and reactive-sized, Grignard-treated (RS-GT) SSZ-13.....	84
Figure 5.6: Mixed gas carbon dioxide permeabilities for 25% Grignard-treated (GT) and 25% reactive-sized, Grignard-treated (RS-GT) SSZ-13/PDMC membranes.	86
Figure 5.7: Mixed gas carbon dioxide/methane selectivities for 25% Grignard-treated (GT) and 25% reactive-sized, Grignard-treated (RS-GT) SSZ-13/PDMC membranes. ..	86
Figure 5.8: TGA analyses for as-received (AR) and reactive-sized, as-received (RS-AR) SSZ-13.	90
Figure 5.9: Mixed gas carbon dioxide permeabilities for 25% reactive-sized, Grignard-treated (RS-GT) and 25% reactive-sized, as-received (RS-AR) SSZ-13/PDMC membranes.	92
Figure 5.10: Mixed gas carbon dioxide/methane selectivities for 25% reactive-sized, Grignard-treated (RS-GT) and 25% reactive-sized, as-received (RS-AR) SSZ-13/PDMC membranes.	92
Figure 5.11: Mixed gas carbon dioxide permeabilities for neat PDMC and 25% reactive-sized, uncalcined (RS-UNC) SSZ-13/PDMC membranes. Error bars represent one standard deviation.	94
Figure 5.12: Mixed gas carbon dioxide/methane selectivities for neat PDMC and 25% reactive-sized, uncalcined (RS-UNC) SSZ-13/PDMC membranes. Error bars represent one standard deviation.	94
Figure 5.13: Hypothetical polymer chain in solution and after solvent removal.....	97
Figure 5.14: Hypothetical adsorbed polymer chain before and after solvent removal.	98
Figure 5.15: Hypothesized interaction of material on the surface of sized sieves with bulk polymer chains.	101

Figure 6.1: Mixed gas carbon dioxide permeabilities for neat PDMC dense film membranes.....	108
Figure 6.2: Mixed gas carbon dioxide/methane selectivities for neat PDMC dense film membranes.....	109
Figure 6.3: Normalized mixed gas carbon dioxide permeabilities/permeances for neat PDMC dense film and hollow fiber membranes. Hollow fiber data from [4].	110
Figure 6.4: Normalized mixed gas carbon dioxide/methane selectivities for neat PDMC dense film and hollow fiber membranes. Hollow fiber data from [4].	111
Figure 6.5: Representation of possible free volume differences between hollow fiber and dense film membranes. FFV refers to membrane state prior to toluene exposure; FFV _{mix} refers to state during toluene exposure. (A) refers to hollow fiber membrane; (B) refers to dense film. Black spheres represent sorbed toluene molecules.	114
Figure 6.6: Mixed gas carbon dioxide permeabilities for PDMC dense film membranes.	116
Figure 6.7: Mixed gas carbon dioxide/methane selectivities for PDMC dense film membranes.....	117
Figure 6.8: Mixed gas carbon dioxide permeabilities for neat PDMC dense film and 25% as-received (AR) SSZ-13/PDMC mixed matrix membranes.....	119
Figure 6.9: Mixed gas carbon dioxide/methane selectivities for neat PDMC dense film and 25% as-received (AR) SSZ-13/PDMC mixed matrix membranes.	119
Figure 6.10: Mixed gas carbon dioxide permeabilities for 25% Grignard-treated (GT) and 25% as-received (AR) SSZ-13/PDMC mixed matrix membranes.	121
Figure 6.11: Mixed gas carbon dioxide/methane selectivities for 25% Grignard-treated (GT) and 25% as-received (AR) SSZ-13/PDMC mixed matrix membranes.	122
Figure 6.12: Mixed gas carbon dioxide permeabilities for 25% Grignard-treated (GT) and 25% reactive-sized, Grignard-treated (RS-GT) SSZ-13/PDMC mixed matrix membranes.	124
Figure 6.13: Mixed gas carbon dioxide/methane selectivities for 25% Grignard-treated (GT) and 25% reactive-sized, Grignard-treated (RS-GT) SSZ-13/PDMC mixed matrix membranes.....	125
Figure 6.14: Mixed gas carbon dioxide permeabilities for 25% reactive-sized, Grignard-treated (RS-GT) and 25% reactive-sized, as-received (RS-AR) SSZ-13/PDMC mixed matrix membranes.....	127

Figure 6.15: Mixed gas of carbon dioxide/methane selectivities for 25% reactive-sized, Grignard-treated (RS-GT) and 25% reactive-sized, as-received (RS-AR) SSZ-13/PDMC mixed matrix membranes..... 128

Figure A.1: Proposed attachment mechanisms for material deposited on sieve surfaces during reactive sizing..... 141

Figure B.1: Flowchart describing the steps necessary to predict interphase properties using the 3-phase Maxwell model. 145

SUMMARY

The case has been made—here and elsewhere—for developing mixed matrix membranes for industrial gas separations. These materials offer substantial improvements in separation performance over currently available commercial polymer membranes. Moreover, the paradigm shift from thermally- to non-thermally-driven separations that these materials represent holds promise for significant reductions in both equipment and operational costs as compared to more traditional separations. The development of these hybrid membrane materials is, however, not without its challenges. Achieving ideal adhesion at the interface between the polymer matrix and dispersed sieving phase is critical to achieve the full separation potential of hybrid membranes; yet this remains one of—if not *the*—most challenging hurdles to overcome.

The work reported here focuses on the separation of carbon dioxide and methane for the purification of natural gas. Initial mixed matrix membranes studied in this work appear to suffer from poor interfacial adhesion. A sieve surface treatment that has previously been shown to improve polymer/sieve adhesion is used to enhance adhesion in these membranes. However, evidence is presented that suggests the surface treatment results in the formation of non-selective voids within the surface layer deposited on the modified sieves. A reactive sizing procedure is developed to *caulk* these voids to prevent gas bypass around sieve particles. Hybrid membranes containing these twice-treated sieves exhibit marked performance improvement over neat polymer membranes. It is also shown that similarly sized as-received sieves result in similar mixed matrix membrane performance. This serendipitous discovery—as well as inconsistencies in

membrane behavior—leads to the development of a non-ideal transport mechanism in mixed matrix membranes.

CHAPTER 1

INTRODUCTION

1.1 Natural Gas Overview

Global population forecasts estimate that over 9 billion people will inhabit our planet by 2050 with the most aggressive expansion expected to occur in newly industrialized nations [1]. As this expanding population adopts an increasingly modern lifestyle, energy consumption is expected to grow accordingly. Owing to its low cost, abundance, and relative cleanliness in comparison to coal and liquid fuels, natural gas has recently been—and is expected to continue to be—an important energy source for new power generation installations. Estimates suggest annual global natural gas production may reach 153 trillion standard cubic feet by 2030—an increase of nearly 50% based on production in 2006 [2].

A substantial number of natural gas deposits contain a variety of contaminants that must be removed to meet sales and pipeline specifications. Table 1.1 lists typical raw natural gas components and their respective concentrations required to meet sales specifications. It is desirable to remove non-fuel gases in order to minimize compression costs and maximize the heating value of the gas. More importantly, natural gas must typically be dehydrated, and acid gases, such as carbon dioxide and hydrogen sulfide, must be removed to prevent corrosion in pipelines and processing equipment. Carbon dioxide is the most abundant contaminant in many gas deposits, and the vast majority of natural gas purification research has been dedicated to its removal. As natural gas demand increases over the coming years, more efficient purification technologies that

allow increased throughput with minimal processing cost will be necessary to keep natural gas costs manageable [3].

Table 1.1: Typical natural gas components and pipeline sales specifications. Adapted from [3].

Component	Typical Concentration	Sales Specification (US)
Methane	75 – 90%	90%
Carbon Dioxide	<1 – 10+%	<2%
Hydrogen Sulfide	<4 – 10000 ppm	<4 ppm
Water	800 – 1200 ppm	<120 ppm
Inert Gases (He, N ₂)	>4%	<4%
C ₃₊ Content	varies	Dew point < -20 °C

1.2 Natural Gas Purification

Natural gas is most commonly purified using cryogenic distillation or amine absorption. However, while these methods are quite successful in removing targeted contaminants, they are both quite expensive and energy intensive operations. Cryogenic distillation is very energy intensive since the gas stream must typically be chilled to below -160 °C; distillation capital costs are also considerably expensive. Amine absorption is very efficient in acid gas removal and is especially preferred when contaminant levels are low [3, 4]. However, capital costs can be significant and are very sensitive to economies of scale [5]. Moreover, amine absorbents—commonly monoethanolamine (MEA) or diethanolamine (DEA)—are employed as aqueous solutions and require regeneration for reuse. This regeneration leads to significant operating costs for absorption units.

The past few decades have seen increasing interest in polymeric membranes for natural gas purification. Membrane separations are non-thermally driven, and therefore generally do not suffer from the high operating costs associated with the more traditional separations discussed above. Most commercial membranes for natural gas purification utilize highly available, low cost polymers and, therefore, have significantly lower capital costs as compared to distillation or absorption units. Furthermore, hollow fiber membrane modules, which will be discussed further in the following section, can provide membrane surface area to volume ratios in excess of 10,000 m²/m³. These high ratios allow for very high productivity from skid-based, small-footprint units that can be easily located on offshore platforms, unlike distillation or absorption towers [3-6].

1.3 Membrane Technology for Natural Gas Purification

Available membrane modules for natural gas purification primarily include asymmetric hollow fiber and spiral wound flat sheet types. The asymmetric geometry is defined by a very thin selective “skin” layer, typically on the order of ~100 – 1000 nm, supported by a non-selective porous substructure. In most applications, hollow fiber modules are preferred due to the high surface area to volume ratios possible, as well as the impressive trans-membrane pressures small diameter fibers can withstand.

As mentioned in the previous section, most commercial membranes for natural gas service utilize relatively inexpensive glassy polymers such as cellulose acetate or polysulfone. Though these materials are selective for the targeted carbon dioxide/methane separation, their productivity is somewhat low. As a result, a large overall surface area is necessary to provide desirable throughput. Furthermore, these materials are also prone to plasticization. Plasticization—covered in more detail in

Chapter 2—is a phenomenon whereby a strongly adsorbing penetrant, such as carbon dioxide, effectively swells a polymer and enhances segmental motion. The result is a simultaneous increase in membrane permeability (productivity) and decrease in selectivity (efficiency). The decrease in selectivity leads to a greater loss of product and, therefore, loss of profit. The typical solution to this problem has been to: 1) operate membrane units at pressures low enough to minimize plasticization-enhanced product loss; and/or 2) design more complex, multistage membrane units. However, both of these options lead to greater overall costs.

Another disadvantage of polymer membranes is the permeability/selectivity tradeoff first noted by Robeson in 1991 [7, 8]. This limitation is depicted in Figure 1.1 as the “upper bound” dashed line. In order to advance commercial interest in polymer membranes for natural gas purification, new materials are needed to transcend this upper bound into the area labeled “Commercially Attractive Region”. Moreover, these materials should be cost-competitive with current membrane technology to further increase commercial interest.

One promising solution to membrane plasticization is to design a crosslinkable polymer appropriate for membrane separations. In such materials, chemical crosslinks have been shown to provide swelling resistance that reduce or eliminate the loss of selectivity under conditions that plasticize typical membranes [9, 10]. Additionally, it is possible to further tailor membrane transport properties by modifying the polymer backbone and/or crosslinking structures [10, 11].

Crosslinkable polymer membranes have been extended to address both plasticization and permeability/selectivity tradeoff limitations with the concept of

crosslinkable mixed matrix membranes [9]. Mixed matrix membranes typically combine an inorganic molecular sieve phase with a continuous polymer matrix. This hybrid material aims to merge the high separation efficiencies obtainable with size-discriminating molecular sieves with the low cost and ease of processing of a polymer. A few studies report mixed matrix membranes that have successfully crossed Robeson's upper bound, but overall there appears to be much work needed to better develop these materials. Only one study has thus far investigated crosslinkable mixed matrix membranes, and it reported only limited success [9]. This suggests that a significant opportunity exists to further investigate and refine these materials.

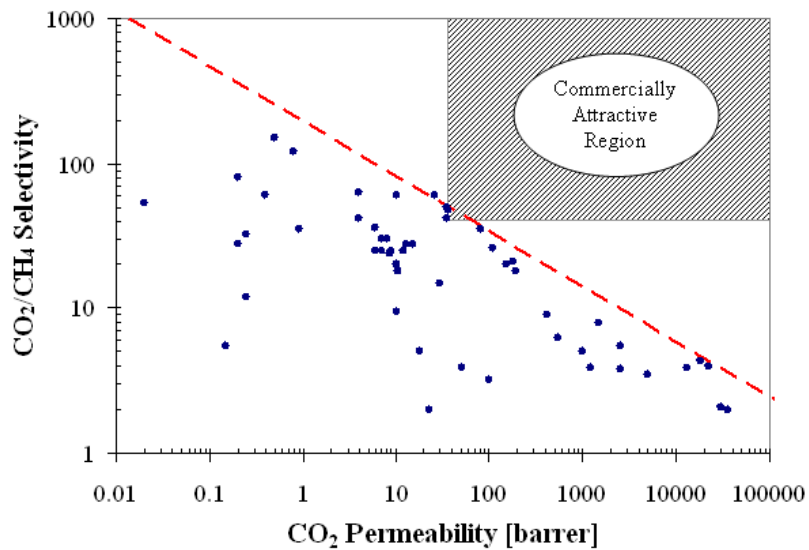


Figure 1.1: Robeson's 1991 permeability/selectivity tradeoff "upper bound" curve for selected high-performance polymer membranes. Adapted from [7, 8].

The overarching goal of this research is to further develop crosslinkable mixed matrix membranes for natural gas purification using previously identified materials. Previous work has suggested inadequate polymer/sieve adhesion, so significant attention

will be given to this area. Material development will focus on dense film membranes owing to their relative ease of fabrication and analysis. Once satisfactory membrane productivity and efficiency gains have been realized, the technology can be transferred to commercially-preferred asymmetric hollow fiber membranes.

1.4 Research Objectives

(1) Engineer the molecular sieve surface so that ideal polymer/sieve adhesion is achieved, allowing for successfully functioning mixed matrix membranes.

Proper interfacial adhesion in mixed matrix membranes is crucial for achieving the productivity enhancements desired for membrane-based natural gas purification. This has been, perhaps, the most significant challenge in developing advanced gas separation membranes. Adhesion appears to be even more challenging when using a stiff-backed, crosslinkable polyimide as the matrix material. A couple of different techniques will be investigated in this work to improve polymer/sieve adhesion and transport properties.

(2) Explore the feasibility of higher molecular sieve loadings to further enhance mixed matrix effects.

As previously discussed, the mixed matrix membrane concept ideally aims to enhance both membrane permeability and selectivity by dispersing an appropriate molecular sieve throughout a polymeric matrix. Due to the dependence of transport properties of an ideal mixed matrix membrane on the volume loading of molecular sieving phase, it is desirable to maximize the loading of this phase in order to maximize membrane productivity. Once adequate polymer/sieve adhesion is achieved as outlined

in Objective 2, the feasibility of increasing sieve loading for further enhancing membrane productivity will be investigated.

(3) Investigate the efficacy of mixed matrix membranes in the presence of more realistic feed streams.

The membranes developed in this work will be primarily characterized using an idealized natural gas mix consisting only of carbon dioxide and methane. Actual natural gas feeds generally contain a variety of strongly adsorbing species, and it is desirable to characterize the impact of these materials on a mixed matrix membrane. Toluene has been selected as a representative contaminant based on previous research [12].

1.5 Dissertation Organization

This dissertation is organized such that general information is covered before introducing the specific findings of this work. Chapter 2 summarizes background information and the fundamental theory of the topics investigated in this work. Chapter 3 details the methods, materials, and equipment used throughout this research. Chapter 4 contains the analysis of mixed matrix membranes incorporating non-treated molecular sieves. Mixed matrix membranes incorporating sieves with various surface treatments are covered in Chapter 5. Chapter 6 contains the analysis of mixed matrix membrane performance in the presence of toluene-contaminated feed streams. And finally, Chapter 7 summarizes the findings of this work and includes recommendations for future work in this area.

1.6 References

1. Sadik, N., *The State of World Population - 6 Billion, A Time for Choices*. 1999, United Nations Population Fund.

2. *International Energy Outlook*, E.I. Administration, Editor. 2009.
3. Baker, R.W. and K. Lokhandwala, *Natural gas processing with membranes: An overview*. Industrial & Engineering Chemistry Research, 2008. **47**(7): p. 2109-2121.
4. Kohl, A.L. and R.B. Nielsen, *Gas Purification*. 1997, Houston, TX: Gulf Publishing.
5. Spillman, R.W., *ECONOMICS OF GAS SEPARATION MEMBRANES*. Chemical Engineering Progress, 1989. **85**(1): p. 41-62.
6. Bernardo, P., E. Drioli, and G. Golemme, *Membrane Gas Separation: A Review/State of the Art*. Industrial & Engineering Chemistry Research, 2009. **48**(10): p. 4638-4663.
7. Robeson, L.M., *CORRELATION OF SEPARATION FACTOR VERSUS PERMEABILITY FOR POLYMERIC MEMBRANES*. Journal of Membrane Science, 1991. **62**(2): p. 165-185.
8. Robeson, L.M., *The upper bound revisited*. Journal of Membrane Science, 2008. **320**(1-2): p. 390-400.
9. Hillock, A.M.W., S.J. Miller, and W.J. Koros, *Crosslinked mixed matrix membranes for the purification of natural gas: Effects of sieve surface modification*. Journal of Membrane Science, 2008. **314**(1-2): p. 193-199.
10. Wind, J.D., et al., *The effects of crosslinking chemistry on CO₂ plasticization of polyimide gas separation membranes*. Industrial & Engineering Chemistry Research, 2002. **41**(24): p. 6139-6148.
11. Kim, T.H., et al., *RELATIONSHIP BETWEEN GAS SEPARATION PROPERTIES AND CHEMICAL-STRUCTURE IN A SERIES OF AROMATIC POLYIMIDES*. Journal of Membrane Science, 1988. **37**(1): p. 45-62.
12. Omole, I.C., *Crosslinked Polyimide Hollow Fiber Membranes for Aggressive Natural Gas Feed Streams*, in *School of Chemical and Biomolecular Engineering*. 2008, Georgia Institute of Technology: Atlanta, GA.

CHAPTER 2

THEORY AND BACKGROUND

2.1 Polymer Membranes for Gas Separations

Polymer membranes have experienced success in a number of industrially relevant gas separations including nitrogen from air, hydrogen recovery from ammonia, and natural gas purification [1-3]. The ease of polymer processing and relative low cost of membrane separations give polymer membranes a significant advantage over more conventional thermally-driven separations. Moreover, with the development of better performing materials in recent decades, polymer membranes continue to generate interest in the common separations listed above, as well as less common and more difficult applications such as olefin/paraffin separations [4].

Polyimides are one class of high performance polymers that have received considerable attention, especially for natural gas purification. Excellent thermal and chemical stability and high intrinsic separation efficiencies make this class of polymers ideal for gas separations. Moreover, these polymers can be tailored to yield varying transport properties for optimized separations [5-7].

2.1.1 General Transport Theory

Gas transport in polymer membranes is best described by a solution diffusion mechanism [8]. In such materials, the partitioning of penetrant molecules in the membrane is strongly influenced by penetrant condensability and the chemical affinity between polymer and penetrant. Sorption dominates gas transport in rubbery polymer membranes, and a strong correlation exists between permeation rate and gas

condensability (which, itself, correlates well with critical temperature). However, both sorption and diffusion are significant factors influencing performance in glassy polymer membranes, with diffusion typically being the dominant mechanism. Smaller molecules are generally transported more quickly than larger molecules in glassy polymers, and the permeation rate in these materials correlates well with penetrant kinetic diameter [9]. Kinetic diameters and critical temperatures for a number of industrially relevant gases are compared in Table 2.1.

Table 2.1: Kinetic diameters [10] and critical temperatures [11] for selected gases.

	Helium	Carbon Dioxide	Oxygen	Nitrogen	Methane
Kinetic Diameter (Å)	2.6	3.3	3.46	3.64	3.8
Critical Temperature (K)	5.2	304.2	154.4	126.1	190.7

A penetrant molecule first sorbs into a polymer before diffusing in the material via jumps through thermally activated transient gaps that form between polymer chains.

This process is illustrated in Figure 2.1.

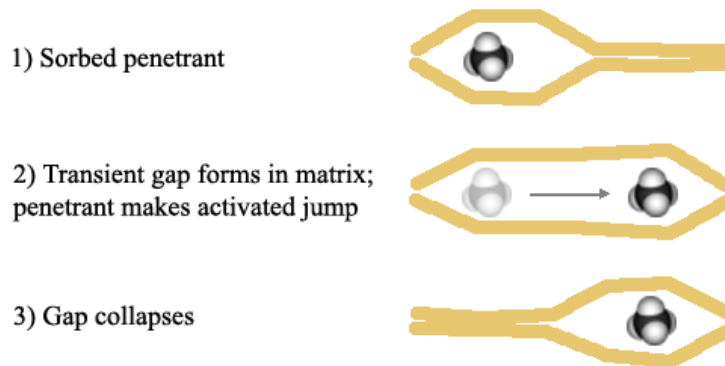


Figure 2.1: Illustration of gas molecule transport through a polymer via transient gap formation.

The diffusivity of a penetrant gas molecule (D_i) through an isotropic material can be fundamentally described as a function of the frequency of activated jumps (f_i) and the mean jump length (λ_i), which is controlled by the size of the transient gaps described above [12]. This relationship is captured in Equation 2.1:

$$D_i = \frac{f_i \cdot \lambda_i^2}{6} \quad (2.1)$$

The solubility of a penetrant in a polymer is defined in terms of its sorptive capacity at a given pressure. If we consider sorption of a penetrant, i , in a polymer, we define its sorption coefficient (S_i) as the specific penetrant capacity (C_i) in the polymer divided by the sorbent pressure (p_i), viz.,

$$S_i = \frac{C_i}{p_i} \quad (2.2)$$

In the case of polymer membrane characterization, permeate pressure is assumed negligible in comparison to feed pressure in Equation 2.2. Moreover, in this case the sorption coefficient should actually be considered an average coefficient since penetrant capacities will differ between the feed and permeate sides of the membrane. This is addressed in more detail later in this section.

Membranes are generally characterized in terms of their productivity (permeability) and efficiency (selectivity). Fundamentally, penetrant permeability (P_i) is defined as diffusive flux (n_i) normalized by membrane thickness (l) and the pressure drop—or more accurately, fugacity—across the membrane (Δp_i) [2, 8], viz.,

$$P_i = \frac{n_i \cdot l}{\Delta p_i} \quad (2.3)$$

Permeabilities are commonly reported in units of barrer, defined as:

$$barrer = 10^{-10} \frac{cm^3 (STP) \cdot cm}{cm^2 \cdot s \cdot cmHg} \quad (2.4)$$

If we assume that the diffusion coefficient is independent of penetrant concentration, then from Fick's first law we find:

$$n_i = -D_i \frac{dC_i}{dx} \quad (2.5)$$

Rearranging and substituting Equation 2.5 into Equation 2.3, we find:

$$\frac{P_i}{l} = \frac{-D_i \frac{dC_i}{dx}}{\Delta p_i} \quad (2.6)$$

If we then integrate over the membrane thickness and define the penetrant concentrations in the upstream and downstream relative to the membrane as $C_{i,u}$ and $C_{i,d}$, respectively, we find:

$$\int_0^l \frac{P_i}{l} dx = \int_{C_{i,d}}^{C_{i,u}} \frac{D_i}{\Delta p_i} dC_i \quad (2.7)$$

It has been noted that diffusion coefficients can actually be a strong function of local penetrant concentration [8, 13], so D_i in Equations 2.5 – 2.7 is actually an average diffusion coefficient in the membrane. It is generally accepted as adequate to treat the diffusion coefficient as such, and we can simply define this average as:

$$\bar{D}_i = \frac{\int_{C_{i,d}}^{C_{i,u}} D_i dC_i}{C_{i,u} - C_{i,d}} \quad (2.8)$$

It therefore follows that:

$$P_i = \bar{D}_i \cdot \frac{C_{i,u} - C_{i,d}}{\Delta p_i} \quad (2.9)$$

We can also define an average penetrant solubility coefficient in the membrane as:

$$\bar{S}_i = \frac{C_{i,u} - C_{i,d}}{\Delta p_i} \quad (2.10)$$

Substituting Equation 2.10 into 2.9, we find:

$$P_i = \bar{D}_i \cdot \bar{S}_i \quad (2.11)$$

This illustrates that when membrane transport is Fickian in nature, the permeability can also be expressed in terms of its governing kinetic and thermodynamic properties, the diffusion coefficient and sorption coefficient, respectively.

The selectivity of a membrane describes how efficiently one gas can permeate relative to another. Under conditions of negligible permeate pressure, the ideal selectivity of a membrane is defined as the ratio of fast gas (i) to slow gas (j) permeabilities, viz.,

$$\alpha_{i/j} = \frac{P_i}{P_j} = \frac{\bar{D}_i}{\bar{D}_j} \cdot \frac{\bar{S}_i}{\bar{S}_j} \quad (2.12)$$

Ideal selectivity is generally evaluated from pure gas permeation experiments. In the case of mixed gas feeds, when sorption site competition or swelling effects may affect transport through a membrane, the separation factor may be written as:

$$S.F._{i/j} = \frac{y_i/y_j}{x_i/x_j} \quad (2.13)$$

Here x and y refer to feed and permeate stream molar compositions, respectively.

Conditions of negligible permeate pressure are assumed for Equation 2.13 [8].

2.1.2 Modeling Polymer Membrane Transport Properties

2.1.2.1 *Dual-Mode Sorption*

While gas sorption in rubbery polymers is sufficiently described by a Henry's law relation, a more appropriate model for glassy polymers describes two separate environments for sorption. The first arises from penetrant dissolution into the polymer and is described by a Henry's law relation, just as for rubbery polymers. The second arises from unequilibrated free volume microvoids that are trapped in the polymer as it is cooled from above its glass transition temperature and can be described using a Langmuir relation. The dual-mode sorption capacity is then the sum of these two contributions, and for a penetrant, i , in a polymer we find [14, 15]:

$$C_i = k_{D,i} p_i + \frac{C'_{H,i} b_i p_i}{1 + b_i p_i} \quad (2.14)$$

where k_D is the Henry's constant, C'_H is the Langmuir hole-filling constant, b is the Langmuir affinity constant, and p_i is the penetrant partial pressure, or more accurately, fugacity.

A convenient feature of the dual-mode model is that it can describe sorption uptake in the presence of more than one penetrant. Under mixed gas conditions, different penetrant species compete for Langmuir holes; the result is a deviation in capacity from predicted pure gas capacity. In the case of a binary feed, Equation 2.14 can be modified as follows to predict the sorption capacity of penetrant i [13]:

$$C_i = k_{D,i} p_i + \frac{C'_{H,i} b_i p_i}{1 + b_i p_i + b_j p_j} \quad (2.15)$$

The Langmuir sorption population in a glassy polymer has finite capacity for a given penetrant. As such, Langmuir microvoids are saturated as membrane feed pressure increases. After Langmuir saturation, additional capacity in the membrane is described by sorption in the Henry's domain. This results in a decreasing sorption coefficient—as defined by Equation 2.2—with increasing pressure, which also results in a decrease in permeability with increasing pressure.

2.1.2.2 Partial Immobilization Model (Dual-Mode Extension)

The dual-mode sorption model for glassy polymers can be extended to membrane permeation analysis. If we modify Equation 2.5 to include flux terms arising from both Henry's and Langmuir concentrations, we find:

$$n_i = -D_{D,i} \frac{dC_{D,i}}{dx} - D_{H,i} \frac{dC_{H,i}}{dx} \quad (2.16)$$

This flux relationship can be substituted into Equation 2.3 in order to arrive at an expression for permeability. After a derivation similar to that above for permeability—the full details of which can be found in the reference [14]—we find the most common form of the model (assuming a binary feed and negligible permeate pressure):

$$P_i = k_{D,i} D_{D,i} \left[1 + \frac{F_i K_i}{1 + b_i p_i + b_j p_j} \right] \quad (2.17)$$

$$F_i = \frac{D_{H,i}}{D_{D,i}} \quad (2.18)$$

$$K_i = \frac{C'_{H,i} b_i}{k_{D,i}} \quad (2.19)$$

In the above equations, the D and H subscripts refer to Henry's and Langmuir parameters, respectively. F is simply the ratio of penetrant diffusivity within the

Langmuir population to that in the Henry's population; and K represents the equilibrium relationship between Langmuir and Henry's populations at infinite dilution.

A significant result of this model is that it readily allows calculation of the lower limit of permeability in the case of Langmuir saturation. At Langmuir saturation, the denominator in the right hand side of Equation 2.17 grows large, resulting in $P_i = k_{D,i}D_{D,i}$. This defines the permeability that is asymptotically approached with increasing pressure.

2.1.2.3 Bulk Flow (Frame of Reference) Model

In the preceding analyses, the contribution of the bulk diffusion term of Fick's first law has been assumed to be negligible. Penetrant flux and/or concentration in many materials is often low enough to make this assumption valid. However, in membranes having high sorption capacity and/or high diffusivity for at least one component of a mixed feed, the bulk flux contribution is often significant and cannot be ignored [15]. In general this simply means:

$$n_i = n_i^{diff} + n_i^{bulk} \quad (2.20)$$

The full derivation is rather tedious and can be found in detail in the literature [15]. For reference, however, the resulting model is included below:

$$n_i = \rho D_{D,i} \cdot \frac{\ln \left[\frac{1 - \omega_{i,d}(1 + 1/r)}{1 - \omega_{i,u}(1 + 1/r)} \right]}{1 + 1/r} \quad (2.21)$$

$$n_j = \rho D_{D,j} \cdot \frac{\ln \left[\frac{1 - \omega_{j,d}(1 + r)}{1 - \omega_{j,u}(1 + r)} \right]}{1 + r} \quad (2.22)$$

$$\omega_i = \frac{k_{D,i} P_i M_i}{22400 \rho} \left(1 + \frac{F_i K_i}{1 + b_i p_i + b_j p_j} \right) \quad (2.23)$$

$$r = \frac{n_i}{n_j} \quad (2.24)$$

$$P_i = \frac{22400 n_i}{M_i \Delta p_i} \quad (2.25)$$

In the above equations ρ is the polymer density, M is penetrant molecular weight, ω is the penetrant mobile concentration and is defined at both feed and permeate sides of the membrane. The remaining parameters are the same as defined in previous sections. The flux relationships for each feed component and the definition of r (Equation 2.24) can be solved simultaneously, and the results can be used to predict permeability according to Equation 2.25.

2.1.3 Non-Ideal Polymeric Membrane Transport Phenomena

2.1.3.1 *Plasticization*

Plasticization occurs in glassy polymers when a strongly sorbing penetrant reaches a concentration such that it physically swells the polymer matrix and enhances segmental mobility [17, 18]. This enhancement in chain mobility results in the loss of size and shape discrimination, and leads to increased diffusivity for all penetrants in the membrane. The slowest penetrant is impacted the greatest, and thus, a drop in selectivity is observed concurrent with an increase in permeability. High critical temperature gases, such as carbon dioxide, are known to strongly interact with glassy polymers and have high solubilities in most polymers [8, 16, 17]. Plasticization is, therefore, especially problematic in natural gas purification.

As previously discussed, permeability asymptotically decreases with increasing pressure in glassy polymer membranes due to Langmuir saturation. However, when a membrane plasticizes, a pronounced increase in permeability can be observed instead of the expected approach to $k_D D_D$. The pressure at which permeability begins to increase is defined as the plasticization pressure. This behavior is qualitatively depicted in Figure 2.2.

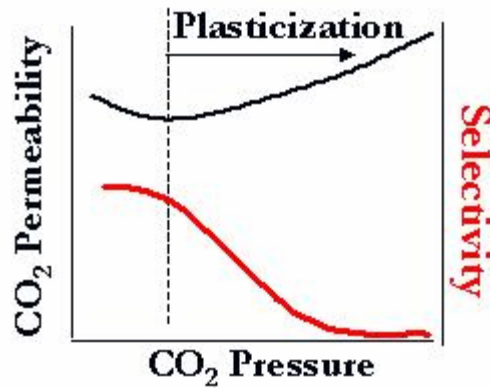


Figure 2.2: Qualitative representation of the permeability increase and selectivity decrease observed due to membrane plasticization.

It has been shown that membranes can be stabilized against plasticization with the use of crosslinkable polymers [18-21]. The networked matrix in these materials is less susceptible to penetrant-induced swelling and exhibits greater stability at higher feed pressures of highly-swelling penetrants. This concept is of fundamental importance to the current work and will be explored further in Section 2.2.

2.1.3.2 Antiplasticization

A phenomenon has been reported in which low concentrations of certain penetrants affect some polymer membranes in a manner contrary to that of plasticization. Instead of enhancing segmental motion, the penetrant apparently retards these fluctuations and slows the diffusion of all penetrants in the membrane [22, 23]. Dubbed antiplasticization, gas permeability is reduced, and the impact on selectivity can vary in a membrane experiencing this effect. For instance, it was observed in work by Maeda and Paul that low concentrations of certain aromatic compounds actually caused an increase in selectivity in poly(phenylene oxide). However, increasing antiplasticizer concentrations beyond certain levels resulted in reduced selectivities as antiplasticization was replaced by a conventional plasticization response [24].

2.1.3.3 Conditioning

As the concentration of a strongly sorbing penetrant in a polymer reaches the point of physical swelling, polymer chain packing reconfigures to accommodate the sorbed penetrant. When the penetrant is removed, the polymer will relax back towards its equilibrium state. If the penetrant is removed more quickly than the polymer can relax, it is left in a swollen state with increased free volume; it is this state of polymer that is considered “conditioned” [25]. The extra free volume of a conditioned membrane allows for a higher sorption capacity at a given pressure and can result in hysteresis in sorption and permeation analyses [26].

2.1.3.4 Physical Aging

Glassy polymers may contain varying amounts of excess free volume depending on processing conditions, thermal history, and exposure to sorbing materials. This free volume—or *unrelaxed* volume—has the tendency to diffuse out of the matrix as polymer chains relax to more equilibrated configurations. This behavior is termed *physical aging* and can result in significant time-dependent membrane transport properties [27-33].

As the polymer matrix densifies during aging, permeabilities decrease and selectivities increase. Owing to its diffusion-like mechanism, physical aging accelerates with thermal annealing and decreasing membrane thickness [31, 32, 34]. Moreover, aging has been observed in crosslinked polymer membranes, suggesting that while crosslinking can enhance resistance to plasticization, the impact of aging on long-term membrane properties should still be considered [19, 28, 34]. Since many commercial membrane applications utilize thin-skinned hollow fibers, physical aging is an important topic of study since this phenomenon can lead to undesirable performance.

2.2 Review of Crosslinkable Polymer Membranes for Gas Separations

As briefly mentioned above, a successful method in combating the deleterious, plasticization-induced reduction of membrane performance is to use a crosslinkable polymer membrane. Owing to the well-known tendency of carbon dioxide to plasticize membranes under industrially relevant conditions, this technique has garnered much interest in the area of natural gas purification. A number of crosslinking techniques are discussed in the below summary, with primary focus on materials most relevant to the current work.

Several researchers have employed UV irradiation as a method to induce crosslinking in polymers for gas separations. Kato et al. synthesized styrene-based photocrosslinked polymers and investigated the crosslinking via FTIR [35]. Similarly, Liu et al. investigated photocrosslinked co-polyimides [36] and Lin et al. investigated a series of poly(ethylene oxide) rubbers for carbon dioxide separations [37]. Shao et al. crosslinked poly(4-methyl-2-pentyne) (PMP) membranes using both UV and thermal methods to obtain membranes having increased light gas selectivities as compared to uncrosslinked PMP [38].

Lindbrathen and Hagg have used a common crosslinked rubbery polymer, poly(dimethylsiloxane) (PDMS), at low temperatures to separate chlorine gas from light gas mixtures. The material is reported to have good selectivity for chlorine but suffers from chemical degradation at industrially relevant temperatures [39]. Raharjo et al. have reported the details of separating methane from mixtures containing n-butane using PDMS membranes [32]. Still other researchers have reported oxygen/nitrogen separations using neat PDMS and PDMS composite materials [40].

A few researchers have investigated methods to crosslink cellulose acetate. Its low cost and widespread acceptance as the de facto membrane material seemingly make this an ideal target for stabilization against plasticization via crosslinking. However, while the reported work was successful in stabilizing cellulose acetate membranes under aggressive feed conditions, the effects on transport properties were mixed [34, 35].

The vast majority of the crosslinkable polymer membrane literature, and the most relevant to the current work, concerns the crosslinking of various polyimides. This class of polymer has proven to be incredibly versatile, having a virtually limitless number of

structures possible by varying and/or modifying diamine and dianhydride monomers. Moreover, the intrinsically high gas transport through many polyimides, coupled with their inherent temperature and chemical resistance, has positioned these materials to be the foundation of next generation gas separation membranes.

Chung et al. have focused on one method of crosslinking polyimides by post-treating membranes with various diamines, such as p-xylenediamine [41-46]. FTIR studies have shown that the penetrating diamine interacts with imide groups by forming amide linkages between adjacent chains [41, 44]. Several investigations have suggested this to be an effective means to stabilize polyimide membranes for carbon dioxide/methane separations. However, it is reported that this method typically results in a reduction of permeability and an increase in selectivity with increasing degrees of crosslinking. Apparently, the addition of the diamine to the polymer reduces its free volume. This reduction in free volume lowers the sorption capacity of penetrant molecules but enhances the size and shape discriminating ability of the membrane [38, 41-46]. More serious, however, is the hydrolytic instability of the resulting polyamic acid backbone. This makes crosslinking in this manner an undesirable approach.

Staudt-Bickel and Wind have investigated a series of crosslinkable polyimides and found an increase in permeability; selectivity in several cases was enhanced. The amount of permeability enhancement was found to be dependent on crosslinking temperature; higher temperature exposure led to higher degrees of crosslinking. It was shown that the crosslinking moieties added free volume to the polymer, allowing for higher carbon dioxide permeabilities while stabilizing membrane selectivity as high as 40

atm of carbon dioxide. The reduced polymer chain mobility caused by the crosslinking was responsible for the reported selectivity stability [21, 42-44].

The work of Staudt-Bickel and Wind involved polyimides based on the commonly used fluorinated dianhydride (4,4'-hexafluoroisopropylidene) diphthalic anhydride (6FDA) and a diamine having a carboxylic acid pendant group, namely 3,5-diaminobenzoic acid (DABA). The DABA acid group can be esterified with a variety of diols. This esterified DABA allows crosslinking in the final polyimide by undergoing a transesterification reaction with neighboring ester groups. Ratios of DABA and other diamines, such as 2,4,6-trimethyl-1,3-phenylenediamine (DAM), were used to control the crosslinking density. Wind showed via NMR and FTIR analyses that various diols have differing esterification reactivities, with 1,4-butanediol yielding nearly 100% conversion while ethylene glycol yielded only ~37%. Wind also reported lower relative membrane performance for membranes crosslinked with 1,4-butanediol, while membranes crosslinked with ethylene glycol experienced enhanced transport properties [21].

Based on the foundation established by Staudt-Bickel and Wind, Wallace [20] and Hillock [18] determined that crosslinking with 1,3-propanediol resulted in membranes having ideal transport properties and plasticization resistance for natural gas purification. This polymer had a DAM:DABA diamine ratio of 3:2 in order to increase the theoretical crosslinking density from that used by Wind, helping maintain membrane productivity while providing ample plasticization resistance. After esterification, the polymer—6FDA-DAM:DABA (3:2), monoesterified with 1,3-propanediol—was referred to as 'PDMC' (PropaneDiol Monoester Crosslinkable polyimide) [18]. Omole advanced this initial work by developing a procedure allowing the synthesis of high molecular weight

PDMC, which he showed was necessary for spinning defect-free crosslinkable asymmetric hollow fiber membranes [47].

2.3 Mixed Matrix Membranes for Gas Separations

As discussed in Chapter 1, mixed matrix membranes (MMMs) have been proposed as next-generation materials capable of transcending the permeability/selectivity tradeoff limitations illustrated by Robeson's upper bound [46, 47]. While some researchers have reported success in developing properly functioning MMMs, the bulk of the literature points to the need for a more fundamental understanding of these materials in order to avoid the myriad non-idealities that have been encountered. Some of these issues will be detailed in subsequent sections, including the need to properly match polymer and sieve properties [48-52]; the subtleties of membrane/dope preparation [48, 53]; and the need to engineer the polymer/sieve interface [54-57].

2.3.1 Gas Transport in Molecular Sieves

Zeolites and other molecular sieves are rigid, microporous materials capable of extremely high selectivities. The materials of greatest interest to this work are typically composed of larger cavities interconnected with smaller channels or apertures. These apertures are what lend size- and shape-selectivity to the sieves, rejecting any species from entering the pore network that is too large. Even in situations where two penetrants can enter the micropores, diffusion of the larger molecule will be hindered more as it will encounter greater resistance when passing through the aperture. Moreover, the larger

penetrant may have only one dimension small enough to access the micropores, adding an entropic penalty to its diffusion through the material [10].

2.3.2 Modeling Mixed Matrix Membrane Performance

The most commonly applied model to predict mixed matrix membrane performance is the Maxwell model. This model was adapted from work reported by James C. Maxwell in 1867 describing electrical properties of suspensions of spherical particles [48]. Other models have been applied to transport in composite membranes such as those developed by Bruggeman [49], Higuchi [50], and Landaur [51], but these are generally more complex and yield similar predictions to the Maxwell model. Maxwell's model is based on certain underlying assumptions. For instance, the dispersed particles should have an aspect ratio of 1 (spherical particles) since no shape factor is included to describe the impact of particle geometry on gas transport. Furthermore, the dispersion is assumed to be dilute enough such that flow around particles is unperturbed by neighboring particles. This implies an inherent high-loading limitation on the model, but Petropolous has noted that the Maxwell model is applicable at moderate loadings most typically studied [52].

The model is defined as:

$$P_{MM} = P_c \left[\frac{P_d + 2P_c - 2\Phi_d(P_c - P_d)}{P_d + 2P_c + \Phi_d(P_c - P_d)} \right] \quad (2.26)$$

where P is permeability, Φ is volume fraction, and the subscripts c and d refer to the continuous polymer phase and dispersed molecular sieving phase, respectively. P_{MM} is the effective permeability of the mixed matrix membrane.

2.3.2.1 Three-Phase Maxwell Model

An extension to the Maxwell model has been proposed to account for more complicated systems in which interfacial voids or non-ideal interphases exist between the bulk polymer matrix and dispersed molecular sieve particles. Termed the *three-phase Maxwell model* (3MM), the two-phase combination of the sieve and surrounding void or interphase is first modeled as a single entity whose transport properties are estimated by application of the Maxwell model, viz.,

$$P_{eff} = P_I \left[\frac{P_d + 2P_I - 2\Phi_s(P_I - P_d)}{P_d + 2P_I + \Phi_s(P_I - P_d)} \right] \quad (2.27)$$

Here, P is permeability, and P_{eff} is the effective permeability of the interphase/sieve combination. The subscripts d and I refer to the dispersed molecular sieving phase and the interphase, respectively. The molecular sieve volume fraction in the two-phase system, Φ_s , is defined as:

$$\Phi_s = \frac{\Phi_d}{\Phi_d + \Phi_I} \quad (2.28)$$

A second application of the Maxwell model using the above P_{eff} as the dispersed phase permeability results in the following:

$$P_{3MM} = P_c \left[\frac{P_{eff} + 2P_c - 2(\Phi_d - \Phi_I)(P_c - P_{eff})}{P_{eff} + 2P_c + (\Phi_d - \Phi_I)(P_c - P_{eff})} \right] \quad (2.29)$$

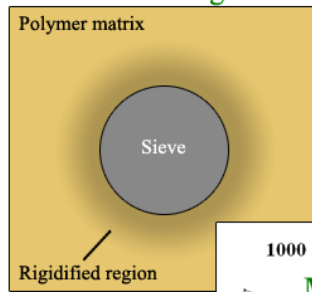
As before, P is permeability and the subscripts c , d , and I refer to the continuous polymer matrix, dispersed molecular sieve phase, and the interphase, respectively [53-55].

This model can be used to estimate the size of interfacial voids or the thickness of non-ideal interphases and used in the analyses of mixed matrix membranes in Chapters 4 and 5.

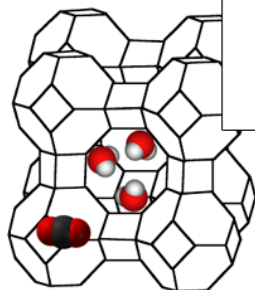
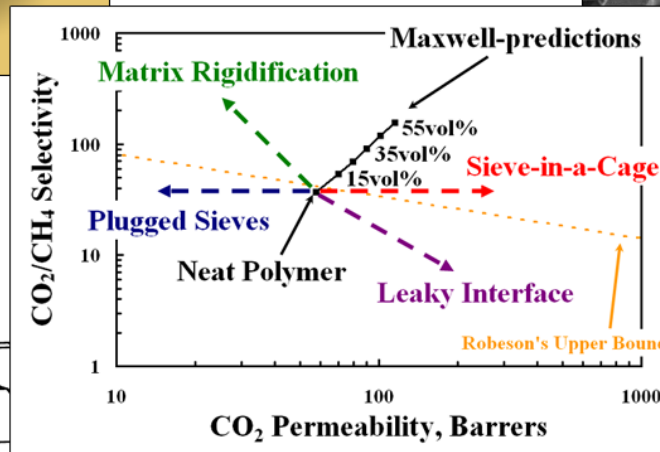
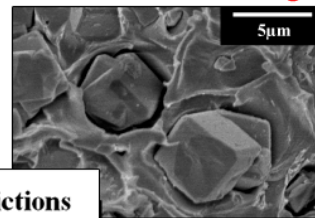
2.3.3 Non-Ideal Interfacial Morphologies

The interface between molecular sieves and the polymer matrix in mixed matrix membranes has been the focus of considerable work, and a number of interfacial morphologies have been identified, each with unique effects on membrane transport properties. These often undesirable effects on transport properties often allow the determination of the specific morphology present in a given membrane. Four common morphologies are illustrated in Figure 2.3 along with their respective qualitative impact on transport properties.

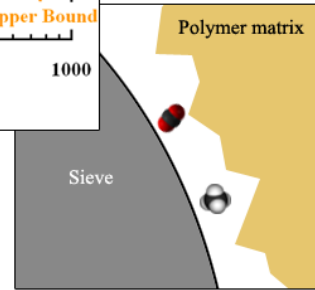
Case I: Matrix Rigidification



Case II: Sieve-in-a-Cage



Case IV: Plugged Sieves



Case III: Leaky Interface

Figure 2.3: Common interfacial morphologies and their respective effects on membrane transport properties.

It has been reported that strong polymer/sieve adhesion in some mixed matrix membranes can result in loss of polymer free volume in the immediate vicinity of the sieve surface. This phenomenon has been dubbed *matrix rigidification* owing to the presumed immobilization of rigidified, surface-bound polymer [56, 57]. Its signature is characterized by lower than predicted permeabilities and near-expected selectivities, which is explained by the lower permeability through the rigidified polymer. Matrix rigidification and its effect on membrane transport is illustrated in the upper left quadrant of Figure 2.3.

Arguably the most common defective morphology, ‘sieve-in-a-cage’ gets its name from the appearance of molecular sieve particles encased in cavities within the polymer matrix [57]. This situation is illustrated by the SEM in the upper right quadrant of Figure 2.3. Clearly the large interfacial voids present a path of much lower transport resistance than either the polymer or the sieve. As such, the signature of sieve-in-a-cage is a much greater than predicted permeability with a selectivity equivalent to that of neat polymer. While the increased membrane productivity is not inherently deleterious to membrane performance, this morphology is generally undesirable since the selectivity enhancement sought by including the molecular sieving phase is not realized due to bypass through the interfacial voids.

Another interfacial morphology exists that is similar to sieve-in-a-cage, only the interfacial void size approaches the dimensions of penetrant molecules. Termed a *leaky interface*, penetrating molecules experience Knudsen diffusion in the interfacial gap, which is a transport regime defined as having a molecular mean free path greater than the void dimensions. This morphology is illustrated in the lower right quadrant of Figure

2.3. Since Knudsen diffusivity scales with the inverse of molecular weight, lighter molecules—not always smaller molecules—are transported more quickly through these extremely narrow defects. Such morphology is identified by an increase in permeability and a reduction in selectivity for most studied gas pairs [54]. Since the smaller, faster gas in most targeted gas pairs (e.g. carbon dioxide/methane or oxygen/nitrogen) is also the heavier gas, the diffusivity of the larger, lighter gas is enhanced more in the Knudsen regime causing the signature drop in selectivity.

Though not technically an interfacial morphology, the final non-ideality to discuss in this section simply concerns the plugging of molecular sieves with water, solvents, or other sorbing contaminants. This situation is depicted in the lower left quadrant of Figure 2.3. Obviously, if the sieve becomes plugged, it can no longer function as a molecular sieve. In this case, since the sieve effectively functions as a nonporous filler, the resulting membrane permeability is less than and the selectivity is equivalent to that of the neat polymer [57].

2.3.4 Review of Mixed Matrix Membranes for Gas Separations

Early gas separation work via mixed matrix membranes generally involved attempts at controlling gas solubility in rubbery polymers. Kemp and Paul reported investigating zeolite 5A in silicone rubber. No substantial separation enhancements were realized, but they did raise important questions concerning the validity of measuring mixed matrix membrane diffusivities via the time lag method [58]. Later, Duval et al. reported that silicalite and zeolites 13X and KY in PDMS and ethylene-propylene diene rubber (EPDM) resulted in enhanced carbon dioxide/methane separation, while only silicalite-1 in these polymers enhanced oxygen/nitrogen separation [59].

The successes with rubbery polymers urged expanded interest in composite membranes using glassy polymers. Shortly after their work with rubbery polymers, Duval et al. investigated a number of glassy polymers with silicalite. They reported poor transport properties and attributed it to the poor polymer/sieve adhesion observed via SEM imaging. Subsequent attempts to enhance adhesion with a sieve treated with a silane coupling agent and by thermal annealing resulted in visibly improved membrane morphology. However, transport properties still suggested a defective membrane [60].

Süer et al. reported work with membranes formed from zeolites 4A and 13X dispersed in polyethersulfone (PES) with no substantial transport property enhancement observed except at very high sieve loading. Their work highlighted the potential problems with mismatched polymer/sieve systems, as well as the impact of membrane formation techniques on morphology and transport properties [61]. These concerns were echoed by Zimmerman et al. [62], Mahajan and Koros [54, 56], and Moore et al. [55, 57].

Vankelecom et al. published similar results noting poor performance in membranes of silicalite and zeolite Y in several different polyimides. In all cases, a lack of interfacial adhesion was blamed for the defective material properties [63]. In subsequent work, the same authors reported somewhat improved polymer adhesion—as determined from mechanical analysis—with silylation of a borosilicate molecular sieve [64].

Although much of the literature has highlighted the problems associated with forming mixed matrix membranes having desirable transport properties, several successful attempts have been reported. Mahajan and Koros reported good results using zeolite 4A in several polyimides and in polyvinylacetate (PVAc). The selectivities of

these membranes matched closely with Maxwell model predictions; however, the permeabilities were considerably lower than expected [50, 70]. This was attributed to matrix rigidification, which was discussed above. Shu and coworkers published a novel surface treatment for zeolites that significantly improved polymer adhesion and membrane properties [65]. The authors subsequently reported good mixed matrix membrane results using zeolite 4A in Ultem[®] polyimide and PVAc [66]. Using the same surface treatment, Husain and Koros reported better than predicted membrane properties using SSZ-13 in Ultem hollow fiber membranes [67].

Additional microporous materials have been investigated as sieves in mixed matrix membranes. Vu and coworkers found that carbon molecular sieve (CMS) particles dispersed in either Ultem or Matrimid[®] polyimide resulted in selectivity enhancements as high as 45% over neat polymer membranes [68, 69]. Similarly, Anson et al. observed permeability enhancements as high as 600% and selectivity enhancements as high as 100% in membranes incorporating activated carbon in acrylonitrile-butadiene-styrene (ABS) copolymer [70]. A number of researchers have also examined the behavior of metal-organic framework (MOF) materials in various polymers. Zhang et al. dispersed Cu-BPY-HFS in Matrimid and reported modest selectivity enhancements [71]. Perez and coworkers evaluated MOF-5 in Matrimid, but determined that only permeabilities were increased [72]. Adams et al. observed modest mixed matrix permeability and selectivity enhancement in Cu-TPA/PVAc membranes [73].

Virtually no research has been published that investigates gas separations via mixed matrix membranes utilizing a crosslinkable polymer matrix. In fact, the only report appears to be from Hillock et al.—the immediate predecessor of the current work.

In their study, modest transport property enhancement in SSZ-13/PDMC membranes with both polymer-sized and silylated sieves was reported. Moreover, impressive plasticization resistance was demonstrated using carbon dioxide feed pressures up to ~30 atm with no observed characteristic upswing in permeability [74]. Hillock's work serves as a proof-of-concept for crosslinkable mixed matrix membranes. These materials are feasible and warrant further investigation as they hold potential for significant advancement in natural gas purification technology.

2.4 References

1. Bernardo, P., E. Drioli, and G. Golemme, *Membrane Gas Separation: A Review/State of the Art*. Industrial & Engineering Chemistry Research, 2009. **48**(10): p. 4638-4663.
2. Ghosal, K. and B.D. Freeman, *Gas separation using polymer membranes: an overview*. Polymers for Advanced Technologies, 1994. **5**(11): p. 673-697.
3. Ockwig, N.W. and T.M. Nenoff, *Membranes for hydrogen separation*. Chemical Reviews, 2007. **107**(10): p. 4078-4110.
4. Das, M., *Membranes for Olefin/Paraffin Separations*, in *School of Chemical & Biomolecular Engineering*. 2009, Georgia Institute of Technology: Atlanta, GA.
5. Kim, T.H., et al., *RELATIONSHIP BETWEEN GAS SEPARATION PROPERTIES AND CHEMICAL-STRUCTURE IN A SERIES OF AROMATIC POLYIMIDES*. Journal of Membrane Science, 1988. **37**(1): p. 45-62.
6. Park, J.Y. and D.R. Paul, *Correlation and prediction of gas permeability in glassy polymer membrane materials via a modified free volume based group contribution method*. Journal of Membrane Science, 1997. **125**(1): p. 23-39.
7. Xiao, Y.C., et al., *The strategies of molecular architecture and modification of polyimide-based membranes for CO₂ removal from natural gas-A review*. Progress in Polymer Science, 2009. **34**(6): p. 561-580.
8. Koros, W.J., et al., *Polymeric membrane materials for solution-diffusion based permeation separations*. Progress in Polymer Science, 1988. **13**(4): p. 339-401.
9. Ho, W.S.W. and K.K. Sirkar, eds. *Membrane Handbook*. 1992, Van Nostrand Reinhold: New York, NY.

10. Breck, D.W., *Zeolite Molecular Sieves: Structure, Chemistry, and Use*. 1974, Malabar, FL: Robert E. Krieger Publishing Co., Inc.
11. Yaws, C.L., ed. *Chemical Properties Handbook*. 1999, McGraw-Hill.
12. Koros, W.J., M.R. Coleman, and D.R.B. Walker, *CONTROLLED PERMEABILITY POLYMER MEMBRANES*. Annual Review of Materials Science, 1992. **22**: p. 47-89.
13. Koros, W.J., *MODEL FOR SORPTION OF MIXED GASES IN GLASSY-POLYMERS*. Journal of Polymer Science Part B-Polymer Physics, 1980. **18**(5): p. 981-992.
14. Koros, W.J., et al., *A MODEL FOR PERMEATION OF MIXED GASES AND VAPORS IN GLASSY-POLYMERS*. Journal of Polymer Science Part B-Polymer Physics, 1981. **19**(10): p. 1513-1530.
15. Kamaruddin, H.D. and W.J. Koros, *Some observations about the application of Fick's first law for membrane separation of multicomponent mixtures*. Journal of Membrane Science, 1997. **135**(2): p. 147-159.
16. Bos, A., et al., *CO₂-induced plasticization phenomena in glassy polymers*. Journal of Membrane Science, 1999. **155**(1): p. 67-78.
17. Wessling, M., et al., *Plasticization of gas separation membranes*. Gas Separation and Purification, 1991. **5**: p. 222-228.
18. Hillock, A.M.W. and W.J. Koros, *Cross-linkable polyimide membrane for natural gas purification and carbon dioxide plasticization reduction*. Macromolecules, 2007. **40**(3): p. 583-587.
19. Omole, I.C., *Crosslinked Polyimide Hollow Fiber Membranes for Aggressive Natural Gas Feed Streams*, in *School of Chemical and Biomolecular Engineering*. 2008, Georgia Institute of Technology: Atlanta, GA.
20. Wallace, D.W., et al., *Characterization of crosslinked hollow fiber membranes*. Polymer, 2006. **47**(4): p. 1207-1216.
21. Wind, J.D., et al., *Solid-state covalent cross-linking of polyimide membranes for carbon dioxide plasticization reduction*. Macromolecules, 2003. **36**(6): p. 1882-1888.
22. Maeda, Y. and D.R. Paul, *EFFECT OF ANTIPLASTICIZATION ON SELECTIVITY AND PRODUCTIVITY OF GAS SEPARATION MEMBRANES*. Journal of Membrane Science, 1987. **30**(1): p. 1-9.

23. Maeda, Y. and D.R. Paul, *EFFECT OF ANTIPLASTICIZATION ON GAS SORPTION AND TRANSPORT .1. POLYSULFONE*. Journal of Polymer Science Part B-Polymer Physics, 1987. **25**(5): p. 957-980.
24. Maeda, Y. and D.R. Paul, *EFFECT OF ANTIPLASTICIZATION ON GAS SORPTION AND TRANSPORT .2. POLY(PHENYLENE OXIDE)*. Journal of Polymer Science Part B-Polymer Physics, 1987. **25**(5): p. 981-1003.
25. Al-Juaied, M. and W.J. Koros, *Performance of natural gas membranes in the presence of heavy hydrocarbons*. Journal of Membrane Science, 2006. **274**(1-2): p. 227-243.
26. Coleman, M.R. and W.J. Koros, *Conditioning of fluorine-containing polyimides. 2. Effect of conditioning protocol at 8% volume dilation on gas-transport properties*. Macromolecules, 1999. **32**(9): p. 3106-3113.
27. Jordan, S.M., W.J. Koros, and G.K. Fleming, *THE EFFECTS OF CO₂ EXPOSURE ON PURE AND MIXED GAS PERMEATION BEHAVIOR - COMPARISON OF GLASSY POLYCARBONATE AND SILICONE-RUBBER*. Journal of Membrane Science, 1987. **30**(2): p. 191-212.
28. Kim, J.H., W.J. Koros, and D.R. Paul, *Effects of CO₂ exposure and physical aging on the gas permeability of thin 6FDA-based polyimide membranes - Part 2. with crosslinking*. Journal of Membrane Science, 2006. **282**(1-2): p. 32-43.
29. Kim, J.H., W.J. Koros, and D.R. Paul, *Physical aging of thin 6FDA-based polyimide membranes containing carboxyl acid groups. Part I. Transport properties*. Polymer, 2006. **47**(9): p. 3094-3103.
30. Moe, M., et al., *EFFECTS OF FILM HISTORY ON GAS-TRANSPORT IN A FLUORINATED AROMATIC POLYIMIDE*. Journal of Applied Polymer Science, 1988. **36**(8): p. 1833-1846.
31. Moe, M.B., W.J. Koros, and D.R. Paul, *EFFECTS OF MOLECULAR-STRUCTURE AND THERMAL ANNEALING ON GAS-TRANSPORT IN 2 TETRAMETHYL BISPHENOL-A POLYMERS*. Journal of Polymer Science Part B-Polymer Physics, 1988. **26**(9): p. 1931-1945.
32. Pfromm, P.H. and W.J. Koros, *ACCELERATED PHYSICAL AGING OF THIN GLASSY POLYMER-FILMS - EVIDENCE FROM GAS-TRANSPORT MEASUREMENTS*. Polymer, 1995. **36**(12): p. 2379-2387.
33. Pope, D.S., G.K. Fleming, and W.J. Koros, *EFFECT OF VARIOUS EXPOSURE HISTORIES ON SORPTION AND DILATION IN A FAMILY OF POLYCARBONATES*. Macromolecules, 1990. **23**(11): p. 2988-2994.
34. Kratochvil, A.M., *Thickness Dependent Physical Aging and Supercritical Carbon Dioxide Conditioning Effects on Crosslinkable Polyimide Membranes for Natural*

Gas Purification, in *School of Chemical & Biomolecular Engineering*. 2008, Georgia Institute of Technology: Atlanta, GA.

35. Kato, N., et al., *SYNTHESIS OF NOVEL ORGANOSILICON-CONTAINING OLIGOMERS WITH REACTIVE FUNCTIONAL-GROUPS THROUGH ANIONIC POLYCONDENSATION REACTIONS*. *Polymer*, 1994. **35**(19): p. 4228-4234.
36. Liu, Y., et al., *Gas permeability and permselectivity of photochemically crosslinked copolyimides*. *Journal of Applied Polymer Science*, 1999. **73**(4): p. 521-526.
37. Lin, H.Q., et al., *Transport and structural characteristics of crosslinked poly(ethylene oxide) rubbers*. *Journal of Membrane Science*, 2006. **276**(1-2): p. 145-161.
38. Shao, L., J. Samseth, and M.B. Hagg. *Crosslinking and stabilization of high fractional free volume polymers for gas separation*. 2008: Elsevier Sci Ltd.
39. Lindbrathen, A. and M.B. Hagg, *Membrane separation of chlorine gas*. *Chemical Engineering and Processing*, 2009. **48**(1): p. 1-16.
40. Rao, H.X., F.N. Liu, and Z.Y. Zhang, *Preparation and oxygen/nitrogen permeability of PDMS crosslinked membrane and PDMS/tetraethoxysilicone hybrid membrane*. *Journal of Membrane Science*, 2007. **303**(1-2): p. 132-139.
41. Cao, C., et al., *Chemical cross-linking modification of 6FDA-2,6-DAT hollow fiber membranes for natural gas separation*. *Journal of Membrane Science*, 2003. **216**(1-2): p. 257-268.
42. Low, B.T., Y.C. Xiao, and T.S. Chung, *Amplifying the molecular sieving capability of polyimide membranes via coupling of diamine networking and molecular architecture*. *Polymer*, 2009. **50**(14): p. 3250-3258.
43. Shao, L., et al., *Transport properties of cross-linked polyimide membranes induced by different generations of diaminobutane (DAB) dendrimers*. *Journal of Membrane Science*, 2004. **238**(1-2): p. 153-163.
44. Shao, L., et al., *The effects of 1,3-cyclohexanebis(methylamine) modification on gas transport and plasticization resistance of polyimide membranes*. *Journal of Membrane Science*, 2005. **267**(1-2): p. 78-89.
45. Shao, L., et al., *Comparison of diamino cross-linking in different polyimide solutions and membranes by precipitation observation and gas transport*. *Journal of Membrane Science*, 2008. **312**(1-2): p. 174-185.

46. Tin, P.S., et al., *Effects of cross-linking modification on gas separation performance of Matrimid membranes*. Journal of Membrane Science, 2003. **225**(1-2): p. 77-90.
47. Omole, I.C., S.J. Miller, and W.J. Koros, *Increased molecular weight of a cross-linkable polyimide for spinning plasticization resistant hollow fiber membranes*. Macromolecules, 2008. **41**(17): p. 6367-6375.
48. Maxwell, J.C., *Treatise on Electricity and Magnetism*. 1873, London: Oxford University Press.
49. Bruggemann, D.A.G., *The calculation of various physical constants of heterogeneous substances. I. The dielectric constants and conductivities of mixtures composed of isotropic substances*. Annalen der Physik V, 1935. **24**.
50. Higuchi, W.I., *A NEW RELATIONSHIP FOR THE DIELECTRIC PROPERTIES OF 2-PHASE MIXTURES*. Journal of Physical Chemistry, 1958. **62**(6): p. 649-653.
51. Landauer, R., *THE ELECTRICAL RESISTANCE OF BINARY METALLIC MIXTURES*. Journal of Applied Physics, 1952. **23**(7): p. 779-784.
52. Petropoulos, J.H., *A COMPARATIVE-STUDY OF APPROACHES APPLIED TO THE PERMEABILITY OF BINARY COMPOSITE POLYMERIC MATERIALS*. Journal of Polymer Science Part B-Polymer Physics, 1985. **23**(7): p. 1309-1324.
53. Mahajan, R., et al., *Challenges in forming successful mixed matrix membranes with rigid polymeric materials*. Journal of Applied Polymer Science, 2002. **86**(4): p. 881-890.
54. Mahajan, R. and W.J. Koros, *Mixed matrix membrane materials with glassy polymers. Part 1*. Polymer Engineering and Science, 2002. **42**(7): p. 1420-1431.
55. Moore, T.T., et al., *Hybrid membrane materials comprising organic polymers with rigid dispersed phases*. Aiche Journal, 2004. **50**(2): p. 311-321.
56. Mahajan, R. and W.J. Koros, *Mixed matrix membrane materials with glassy polymers. Part 2*. Polymer Engineering and Science, 2002. **42**(7): p. 1432-1441.
57. Moore, T.T. and W.J. Koros, *Non-ideal effects in organic-inorganic materials for gas separation membranes*. Journal of Molecular Structure, 2005. **739**(1-3): p. 87-98.
58. Paul, D.R. and D.R. Kemp, *DIFFUSION TIME LAG IN POLYMER MEMBRANES CONTAINING ADSORPTIVE FILLERS*. Journal of Polymer Science Part C-Polymer Symposium, 1973(41): p. 79-93.

59. Duval, J.M., et al. *ADSORBENT FILLED MEMBRANES FOR GAS SEPARATION .I. IMPROVEMENT OF THE GAS SEPARATION PROPERTIES OF POLYMERIC MEMBRANES BY INCORPORATION OF MICROPOROUS ADSORBENTS*. 1993: Elsevier Science Bv.
60. Duval, J.M., et al., *PREPARATION OF ZEOLITE FILLED GLASSY POLYMER MEMBRANES*. Journal of Applied Polymer Science, 1994. **54**(4): p. 409-418.
61. Suer, M.G., N. Bac, and L. Yilmaz, *GAS PERMEATION CHARACTERISTICS OF POLYMER-ZEOLITE MIXED MATRIX MEMBRANES*. Journal of Membrane Science, 1994. **91**(1-2): p. 77-86.
62. Zimmerman, C.M., A. Singh, and W.J. Koros, *Tailoring mixed matrix composite membranes for gas separations*. Journal of Membrane Science, 1997. **137**(1-2): p. 145-154.
63. Vankelecom, I.F.J., et al., *INCORPORATION OF ZEOLITES IN POLYIMIDE MEMBRANES*. Journal of Physical Chemistry, 1995. **99**(35): p. 13187-13192.
64. Vankelecom, I.F.J., et al., *Silylation to improve incorporation of zeolites in polyimide films*. Journal of Physical Chemistry, 1996. **100**(9): p. 3753-3758.
65. Shu, S., S. Husain, and W.J. Koros, *Formation of nanostructured zeolite particle surfaces via a halide/Grignard route*. Chemistry of Materials, 2007. **19**(16): p. 4000-4006.
66. Shu, S., S. Husain, and W.J. Koros, *A general strategy for adhesion enhancement in polymeric composites by formation of nanostructured particle surfaces*. Journal of Physical Chemistry C, 2007. **111**(2): p. 652-657.
67. Husain, S. and W.J. Koros, *Mixed matrix hollow fiber membranes made with modified HSSZ-13 zeolite in polyetherimide polymer matrix for gas separation*. Journal of Membrane Science, 2007. **288**(1-2): p. 195-207.
68. Vu, D.Q., W.J. Koros, and S.J. Miller, *Mixed matrix membranes using carbon molecular sieves - I. Preparation and experimental results*. Journal of Membrane Science, 2003. **211**(2): p. 311-334.
69. Vu, D.Q., W.J. Koros, and S.J. Miller, *Mixed matrix membranes using carbon molecular sieves - II. Modeling permeation behavior*. Journal of Membrane Science, 2003. **211**(2): p. 335-348.
70. Anson, M., et al., *ABS copolymer-activated carbon mixed matrix membranes for CO₂/CH₄ separation*. Journal of Membrane Science, 2004. **243**(1-2): p. 19-28.
71. Zhang, Y.F., et al., *Gas permeability properties of Matrimid (R) membranes containing the metal-organic framework Cu-BPY-HFS*. Journal of Membrane Science, 2008. **313**(1-2): p. 170-181.

72. Perez, E.V., et al., *Mixed-matrix membranes containing MOF-5 for gas separations*. Journal of Membrane Science, 2009. **328**(1-2): p. 165-173.
73. Adams, R.T., et al., *Metal Organic Framework Mixed Matrix Membranes for Gas Separations*. Submitted, 2009.
74. Hillock, A.M.W., S.J. Miller, and W.J. Koros, *Crosslinked mixed matrix membranes for the purification of natural gas: Effects of sieve surface modification*. Journal of Membrane Science, 2008. **314**(1-2): p. 193-199.

CHAPTER 3

MATERIALS AND METHODS

In this chapter, the materials that were studied, material preparation and characterization techniques, and the equipment used to characterize these materials will be detailed. The specific materials selected for this work are described in Section 3.1. Membrane preparation techniques are described in Section 3.2, followed by sieve modification procedures in Section 3.3. Material characterization techniques and equipment are outlined in Section 3.4

3.1 Materials

3.1.1 Polymers

The polymer selected for this work was a crosslinkable polyimide designated 6FDA-DAM:DABA (3:2), 1,3-propanediol monoesterified. This polymer was first developed by Wallace et al. [1, 2] and Hillock [3] based on original work by Staudt-Bickel and Koros [4] and Wind et al. [5, 6] and is most commonly referred to as PDMC (PropaneDiol Monoester Crosslinkable). The PDMC used in this work was either synthesized in the Koros group laboratory at Georgia Institute of Technology or was graciously provided by Chevron Energy Technology Co.

The PDMC was synthesized via a polycondensation reaction between (4,4'-hexafluoroisopropylidene)diphthalic anhydride (6FDA) (99%, Lancaster Synthesis, Ward Hill, MA), 2,4,6-trimethyl-*m*-phenylenediamine (DAM) (96%, Sigma-Aldrich, St. Louis, MO), and 3,5-diaminobenzoic acid (DABA) (98%, Sigma-Aldrich) in 1-methyl-2-

pyrrolidinone (NMP) (anhydrous, 99.5%, Sigma-Aldrich). The polyamic acid resulting from the initial condensation reaction was thermally imidized in NMP with added *o*-dichlorobenzene (ODCB) (anhydrous, 99%, Sigma-Aldrich) to assist in water removal. The reaction scheme is displayed in Figure 3.1.

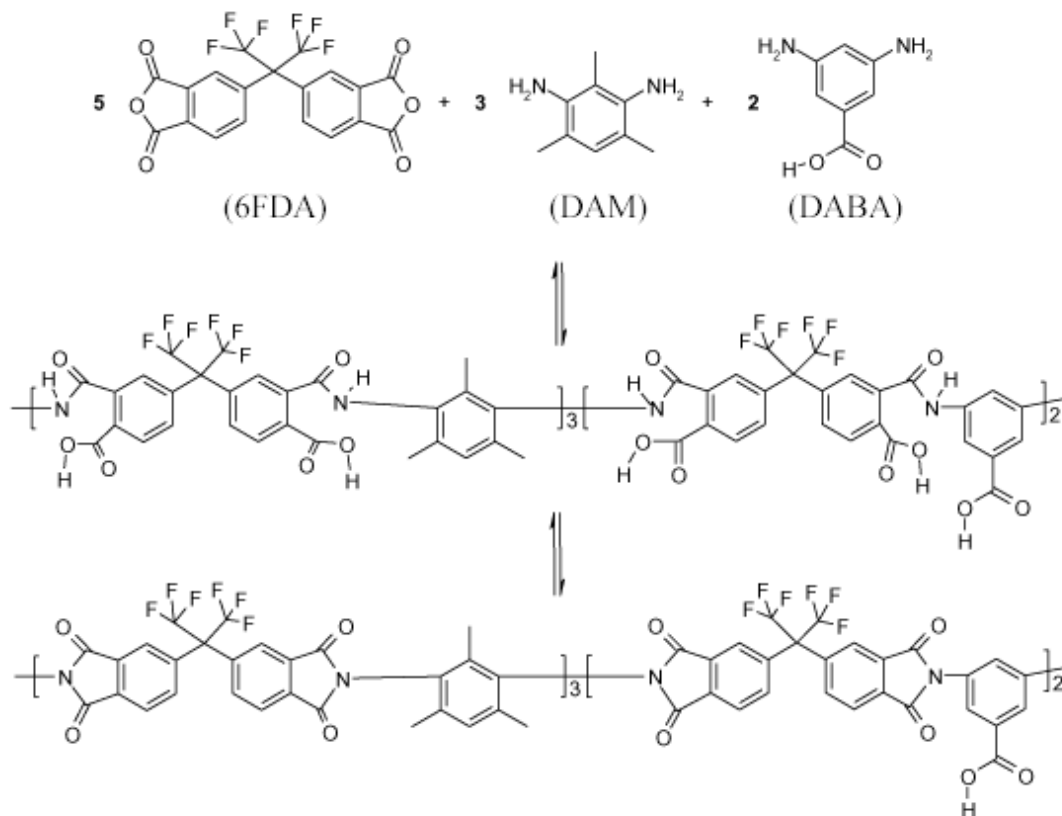


Figure 3.1: Reaction scheme for 6FDA-DAM:DABA (3:2). Adapted from [7].

The imidized polymer was esterified using 1,3-propanediol (99.6%, Sigma-Aldrich) and *p*-toluenesulfonic acid (*p*-TSA) (98.5%, Sigma-Aldrich) as a catalyst. Omole noted that the liberated water and the diol present during the esterification reaction, along with the *p*-TSA catalyst, caused hydrolytic attack of imide rings and

resulted in significant loss of molecular weight. It was found that by reducing the amount of catalyst and lowering the reaction temperature, the molecular weight of the original polyimide could be maintained [7, 8]. This finding was crucial in being able to spin high quality PDMC asymmetric hollow fiber membranes. The reaction scheme for the esterification step is displayed in Figure 3.2. The detailed synthesis procedure can be found in the references [3, 7, 8].

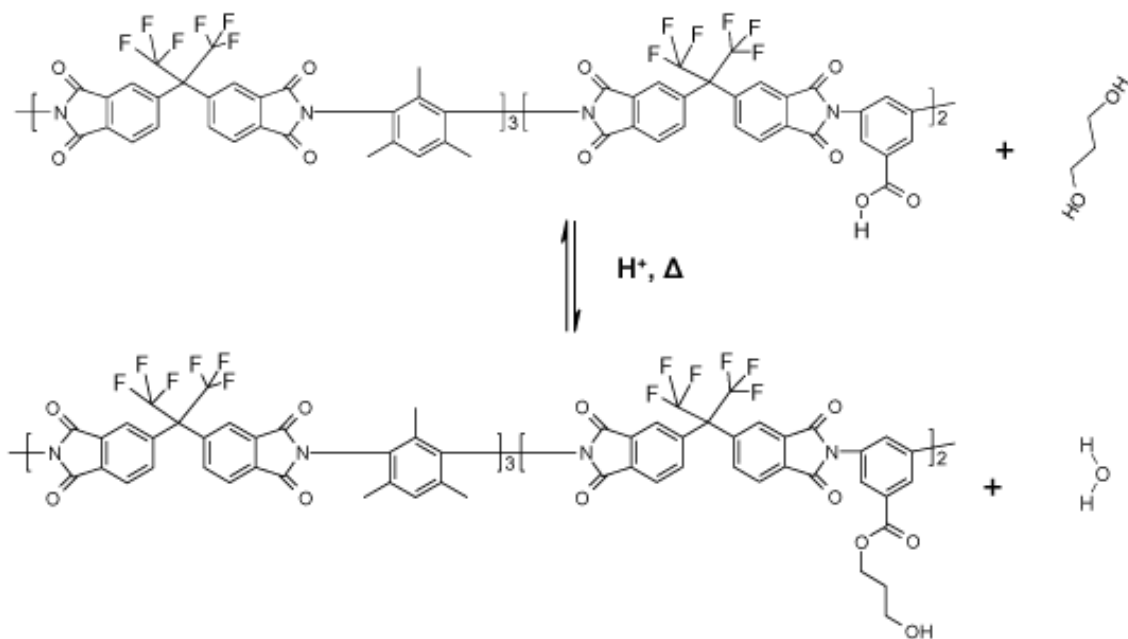


Figure 3.2: Reaction scheme for esterification of 6FDA-DAM:DABA (3:2) with 1,3-propane diol to form PDMC. Adapted from [7].

PDMC can be crosslinked via a transesterification reaction between adjacent ester pendent groups on the DABA monomer. This is accomplished by heating pre-cast membranes to above 150 °C under vacuum. The crosslinking scheme is displayed in Figure 3.3.

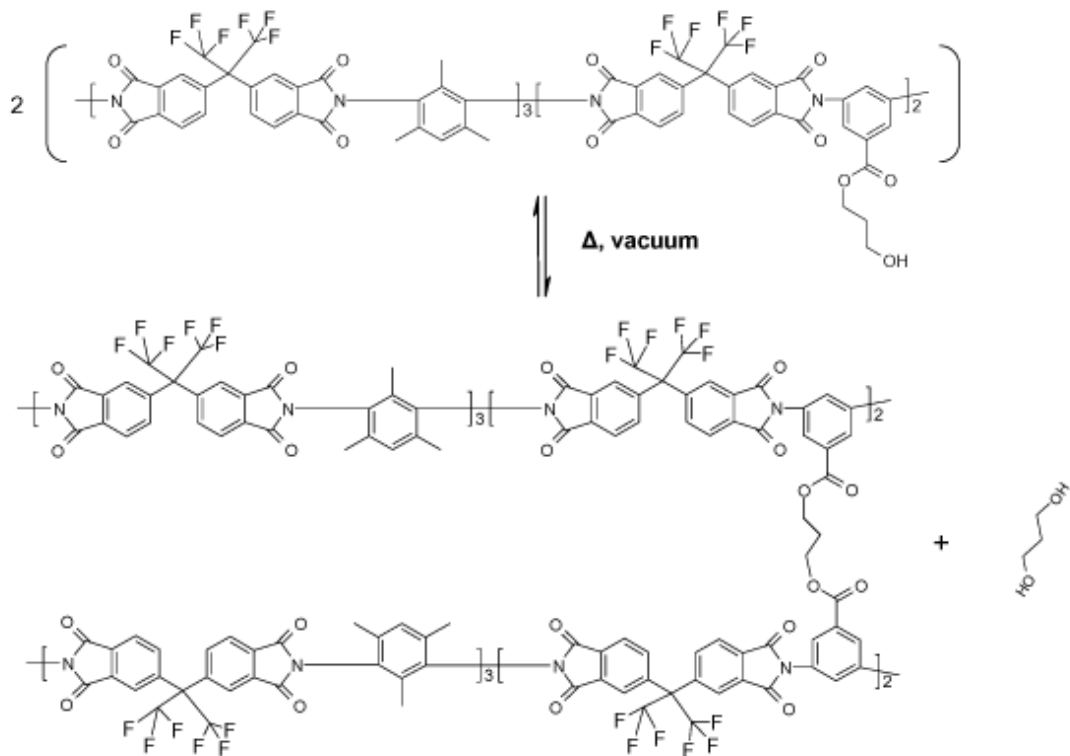


Figure 3.3: Reaction scheme for transesterification crosslinking between adjacent esters. Adapted from [7].

3.1.2 Molecular Sieves

The molecular sieve used in this work was SSZ-13, a microporous aluminosilicate material having a chabazite (CHA) framework with a pore diameter of 3.8 Å (graciously provided by Chevron Energy Technology Co.). Figure 3.4 illustrates a single CHA cage with pore openings entering from multiple directions and shows how these individual cages are arranged into a 3-dimensional framework.

SSZ-13 can be synthesized with varying silicon-to-aluminum ratios; the material used in this work had a Si:Al > 25:1. High silica sieves were preferred in this work since the lower aluminum content requires fewer hydrophilic framework-balancing cations.

Plugged sieves in mixed matrix membranes are often caused by the tendency of these cations to attract water, as discussed in Section 2.3.3.

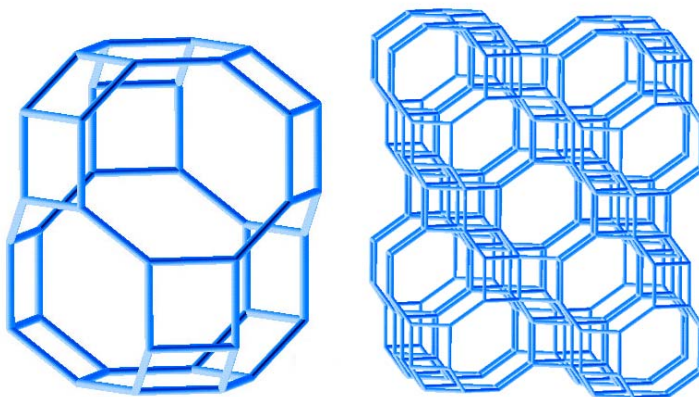


Figure 3.4: Illustration of an individual chabazite cage structure (left) and the assembly of cages into the chabazite framework (right). Adapted from [9].

SSZ-13 has been reported to have impressive carbon dioxide/methane separation properties, with a carbon dioxide permeability of 200 barrer and selectivity over methane of ~ 800 [3]. Its transport properties, along with its intrinsic hydrophobicity, make SSZ-13 an ideal candidate for use in hybrid membranes for natural gas purification.

3.1.3 Gases

All pure gases used throughout this research (i.e., carbon dioxide and methane) were research grade (99.999%) and supplied by Airgas South (Kennesaw, GA). Gas mixtures were supplied by either Airgas South or by Praxair, Inc. (Peachtree City, GA).

3.2 Membrane Formation

3.2.1 Neat Polymer Membranes

While asymmetric hollow fiber membranes are the industrially preferred membrane geometry, dense film membranes are much simpler to prepare and characterize when developing new technology. As such, dense film polymer membranes were exclusively investigated over the course of this work. A typical neat polymer membrane solution, or dope, was prepared from an amount of dried PDMC and sufficient tetrahydrofuran (THF) (anhydrous, 99.9+%, Sigma-Aldrich) to yield 25-30% solids (w/w). The PDMC powder was dried under vacuum at no more than 75 °C for 24-48 hr to remove water. Care was taken to not expose the PDMC to temperatures greater than 120 °C in order to avoid crosslinking the polymer.

After THF was added to the dry PDMC, the container was sealed and mixed on an axial roller until the PDMC was thoroughly dissolved. The vial was subsequently removed from the roller and allowed to remain static in order to remove entrained air bubbles.

All membranes were cast in a controlled atmosphere established in a polyethylene glove bag. The glove bag was purged with dry nitrogen gas several times to displace atmospheric water vapor. Once the glove bag was sealed, several milliliters of THF were poured into an open glass petri dish and allowed to evaporate in order to saturate the local atmosphere. The membrane dope was then slowly poured onto either a GlasClad[®]-treated (Gelest Inc., Morrisville, PA) tempered glass plate or a Teflon[®] plate. The dope was then draw-cast using a 10 mil stainless steel doctor blade (Paul N. Gardner Co.,

Pompano Beach, FL). The freshly drawn dope was subsequently covered by an inverted glass dish to further slow solvent evaporation.

The nascent membrane was allowed to vitrify for at least 24 hr (up to 48 hr) after casting before being removed from the glove bag. Once removed from the bag, the membrane was delaminated from the plate and removed to a sheet of heavy-gauge Teflon[®]-coated aluminum foil. The edges of the membrane were carefully clipped with small binder clips in order to prevent the membrane from curling onto itself during subsequent drying/annealing steps. The clipped membrane was then placed into a vacuum oven and evacuated at ~29 in. Hg at room temperature for at least one hour.

The thermal treatment of uncrosslinked PDMC membranes consisted of increasing the vacuum oven temperature by 10 °C/hr until 75 °C was reached. The membrane remained under these conditions for 48 hr before the oven was allowed to cool. Once the oven temperature was below 40 °C, the membrane was removed and immediately prepared for testing.

Occasionally, a single membrane was divided in half after the previous thermal treatment. This allowed an uncrosslinked section to be tested while the remaining membrane was returned to the oven for crosslinking. To crosslink the remaining section of membrane, vacuum was applied to the oven for at least one hour before increasing the oven temperature to 220 °C for 24 hr. After 24 hr, the oven was allowed to cool while still under vacuum. The membrane was removed and tested once the oven temperature was below 40 °C. When a membrane was to be only tested as crosslinked, the oven temperature was ramped to 75 °C as described above. After being maintained at 75 °C for several hours, the oven temperature was increased to 220 °C for 24 hr. The oven was

then allowed to cool; when the oven was below 40 °C, the membrane was removed and immediately prepared for testing.

3.2.2 Mixed Matrix Membranes

Mixed matrix membranes were prepared similarly to neat polymer dense film membranes with the exception of a sieve dispersion step. An amount of sieve, generally 150-250 mg, was added to an 8 ml glass vial and placed in a vacuum oven. Under vacuum, the sieves were activated overnight (8-12 hr) at 150-180 °C, after which the oven was allowed to cool. When the oven temperature was below 40 °C, the oven was purged with dry nitrogen gas. The vial was quickly removed and 5-6 ml THF was added. The sieves were subsequently dispersed via ultrasonication using either an 80 W sonication horn (Sonics & Materials, Inc., Newton, CT), operating at 40-50% power or a sonication bath (Branson Ultrasonics Corp., Danbury, CT). When the sonication horn was used, several bursts of 30 s of sonication followed by 30 s of rest were applied for up to a total of 3 min of sonication time. When the sonication bath was used, it was found that 2-3 hr resulted in comparable (according to visual comparison) dispersion to the sonication horn.

Once the sieves were dispersed, a small amount of previously dried PDMC powder (dried under vacuum at 75 °C for 48 hr) was added to the vial. This PDMC—amounting to roughly 1-3% of the total PDMC to be added to the dope—was added to prime the sieves; this served to stabilize the dispersion and was previously shown to improve membrane formation [10]. The procedure used to initially disperse the sieves was repeated after adding the priming PDMC. After priming, small amounts of dry PDMC powder were added to the vial, followed by vigorous shaking until the polymer

had mostly dissolved. This was repeated until the required amount of polymer had been added to reach the desired sieve loading (e.g., 15% sieves in PDMC by weight). Once the required amount of PDMC had been added, the vial was placed on an axial roller overnight (8-12 hr) to thoroughly mix.

After mixing, the dope was concentrated by slowly purging with dry nitrogen gas while mixing on an axial roller set at an angle such that the contents of the vial would not pour out. After 5-7 min of purging, the vial was capped and mixing continued until the dope was again homogeneous. It was determined through experience that the optimum dope consistency resembled that of honey, so the dope was concentrated in stages in order to prevent more solvent evaporation than was desired. Dopes having too low a viscosity resulted in particle settling; dopes having too high a viscosity were difficult to pour and draw with a casting knife. Once the ideal dope consistency was reached, the vial was allowed to mix on the axial roller until ready for casting.

At this point, the hybrid membrane dope was cast, dried, and/or crosslinked according to the above description for neat polymer membranes.

3.3 Molecular Sieve Modification

3.3.1 Grignard Procedure

Some molecular sieve samples were Grignard-treated (GT) to investigate the impact of the procedure on polymer/sieve adhesion; the results of this investigation are detailed in Chapter 6. The following procedure was adapted from work by Shu and Husain [11, 12].

Sieves to be treated (approximately 500 mg) were placed in a 100 ml three neck flask and dried under vacuum at 150 °C for 8-12 hr. The oven was cooled and purged with dry nitrogen gas before removing the sieves. Approximately 30 ml anhydrous toluene (anhydrous, 99.8%, Sigma-Aldrich) and 5 ml thionyl chloride (99.5%, Sigma-Aldrich) were added to the dry sieves, maintaining anhydrous conditions. A slow dry nitrogen gas purge was started and the sieves were ultrasonicated in a bath for at least 4 hr (up to 24 hr). The flask was subsequently heated at 100-110 °C with stirring until the solvent had evaporated, leaving a dry cake. Vacuum was applied to the flask to remove any remaining solvent.

The dry cake was dispersed again in 30 ml anhydrous toluene in an ultrasonication bath with slow dry nitrogen purge, as above. In general, the sieves were well dispersed after 4 hr of sonication. Approximately 2-3 ml methyl magnesium bromide (3.0 M in diethyl ether, Sigma-Aldrich) was added to the dispersed sieves; the dispersion was ultrasonicated at least an additional 4 hr (up to 24 hr). It was determined during the course of this work that scaling the amount of Grignard reagent based on sieve mass (as was done in the original development of the treatment) was inappropriate since the ultimate result of the treatment was a deposit of material on the external surface of the sieve. Therefore, it was deemed most proper to scale the reagent amount with the external surface area of the sieve, as determined by nitrogen physisorption.

The flask was subsequently placed in an ice bath with vigorous stirring, and the reaction mixture was quenched via slow addition of 20 ml anhydrous 2-propanol (IPA) (anhydrous, 99.5%, Sigma-Aldrich). The sieves were collected via centrifugation in Teflon[®] centrifuge tubes and subsequently washed three times with anhydrous IPA.

Following the IPA wash, the sieves were washed with deionized water (minimum 18 M Ω) until the supernatant liquid conductivity was below 70 μ S. The sieves were then dried overnight under vacuum at 150 °C.

3.3.2 Reactive Sizing

As will be discussed further in Chapter 5, analysis of Grignard-treated sieves suggested the creation of non-selective voids during the procedure. It is believed that these voids existed *within* the sieve surface layer due to formations stemming from magnesium hydroxide deposits. The following procedure was initially envisioned as a means to *caulk* these voids with PDMC-philic material in order to both maintain improved polymer/sieve adhesion and prevent sieve bypass. However, this procedure also resulted in an unexpected improvement in membrane performance after treating as-received sieves.

A sample of sieves (typically 500 mg) was added to a 100 ml round bottom flask and subsequently dried under vacuum at 150 °C for 8-12 hr. The oven was then cooled and purged with dry nitrogen gas before removing the sieves. Maintaining anhydrous conditions, sufficient NMP was added to yield a 3-4% (w/v) mixture. A slow dry nitrogen purge was started, and the sieves were dispersed via ultrasonication in a bath for at least 4 hr (up to 24 hr). The flask was then removed from the ultrasonication bath and placed on a stir plate; the dispersion was stirred with a Teflon[®]-coated stir bar.

Based on the amount of sieve being treated, the amount of PDMC needed to form a 15% (w/w) sieve/polymer mixture was calculated. This amount of PDMC was used to determine the amounts of monomer (6FDA, DAM, and DABA) to add to the reactive sizing mixture. The molar ratios used for PDMC synthesis were maintained: a ratio of

6FDA:DAM:DABA equaling 1:0.6:0.4. As per the preceding calculations, the appropriate amount of DAM and DABA were added to the flask, and the mixture was stirred for 15 min to fully dissolve the diamines. The appropriate amount of 6FDA was then added, and the mixture was stirred for 12-18 hr.

Instead of the thermal imidization technique typically used in PDMC synthesis, a chemical imidization method was utilized in this procedure. Approximately 0.17 ml 3-methylpyridine (>99.5%, Sigma-Aldrich) per gram of PDMC precursor (6FDA-DAM:DABA (3:2)) was added as a catalyst to the stirring mixture in addition to 1.5 ml acetic anhydride (>98%, Sigma-Aldrich) per gram of precursor. The mixture was stirred for an additional 12-18 hr.

The mixture was precipitated in methanol and washed before collection via high pressure filtration (Pall Corp., Port Washington, NY) using a 0.2 μm filter disc. The collected solids were dried in a fume hood for up to 3 hr before being dried under vacuum at 200 °C for 8-12 hr.

The dried solids were added to a 100 ml round bottom flask, along with a Teflon[®]-coated stir bar, before starting a dry nitrogen gas purge. Sufficient anhydrous NMP was added to the dry solids, with vigorous mixing, to form a 20% (w/w) mixture. Once the polymer had fully dissolved and the mixture appeared homogeneous, the temperature was raised to 100 °C and 70 times molar excess (based on DABA content) 1,3-propanediol was slowly added. Additionally, 0.5 mg *p*-TSA per gram of PDMC theoretically synthesized was added. The temperature was then increased to 140 °C and maintained for 12-18 hr.

Once the mixture had cooled, it was again precipitated in methanol and washed before collection via high pressure filtration. The collected solids were dried in a hood for up to 3 hr before being dried under vacuum at 75 °C for 48 hr. The treated sieves were then recovered by washing/centrifuging the dry solids with THF in Teflon[®] centrifuge tubes for a total of three washes. The treated sieves were again dried under vacuum at 75 °C overnight (8-12 hr) before use.

3.4 Characterization Techniques

3.4.1 Gas Permeation Analysis

3.4.1.1 Membrane Masking

Dense film membranes, as prepared according to Section 3.2, were masked for permeation analysis as described previously [13-15]. An approximately 1 in.² section of membrane, selected to be effectively void of pin holes, sieve agglomerates, and other defects, was sandwiched between two annular pieces of adhesive-backed aluminum foil (Fasson, Mentor, OH). The inner diameter of the annulus was approximately 0.5 in., while the outer diameter was approximately 1.75 in. Care was taken to align the inner circles of the top and bottom pieces of aluminum foil since the membrane area exposed by these holes defines the area used in calculating gas permeabilities. Membrane areas were measured by first scanning an image of the masked membrane and then measuring the masked area using Scion Image software (Scion Corp., Frederick, MD) running on a personal computer. Membrane thickness was determined by averaging ten measurements using a micrometer (B. C. Ames, Inc., Melrose, MA).

The masked membrane sandwich was then sealed onto the bottom half of a permeation cell by means of an additional annulus of adhesive-backed aluminum foil. The inner diameter of this annulus was sized somewhat larger than the exposed membrane diameter of the masked sandwich (~0.625 in.); the outer diameter was also sized larger than the outer diameter of the masked sandwich, but smaller than the inner diameter of the innermost O-ring (~2.25 in.). One or two pieces of filter paper were placed between the stainless steel frit of the permeation cell and the membrane in order to provide support and protect the membrane from damage at high test pressures. A schematic of this arrangement is depicted in Figure 3.5.

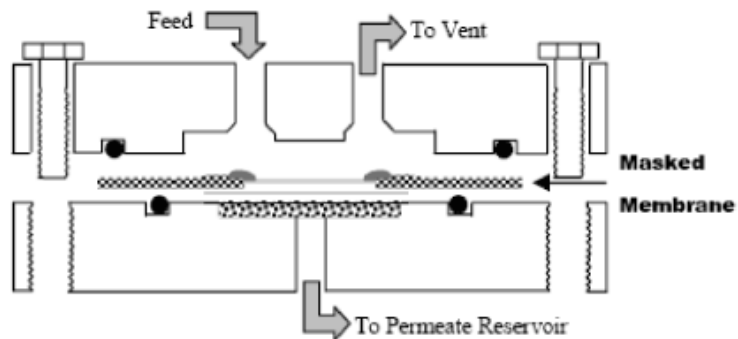


Figure 3.5: Schematic of masked membrane placed in an assembled permeation cell. Adapted from [14].

Under certain test conditions, such as long-term exposure to high pressure feeds containing carbon dioxide or toluene, it was necessary to create a seal on the upstream face of the mask between the membrane and the masking material in order to prevent membrane bypass. In this case, epoxy (Duralco[®] 4525, Cotronics, Brooklyn, NY) was applied such that the interior edges of the masking material were covered, as well as the

outermost portion of the membrane. The epoxy was allowed to cure for 24 hr before the membrane area was measured (as described above) and the permeation cell assembled.

Permeation cell assembly was accomplished by tightening six machine bolts arranged around the periphery of the cell. Inner and outer Viton[®] O-rings pressed against the upper and lower faces of the cell create a leak-tight seal to keep out atmospheric gases. The assembled cell was then placed into a permeation system for testing, as described in the following sections.

3.4.1.2 Permeation Equipment

Membrane permeabilities were determined via use of an in-house constructed constant-volume, variable pressure (isochoric) permeation system originally described elsewhere [16, 17]. The schematic in Figure 3.6 depicts the connection of essential components for constructing such a system.

All system components were constructed from stainless steel (type 316) and were assembled within an insulated box. Connections were welded when possible; otherwise, Swagelok VCR[®] (Swagelok Co., Solon, OH) connections were used to minimize leakage. The permeate pressure transducer was either a type 122A or 622B 0-10 torr Baratron[®] capacitance manometer supplied by MKS Instruments (Andover, MA). The permeate transducer signal was output to a PDR-5-B power supply/pressure readout, also supplied by MKS. During permeation analyses, an output signal from the readout was converted and stored as pressure data via a data acquisition system comprised of an analog/digital input/output card (Keithley Instruments, Inc., Cleveland, OH) installed in a personal computer running a custom LabVIEW[®] (National Instruments Corp., Austin, TX) virtual instrument. The feed pressure transducer was a Sensotec[®] 1000 psia model supplied by

Honeywell International, Inc. (Columbus, OH) connected to a power supply/readout; feed pressures were manually recorded. A fan, (3), and PID-controlled heat source, (4), were used to maintain system temperature at 35 °C.

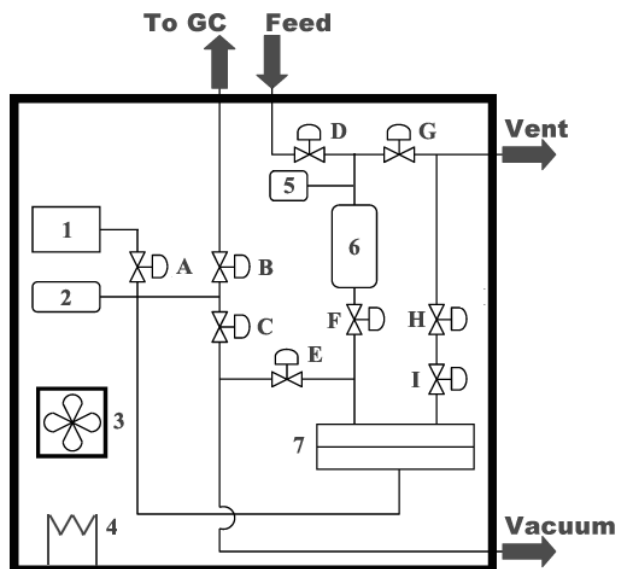


Figure 3.6: Schematic of an isochoric permeation analysis system used throughout this work. Essential components are as follows: (1) permeate pressure transducer; (2) permeate reservoir; (3) circulation fan; (4) heater, controlled by PID temperature controller; (5) feed pressure transducer; (6) feed reservoir; and (7) permeation cell. Important valves are as follows: (A) permeate transducer isolation valve; (B) GC feed valve; (C) permeate vacuum valve; (D) feed valve; (E) feed vacuum valve; (F) feed isolation valve; (G) vent valve; (H) retentate metering valve; and (I) retentate shutoff valve.

3.4.1.3 Pure Gas Permeation

Once a membrane was masked and the permeation cell was placed into the system, permeation analysis proceeded as follows. The system was first evacuated by closing valves (B), (D), (G), (H), and (I) and opening valves (A), (C), (E), and (F) for a length of time sufficient to allow sorbed gases to diffuse out of the membrane and

masking materials. Care was taken to always establish vacuum on the downstream face of the membrane first to avoid buckling or breaking the membrane. It is critical to properly evacuate the system as high leak or outgassing rates can lead to erroneous permeability and selectivity calculations. The *leak rate*, which is a measurement of atmospheric gases leaking into the system and as well as material outgassing from masking materials, is determined by closing all system valves, except for (A), and recording pressure data over a period of time. Throughout this research, fresh membranes were evacuated until the leak rate was less than 0.1% of the methane steady state permeation rate for a given membrane; this typically required an initial vacuum period of 48-72 hr. After measuring the leak rate, the system was again evacuated for several hours prior to beginning a permeation analysis.

To begin the analysis, the gas to be tested was charged into the feed reservoir by opening valve (D); the permeate vacuum valve, (C), and feed vacuum valve, (E), were left open until just before gas was introduced to the feed side of the membrane. The reservoir was purged several times with the test gas to remove any atmospheric gases that may have been in the transfer line. The feed was carefully adjusted to the desired pressure by slowly venting through valve (G). The system was subsequently allowed to thermally equilibrate for about an hour before continuing. The pure gas permeation analyses to be discussed in subsequent chapters were performed at 35 °C and ~65 psia feed pressure.

To begin collecting data, the permeate vacuum valve, (C), and feed vacuum valve, (E), were closed and the feed isolation valve, (F) was opened. Pressure data collection via LabVIEW began simultaneously with the opening of valve (F). Data was typically

collected for 14 time lags before opening the permeate vacuum valve, (C), to evacuate the permeate reservoir. This valve was again closed and pressure data was collected for an additional 2-4 time lags to ensure permeation had truly reached steady state.

Permeabilities were calculated according to Equation 2.3. The flux was calculated from the ideal gas law and the steady state pressure rise (dp/dt [torr/s]) determined from a plot of permeate pressure versus time. The slope of this line was typically determined between 10 and 14 time lags. This calculation is detailed in the references [14, 18].

3.4.1.4 Mixed Gas Permeation

Permeation analysis using mixed gases was performed as described above with a few minor modifications. In order to prevent concentration polarization due to more rapid fast gas depletion (with respect to the slower gas) in the feed reservoir, the feed was continuously purged. This required the feed valve, (D), to remain open to the gas manifold or gas cylinder. By opening the retentate shutoff valve, (I), and adjusting the retentate metering valve, (H), the feed purge rate was set such that a <1% stage cut was maintained. A bubble flow meter was used to measure the purge flow rate.

An Agilent Technologies (Santa Clara, CA) 6890N gas chromatograph (GC) configured with a GS-CarbonPLOT[®] capillary column (J&M Scientific, Folsom, CA) and thermal conductivity detector (TCD) was used to analyze the permeate gas composition. The GC was modified so that the sample loop and transfer line leading from the permeation system to the GC remained under vacuum—eliminating the need for permeate purge gas flow. When sufficient pressure had built in the permeate reservoir, (2), a vacuum shutoff valve at the GC was closed, and the GC feed valve, (B), was

opened to allow permeate gas to equilibrate in the evacuated transfer line. The GC feed pressure was recorded, the feed valve, (B), was closed, and the GC program was executed to analyze the gas.

Whereas permeation data collection was based on time lag information when testing with pure gases, data was collected for mixed gas permeation analysis only after the membrane had reached steady state. It was determined that exposing membranes to gas mixtures for at least an hour before collecting pressure data was sufficient to establish steady state permeation rates. Analyses were repeated after an additional hour of permeation to verify that steady state had been reached.

When testing with toluene-contaminated feeds, membranes were allowed to equilibrate for 24 hr before permeation analysis. This was accomplished by pressurizing the feed reservoir, (6), to the desired feed pressure, opening the feed isolation valve, (F), so that the membrane was exposed to the feed gas, and closing all remaining valves. After equilibration, the permeate reservoir, (2), was evacuated by opening the permeate vacuum valve, (C); the permeate transducer isolation valve, (A), was also opened. The feed reservoir was purged with fresh feed gas and the feed purge rate was adjusted as before to maintain a stage cut of <1%. The system was allowed to equilibrate in this condition for at least one hour before collecting permeation data as before.

3.4.2 Cryogenic Nitrogen Physisorption (BET)

Molecular sieve surface area and porosity were characterized using nitrogen physisorption at 77 K. This technique was pioneered by Brunauer, Emmett, and Teller, and thus, is often referred to by their initials: BET [19]. A Micromeritics Instrument Corp. (Norcross, GA) ASAP 2020 was used to analyze the sieves used in this work.

3.4.3 Scanning Electron Microscopy (SEM)

Molecular sieves and hybrid membranes were visually characterized via scanning electron microscopy (SEM). A LEO (now Zeiss, Oberkochen, Germany) thermally-assisted field emission (TFE) SEM was used to image materials used through this work. Dilute suspensions of molecular sieve samples in acetone were prepared and dropped onto aluminum sample stages. Samples were allowed to thoroughly dry before imaging. Membrane samples were prepared by fracturing under liquid nitrogen to obtain a clean break for cross-section imaging. Membranes were sputter coated with ~10 nm of gold to reduce charging during imaging.

3.4.4 Thermogravimetric Analysis (TGA)

Thermogravimetric analysis (TGA) was used to characterize several materials used in this work. The amount of magnesium hydroxide deposited on sieves as a result of the Grignard procedure could be determined from the mass loss due to dehydration at ~330 °C. The mass lost upon calcining molecular sieves—in addition to the calcined sieve density—was used to calculate the density of the uncalcined material; this was important for predicting permeabilities in several hybrid membranes using the Maxwell model. TGA was also used to determine the amount of surface-deposited material resulting from the reactive sizing procedure. These analyses were performed using a Netzsch (Selb, Germany) STA 409 PC Luxx[®] thermobalance.

3.4.5 X-Ray Photoelectron Spectroscopy (XPS)

X-Ray photoelectron spectroscopy (XPS), also known as electron spectroscopy for chemical analysis (ESCA), was used to determine the elemental composition of

surface material deposited during the reactive sizing procedure. Samples were characterized using a Surface Science Labs (Mountain View, CA) SSX-100 spectrometer emitting monochromatic Al K α x-rays (1.4866 keV).

3.4.6 Gel Permeation Chromatography (GPC)

Polymer samples, both those synthesized in-house and externally, were analyzed using gel permeation chromatography (GPC) to determine the molecular weight and polydispersity index (PDI) of various batches. Samples were analyzed by American Polymer Standards Corp. (Mentor, OH).

3.5 References

1. Wallace, D., *Crosslinked Hollow Fiber Membranes for Natural Gas Purification and Their Manufacture from Novel Polymers*, in *School of Chemical Engineering*. 2004, University of Texas at Austin: Austin, TX.
2. Wallace, D.W., et al., *Characterization of crosslinked hollow fiber membranes*. *Polymer*, 2006. **47**(4): p. 1207-1216.
3. Hillock, A.M.W., *Crosslinkable Polyimide Mixed Matrix Membranes for Natural Gas Purification*, in *School of Chemical & Biomolecular Engineering*. 2005, Georgia Institute of Technology: Atlanta, GA. p. 197.
4. Staudt-Bickel, C. and W.J. Koros, *Improvement of CO₂/CH₄ separation characteristics of polyimides by chemical crosslinking*. *Journal of Membrane Science*, 1999. **155**(1): p. 145-154.
5. Wind, J.D., et al., *The effects of crosslinking chemistry on CO₂ plasticization of polyimide gas separation membranes*. *Industrial & Engineering Chemistry Research*, 2002. **41**(24): p. 6139-6148.
6. Wind, J.D., et al., *Solid-state covalent cross-linking of polyimide membranes for carbon dioxide plasticization reduction*. *Macromolecules*, 2003. **36**(6): p. 1882-1888.
7. Omole, I.C., *Crosslinked Polyimide Hollow Fiber Membranes for Aggressive Natural Gas Feed Streams*, in *School of Chemical and Biomolecular Engineering*. 2008, Georgia Institute of Technology: Atlanta, GA.

8. Omole, I.C., S.J. Miller, and W.J. Koros, *Increased molecular weight of a cross-linkable polyimide for spinning plasticization resistant hollow fiber membranes*. *Macromolecules*, 2008. **41**(17): p. 6367-6375.
9. Baerlocher, C. and L.B. McCusker. *Database of Zeolite Structures*. 1996 [cited; Available from: <http://www.iza-structure.org/databases/>].
10. Mahajan, R. and W.J. Koros, *Factors controlling successful formation of mixed-matrix gas separation materials*. *Industrial & Engineering Chemistry Research*, 2000. **39**(8): p. 2692-2696.
11. Shu, S., S. Husain, and W.J. Koros, *A general strategy for adhesion enhancement in polymeric composites by formation of nanostructured particle surfaces*. *Journal of Physical Chemistry C*, 2007. **111**(2): p. 652-657.
12. Shu, S., S. Husain, and W.J. Koros, *Formation of nanostructured zeolite particle surfaces via a halide/Grignard route*. *Chemistry of Materials*, 2007. **19**(16): p. 4000-4006.
13. Damle, S. and W.J. Koros, *Permeation equipment for high-pressure gas separation membranes*. *Industrial & Engineering Chemistry Research*, 2003. **42**(25): p. 6389-6395.
14. Moore, T.T., *Effects of Materials, Processing, and Operating Conditions on the Morphology as Gas Transport Properties of Mixed Matrix Membranes*, in *Department of Chemical Engineering*. 2004, University of Texas: Austin, TX.
15. Zimmerman, C.M., *Advanced Gas Separation Membrane Materials: Hyper Rigid Polymers and Molecular Sieve-Polymer Mixed Matrixes*, in *Department of Chemical Engineering*. 1998, University of Texas: Austin, TX.
16. O'Brien, K.C., et al., *A NEW TECHNIQUE FOR THE MEASUREMENT OF MULTICOMPONENT GAS-TRANSPORT THROUGH POLYMERIC FILMS*. *Journal of Membrane Science*, 1986. **29**(3): p. 229-238.
17. Pye, D.G., H.H. Hoehn, and M. Panar, *MEASUREMENT OF GAS PERMEABILITY OF POLYMERS .1. PERMEABILITIES IN CONSTANT VOLUME-VARIABLE PRESSURE APPARATUS*. *Journal of Applied Polymer Science*, 1976. **20**(7): p. 1921-1931.
18. Crank, J. and G.S. Park, eds. *Diffusion in Polymers*. 1968, Academic Press: London and New York. 452.
19. Brunauer, S., P.H. Emmett, and E. Teller, *Adsorption of gases in multimolecular layers*. *Journal of the American Chemical Society*, 1938. **60**: p. 309-319.

CHAPTER 4

CROSSLINKABLE MIXED MATRIX MEMBRANES FOR NATURAL GAS PURIFICATION

4.1 Introduction

In Chapter 1, the case was made for pursuing next-generation polymeric membranes—especially mixed matrix membranes—for natural gas purification. Chapters 2 and 3 followed up with background information related to membrane development and characterization, as well as common difficulties encountered during membrane development. In this chapter, the results of material characterization are presented and used to predict expected membrane transport properties. The analyses of crosslinkable mixed matrix membranes using as-received molecular sieves are compared to these predictions, and apparent defects are discussed. Finally, the possibility of crosslinking-induced defect formation is probed via analysis of an uncrosslinked mixed matrix membrane. The membranes investigated in this chapter will be used to establish a baseline against which the performance of membranes developed in subsequent chapters will be benchmarked.

4.2 Polymer and Molecular Sieve Transport Properties

4.2.1 PDMC Characterization

As discussed in Chapter 3, the crosslinkable polyimide used in this research—6FDA-DAM:DABA (3:2), propane diol esterified (PDMC)—was originally developed by Wallace et al. [1, 2] and Hillock et al. [3, 4] based on materials first investigated by

Staudt-Bickel and Koros [5] and Wind et al. [6, 7]. This material possesses attractive carbon dioxide/methane separation properties and exhibits impressive plasticization resistance—qualities that position PDMC as an ideal matrix material for hybrid gas separation membranes.

In order to characterize membrane performance, it is necessary to account for batch-to-batch variances in transport properties that can arise from molecular weight or polydispersity differences. During the course of this research, two separate batches of PDMC having similar molecular weights and polydispersity indices were used (MW: >100 kdaltons; PDI: ~3.0). Several neat PDMC dense film membranes were prepared and tested from each batch of polymer (for a total of 8 membranes) to give an average carbon dioxide permeability of 66.9 ± 4.1 barrer and a selectivity over methane of 36.4 ± 0.6 (at 35 °C and ~65 psia). The reported errors represent one standard deviation for the respective data sets, corresponding to 6% and 0.6% error in permeability and selectivity, respectively. These neat PDMC data will be used in the remainder of this dissertation to compare with mixed matrix results and for use in Maxwell model predictions.

The plasticization resistance of the crosslinked PDMC used in this work was also verified and compared to that of uncrosslinked polymer. As evidenced by the pure carbon dioxide permeation isotherms presented in Figure 4.1, crosslinked PDMC dense film membranes were stable to a carbon dioxide feed pressure of ~450 psia, whereas uncrosslinked PDMC membranes were plasticization resistant to only ~150 psia. These results are similar to those reported by Wallace [1] and Hillock [3], and suggest that crosslinked PDMC membranes would be stable in the field at feed pressures up to ~4500 psia (assuming 10% carbon dioxide).

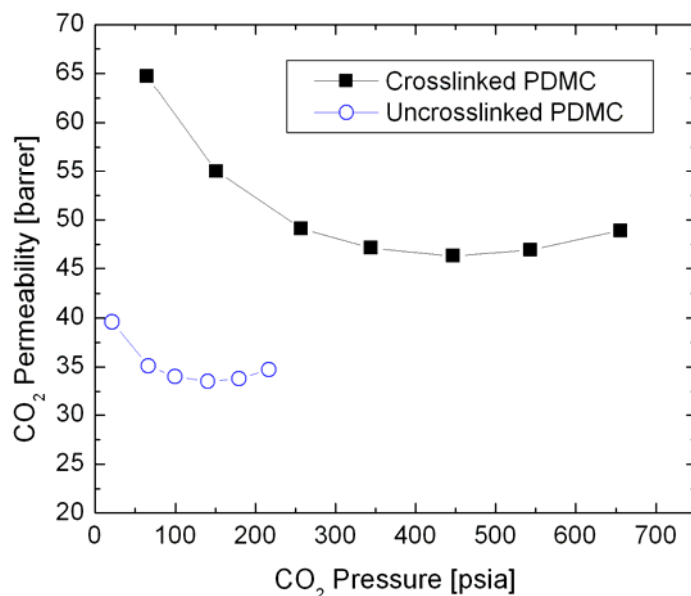


Figure 4.1: Comparison of pure carbon dioxide isotherms for uncrosslinked and crosslinked PDMC dense film membranes.

4.2.2 SSZ-13 Characterization

The measurement of polymer permeabilities is considerably easier than for molecular sieves. While some success has been had in forming and testing pure molecular sieve membranes, pure sieve membranes in general are difficult and expensive to produce [8]. It is possible in some instances to independently measure and combine the sorption and diffusion coefficients for molecular sieve particles in order to determine the permeability (see Equation 2.11). However, the diffusion of small molecules in microporous materials is quite rapid, and direct measurement of adsorption/desorption kinetics has typically only been measurable for particles having dimensions of several microns—orders of magnitude larger than the SSZ-13 available for this research. Further complicating these measurements are thermal effects arising from the intrinsic heats of

adsorption associated with sorbate/sorbent interactions [9]. The development of pulsed field gradient nuclear magnetic resonance (PFG-NMR) techniques to measure diffusivities in microporous materials under equilibrium conditions has allowed dynamic measurements to be made in the absence of such nonidealities. However, diffusivities measured using PFG-NMR are often an order of magnitude or more greater than those measured by other techniques [10].

The accepted SSZ-13 transport properties ($P_{\text{CO}_2} = 200$ barrer; $\alpha_{\text{CO}_2/\text{CH}_4} = 800$) were determined in earlier research by Medal, L.P (Newark, DE). In this work, the Maxwell model (see Section 2.3.2) was used to back-calculate SSZ-13 properties from measured permeabilities of mixed matrix membranes composed of a well-characterized polymer matrix—polyvinyl acetate (PVAc). These membranes showed ideal mixed matrix enhancement so the resulting back-calculated sieve properties are believed to be reasonably accurate [3, 11].

4.2.3 Maxwell Model Permeability Predictions

As discussed in Section 2.3.2, the Maxwell model is often used to predict mixed matrix membrane permeabilities using the individual pure polymer and sieve transport properties. The values estimated by this model are generally used as a baseline to which experimental values are compared, allowing for the characterization of a membrane as either successful or defective. In the case of defective membranes, the comparison of predicted to experimental transport properties can help determine the predominant type of defect affecting membrane performance. Using the above pure component properties, the Maxwell-predicted permeabilities for 15% and 25% (w/w) SSZ-13 in PDMC were calculated and are compared to neat PDMC values in Table 4.1. The side-by-side

comparison of the transport properties in the table illustrates the potential benefits of utilizing these materials for natural gas purification. These Maxwell-predicted estimates will be used in the remainder of this dissertation to gauge the success of membrane development.

Table 4.1: Comparison of neat PDMC and Maxwell-predicted pure gas carbon dioxide permeabilities and ideal carbon dioxide/methane selectivities. Numbers in parentheses are total membranes tested; errors represent one standard deviation.

	P_{CO2} [barrer]	$\alpha_{CO2/CH4}$
Neat PDMC (8)	66.9 ± 4.1	36.4 ± 0.6
15% SSZ-13/PDMC Maxwell Prediction	78.8	51.1
25% SSZ-13/PDMC Maxwell Prediction	87.8	64.7

4.2.4 Permeation Analysis

A number of 15% and 25% (w/w) as-received (AR) SSZ-13/PDMC membranes were prepared and tested according to the procedures detailed in Chapter 3. A total of 6 different membranes were tested at 15% loading and 2 at 25%. The averaged results of these analyses are compared with neat PDMC and Maxwell-predicted transport properties in Table 4.2. As before, the reported errors represent one standard deviation for the respective data sets.

The membranes were clearly defective as evidenced by the greater than Maxwell-predicted permeabilities and approximately neat-polymer selectivities reported in the table. Moreover, significant variance in measured carbon dioxide permeabilities (as high as 25%) were observed for mixed matrix membranes; neat PDMC permeabilities varied

only 6%. Membrane selectivities for carbon dioxide over methane generally varied 2% or less.

Table 4.2: Comparison of measured and Maxwell-predicted pure gas carbon dioxide permeabilities and ideal carbon dioxide/methane selectivities for 15% and 25% as-received SSZ-13/PDMC membranes. Numbers in parentheses are total membranes tested; errors represent one standard deviation. Tested at 35 °C and ~65 psia.

Membrane	P_{CO_2} [barrer]	α_{CO_2/CH_4}
Neat PDMC (8)	66.9 ± 4.1	36.4 ± 0.6
15% AR-SSZ-13/PDMC (6)	98.6 ± 25.0	36.3 ± 0.3
15% Maxwell Prediction	78.8	51.1
25% AR-SSZ-13/PDMC (2)	153 ± 33	34.7 ± 0.8
25% Maxwell Prediction	87.8	64.7

The variability in mixed matrix permeabilities may have been due to two factors: sieve agglomeration and varying degrees of defective interfaces. Submicron particles are notoriously difficult to disperse, even with high-intensity ultrasonication. Agglomerates of submicron particles can restrict polymer chain penetration, creating a non-selective, low-resistance pathway for gas transport. Since the primary batch of SSZ-13 used in this research had particle diameters ranging from <300-500 nm, some agglomeration may have been present, though the majority of the membranes tested contained no agglomerates that were immediately apparent. Another factor that likely contributed to inconsistent hybrid membrane permeabilities is variability in the polymer/sieve interfacial morphology, which will be discussed further in the following section.

4.3 Characterization of Apparent Mixed Matrix Membrane Defects

4.3.1 Sieve-in-a-Cage Defects

The high permeabilities and neat-polymer selectivities for SSZ-13/PDMC mixed matrix membranes reported in Table 4.2 are typical of sieve-in-a-cage defects (discussed in Section 2.3.3). This defect type is characterized by voids at the polymer/sieve interface which are believed to result from poor material interaction and/or membrane formation stresses. These voids are often visible in scanning electron microscopy (SEM) imaging, as illustrated by the sieve-in-a-cage example in Figure 2.3. However, SEM images of SSZ-13/PDMC mixed matrix membranes seem to suggest rather good adhesion. A representative SEM image of the AR-SSZ-13/PDMC hybrid membranes analyzed in this work is presented in Figure 4.2.

As evidenced by the figure, no interfacial voids are readily apparent. In fact, the polymer appears to be quite well adhered to the sieve, which contradicts the measured transport properties given in Table 4.2. To further investigate the nature of the membrane defects, the 3-phase Maxwell model (3MM) discussed in Section 2.3.2.1 was used to estimate the interfacial void size that would result in the observed transport properties. The results of the model are compared to observed values in Table 4.3.

Table 4.3: Comparison of measured and 3-phase Maxwell model-estimated pure gas transport properties for 15% and 25% AR-SSZ-13/PDMC hybrid membranes.

Membrane	P_{CO_2} [barrer]	α_{CO_2/CH_4}	Est. Void Size [nm]
15% AR-SSZ-13/PDMC	98.6	36.3	---
15% 3MM Estimate	98.6	35.4	~3
25% AR-SSZ-13/PDMC	153	34.7	---
25% 3MM Estimate	153	36.3	~15

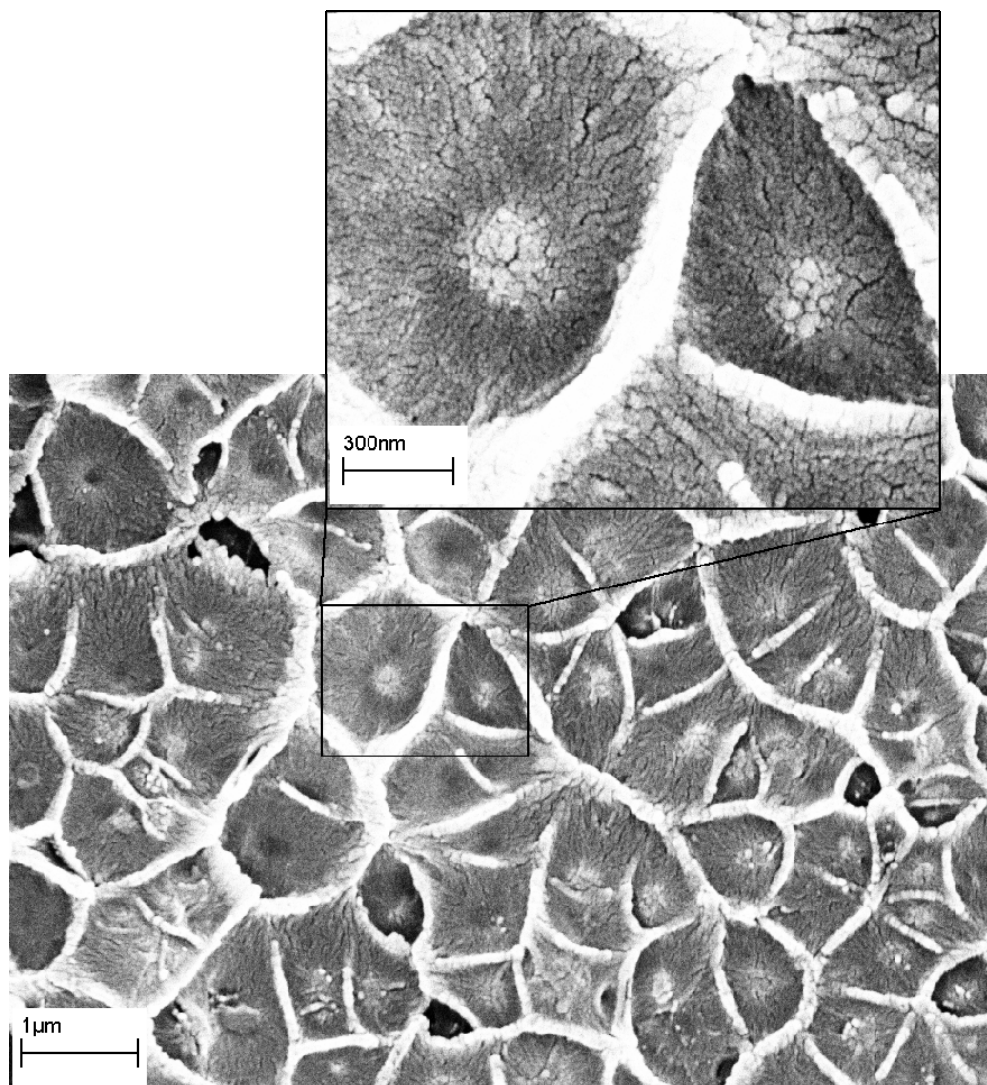


Figure 4.2: Representative SEM image of as-received SSZ-13/PDMC mixed matrix membranes.

The 3-phase Maxwell model predicts a ~ 3 nm interfacial void in 15% loaded membranes and a ~ 15 nm void in 25% loaded membranes. Voids of these dimensions would not typically be visible in SEM images since a layer of 10-20 nm gold particles is sputtered onto the samples to reduce charging during SEM imaging. The disagreement in predicted void sizes for 15% and 25% loadings likely stems from the variability in

observed membrane permeabilities discussed above. However, uncertainty in sieve transport properties could also contribute to inaccuracies in model predictions. This is addressed in the following section.

4.3.2 Leaky Interface Defects

The Maxwell model is a useful tool for analyzing gas transport in hybrid membranes, but it requires that the properties of the individual materials be well-characterized. As previously discussed, gas permeabilities for polymers are relatively easy to measure, but molecular sieve permeabilities have proven quite difficult to determine. While it is believed that the properties used for SSZ-13 are fairly representative, small errors in permeability or selectivity could result in substantial deviations in model predictions. It is, therefore, desirable to investigate the polymer/sieve interface in the absence of transport through the sieve. By utilizing a nonporous sieve—uncalcined SSZ-13 in this case—and the Maxwell model, the observed and predicted membrane transport properties can again be compared to diagnose non-idealities without inaccuracies in sieve properties affecting the analysis. Moreover, the use of uncalcined SSZ-13 would provide an interface essentially identical to that formed with calcined SSZ-13, which is more desirable than using a nonporous surrogate particle, such as pure silica. As such, a 25% (w/w) uncalcined (UNC) SSZ-13/PDMC mixed matrix membrane was prepared and tested as before. The results of permeation testing and Maxwell-model predictions are presented in Table 4.4.

The permeability of mixed matrix membranes is expected to decrease when a nonporous material is dispersed throughout the polymer matrix since the diffusive path of penetrant molecules is lengthened. However, this path length increases equally for all

penetrants, so the hybrid membrane is expected to maintain neat-polymer selectivity. Comparing the measured and Maxwell-predicted permeability and selectivity values in Table 4.4, it appears that SSZ-13/PDMC membrane defects fall under the category of leaky interfaces (discussed in Section 2.3.3) instead of the sieve-in-a-cage voids discussed above. These defect types differ only in the size of the interfacial voids that form. While sieve-in-a-cage defects are large enough to allow for bulk flow, leaky interface defects are sized such that Knudsen diffusion dominates gas transport through the voids. In the case of carbon dioxide/methane separation, Knudsen diffusivity results in reverse-selectivity, effectively lowering the selectivity of the overall membrane.

Table 4.4: Comparison of measured and 3-phase Maxwell model-predicted pure gas transport properties for 25% UNC-SSZ-13/PDMC hybrid membranes. Tested at 35 °C and ~65 psia.

Membrane	P_{CO_2} [barrer]	α_{CO_2/CH_4}	Est. Void Size [nm]
25% UNC-SSZ-13/PDMC	155	25.5	---
25% Maxwell Prediction	48.5	36.4	---
25% 3MM Estimate (P-Based)	155	36.4	~26
25% 3MM Estimate (α -Based)	49.3, 82.3	25.5	~0.3, ~1

Using the 3-phase Maxwell model, the interfacial void size in the 25% UNC-SSZ-13/PDMC membrane was estimated by requiring either the predicted permeability or the selectivity to converge to the observed values reported in Table 4.4. Permeability-based estimates suggest interfacial voids roughly 26 nm in size. However, selectivity-based estimates suggest voids either ~0.3 or ~1.0 nm in size. The two solutions are possible for the selectivity-based estimation because the 3MM-predicted selectivities experience a minimum as void size increases from 0 nm to ~0.5 nm; beyond this minimum, the

estimated selectivity increases towards neat-polymer selectivity. This behavior is illustrated in the 3MM predictions presented in Figure 4.3.

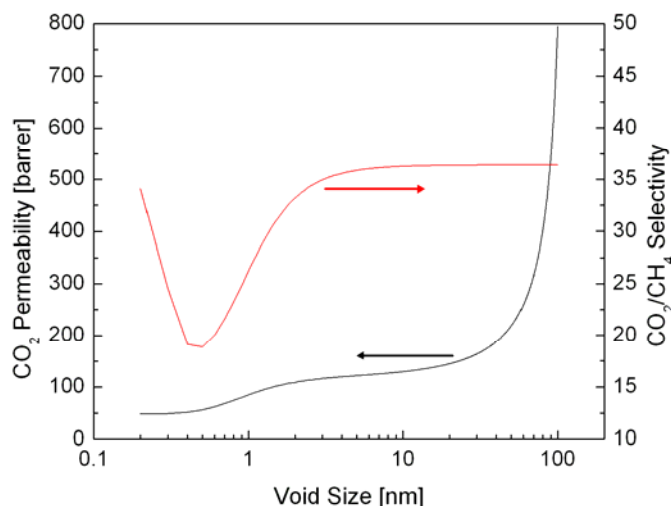


Figure 4.3: 3-Phase Maxwell model predictions of carbon dioxide permeability and carbon dioxide/methane selectivity for 25% uncalcined SSZ-13/PDMC membranes.

4.4 Investigation of Potential for Crosslinking-Induced Void Formation

It has been noted that stresses arising during crosslinking may lead to the apparent interfacial defects in SSZ-13/PDMC membranes. Hillock used transmission electron microscopy (TEM) imaging to support this hypothesis, noting that apparent voids were visible at polymer/sieve interfaces in crosslinked membranes. However, it was also noted that uncrosslinked membranes similarly appeared to be at least partially defective in some samples [3]. While the direct observation of these voids may hint at crosslinking as the culprit, the possibility exists that defects may result from microtoming during TEM sample preparation.

In order to rule out the creation of defects during sample preparation, another 25% (w/w) UNC-SSZ-13/PDMC membrane was prepared and tested as before, though this membrane was not crosslinked. The results of permeation testing and Maxwell-model predictions are compared with neat uncrosslinked PDMC transport properties in Table 4.5.

Table 4.5: Comparison of measured uncrosslinked neat PDMC and 25% uncalcined (UNC) SSZ-13/PDMC pure gas transport properties to Maxwell model-predicted values. Numbers in parentheses are total membranes tested; errors represent one standard deviation. Tested at 35 °C and ~65 psia.

Membrane	P_{CO2} [barrer]	$\alpha_{CO2/CH4}$	Est. Void Size [nm]
Neat PDMC – Uncrosslinked (3)	32.4 ± 2.8	31.3 ± 1.1	---
25% UNC-SSZ-13/PDMC – Uncrosslinked	58.4	26.8	---
25% Maxwell Prediction	22.6	31.3	---
25% 3MM Estimate (P-Based)	58.4	29.6	~2
25% 3MM Estimate (α -Based)	22.6, 52.4	26.8	~0.2, ~1.2

The higher than Maxwell-predicted permeability and lower selectivity observed for the uncrosslinked 25% UNC-SSZ-13/PDMC membrane suggests leaky interface defects similar to those found in the preceding analysis. However, in this investigation the good agreement between the 3-phase Maxwell model applied to both permeability and selectivity suggests that interfacial voids between 1-2 nm can be assumed to exist with reasonable certainty.

Preexisting voids in uncrosslinked membranes may be exacerbated during crosslinking due to matrix densification and stress accumulation at defective interfaces. These phenomena may account for the inconsistencies observed in the crosslinked UNC-

SSZ-13/PDMC membrane analysis. Considering the foregoing observations, it may be concluded that as-received SSZ-13 and PDMC do not sufficiently interact for successful mixed matrix membrane formation. Modification of the external sieve surface, however, may be a viable solution for obtaining improved polymer/sieve adhesion. The modification of sieves for this purpose will be explored in Chapter 5.

4.5 Summary and Conclusions

Inconsistencies in the analyses of calcined and uncalcined SSZ-13/PDMC membranes and the respective comparisons to Maxwell model predictions point to the complex and difficult-to-study nature of the particle/sieve interface in mixed matrix membranes. From the work presented in this chapter, it appears that interfacial voids plague SSZ-13/PDMC mixed matrix membranes. While such voids do enhance membrane productivity by substantially increasing gas permeabilities, the objective of this research is to enhance both permeability *and* selectivity. Work reported in Chapter 5 will detail efforts to eliminate the nanoscale voids suggested by the above analyses and will culminate in the description of a novel, non-ideal transport mechanism for mixed matrix membranes.

4.6 References

1. Wallace, D., *Crosslinked Hollow Fiber Membranes for Natural Gas Purification and Their Manufacture from Novel Polymers*, in *School of Chemical Engineering*. 2004, University of Texas at Austin: Austin, TX.
2. Wallace, D.W., et al., *Characterization of crosslinked hollow fiber membranes*. *Polymer*, 2006. **47**(4): p. 1207-1216.

3. Hillock, A.M.W., *Crosslinkable Polyimide Mixed Matrix Membranes for Natural Gas Purification*, in *School of Chemical & Biomolecular Engineering*. 2005, Georgia Institute of Technology: Atlanta, GA. p. 197.
4. Hillock, A.M.W. and W.J. Koros, *Cross-linkable polyimide membrane for natural gas purification and carbon dioxide plasticization reduction*. *Macromolecules*, 2007. **40**(3): p. 583-587.
5. Staudt-Bickel, C. and W.J. Koros, *Improvement of CO₂/CH₄ separation characteristics of polyimides by chemical crosslinking*. *Journal of Membrane Science*, 1999. **155**(1): p. 145-154.
6. Wind, J.D., et al., *The effects of crosslinking chemistry on CO₂ plasticization of polyimide gas separation membranes*. *Industrial & Engineering Chemistry Research*, 2002. **41**(24): p. 6139-6148.
7. Wind, J.D., et al., *Solid-state covalent cross-linking of polyimide membranes for carbon dioxide plasticization reduction*. *Macromolecules*, 2003. **36**(6): p. 1882-1888.
8. McLeary, E.E., J.C. Jansen, and F. Kapteijn, *Zeolite based films, membranes and membrane reactors: Progress and prospects*. *Microporous and Mesoporous Materials*, 2006. **90**(1-3): p. 198-220.
9. Lee, L.K. and D.M. Ruthven, *ANALYSIS OF THERMAL EFFECTS IN ADSORPTION RATE MEASUREMENTS*. *Journal of the Chemical Society-Faraday Transactions I*, 1979. **75**: p. 2406-2422.
10. Ruthven, D.M., *Past progress and future challenges in adsorption research*. *Industrial & Engineering Chemistry Research*, 2000. **39**(7): p. 2127-2131.
11. Moore, T.T., *Effects of Materials, Processing, and Operating Conditions on the Morphology as Gas Transport Properties of Mixed Matrix Membranes*, in *Department of Chemical Engineering*. 2004, University of Texas: Austin, TX.

CHAPTER 5

CROSSLINKABLE MIXED MATRIX MEMBRANES WITH MODIFIED MOLECULAR SIEVES

5.1 Introduction

In Chapter 4, crosslinkable mixed matrix membranes composed of as-received SSZ-13 and PDMC were found to suffer from apparent sieve-in-a-cage and leaky interface defects based on comparisons to neat polymer and Maxwell model-predicted transport properties. Such defects preclude the separation performance enhancement sought in developing these hybrid membranes. In order to improve polymer/sieve adhesion, SSZ-13 was modified using a procedure developed by Shu and Husain that reportedly led to improved membrane performance [1-3]. It was found in the present case, however, that this treatment actually resulted in poorer membrane performance as the result of a previously unreported transport mechanism. Modified sieves were treated with a second procedure developed in this work aimed at preventing hypothesized non-selective bypass. Membranes containing these twice-treated sieves showed substantial enhancement in both carbon dioxide permeability and selectivity over methane. However, it was found that PDMC membranes containing SSZ-13 modified using *only* the newly developed procedure also showed similar separation improvement. The characterization of these membranes and the analysis of a complex transport mechanism in mixed matrix membranes are discussed in the remainder of this chapter.

5.2 Grignard-Treated SSZ-13/PDMC Mixed Matrix Membranes

5.2.1 Characterization of Grignard-Treated SSZ-13

The Grignard procedure (see Section 3.3.1) pioneered by Shu and Hussain [2, 3] was used to modify the external surface of SSZ-13 in an attempt to improve polymer adhesion. This treatment results in the deposition of magnesium hydroxide nanostructures on the sieve surface and has been hypothesized to enhance polymer adhesion via both enthalpic and entropic effects [2, 4]. The amount of material deposited onto the sieve should be considered when preparing membranes and predicting transport properties due to the increase in particle density caused by the magnesium hydroxide deposits ($\rho_{\text{SSZ-13}} = 1.51 \text{ g cm}^{-3}$; $\rho_{\text{Mg(OH)}_2} = 2.34 \text{ g cm}^{-3}$). Since magnesium hydroxide dehydrates at $\sim 330 \text{ }^\circ\text{C}$, thermogravimetric analysis (TGA) can be used to determine the amount deposited in a given batch of Grignard-treated SSZ-13 (GT-SSZ-13). A typical TGA analysis for GT-SSZ-13 is presented in Figure 5.1.

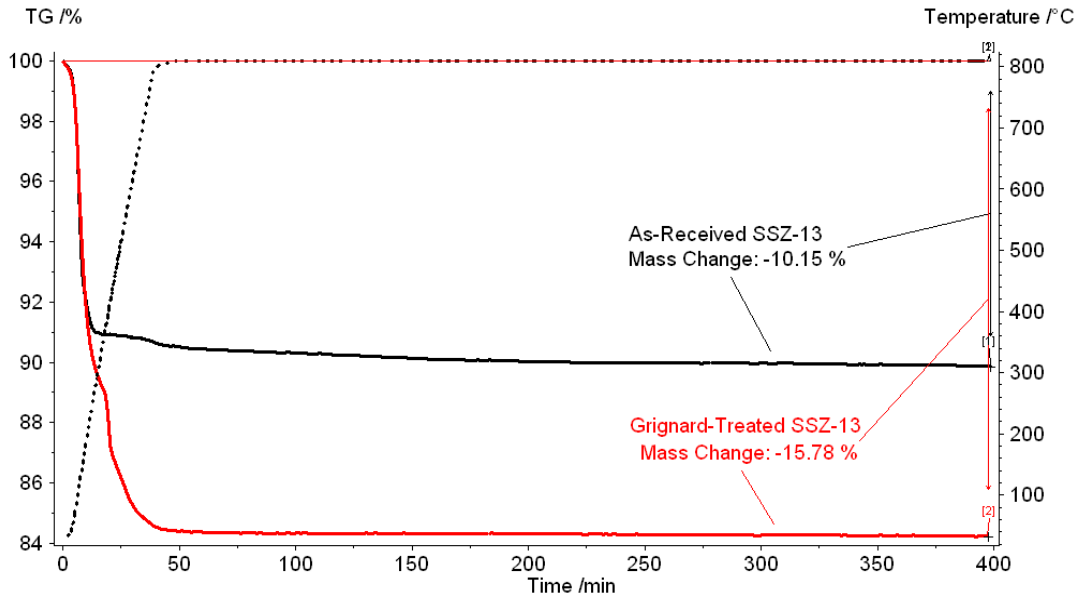
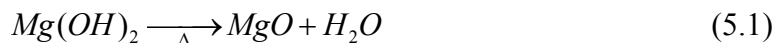


Figure 5.1: Typical TGA analyses of as-received (AR) and Grignard-treated (GT) SSZ-13.

In the above TGA analyses, the mass lost from the as-received sieve can be attributed to physisorbed water, and the additional mass lost from the treated sieve can be attributed to the dehydration of magnesium hydroxide. According to the dehydration reaction of magnesium hydroxide, 1 mol of water is lost per mole of magnesium hydroxide, viz.,



The mass of TGA-analyzed sieve, along with the mass of water lost due to dehydration, can be used to ultimately determine the mass of magnesium hydroxide deposited on the sieve. Using this technique, it was found that the batches of GT-SSZ-13 treated in this research typically contained ~8-12% (w/w) magnesium hydroxide. This information was used to adjust the apparent density of each treated batch of SSZ-13 when preparing membranes or using the Maxwell model to predict transport properties.

Cryogenic nitrogen physisorption (BET) was also used to characterize surface area and pore volume in pre- and post-treated SSZ-13 to ensure that micropores were not significantly blocked during the Grignard treatment. Such blockage is clearly undesirable since transport through the sieve would be compromised and possibly not well matched with the polymer permeability for the desired separation. In a worst-case scenario, the sieve may even become completely impermeable. Typical as-received and Grignard-treated SSZ-13 BET surface areas and pore volumes are presented in Table 5.1.

The BET surface area and pore volume data reported in Table 5.1 suggest that the modified SSZ-13 microporosity remains essentially unchanged as compared to the as-received sieve. These results are comparable to those previously observed for similarly modified SSZ-13 [4].

Table 5.1: Typical nitrogen physisorption results for as-received (AR) and Grignard-treated (GT) SSZ-13. Pore volume determined using the Horvath-Kawazoe method (cylindrical pores).

Sample	BET Surface Area [m² g⁻¹]	Pore Volume [cm³ g⁻¹]
AR-SSZ-13	686 ± 19	0.310 ± 0.040
GT-SSZ-13	687 ± 19	0.299 ± 0.039

5.2.2 Mixed Matrix Membranes with Grignard-Treated Sieves

A number of 15% and 25% (w/w) Grignard-treated SSZ-13/PDMC mixed matrix membranes were prepared and tested: 4 at 15% loading and 3 at 25% loading. The averaged results of the permeation analyses are compared with neat PDMC and Maxwell-predicted transport properties in Table 5.2.

Table 5.2: Measured and Maxwell-predicted pure gas carbon dioxide permeabilities and ideal carbon dioxide/methane selectivities for 15% and 25% Grignard-treated (GT) SSZ-13/PDMC membranes. Numbers in parentheses are total membranes tested; errors represent one standard deviation. All membranes tested at 35 °C and ~65 psia.

Membrane	P_{CO2} [barrer]	α_{CO2/CH4}
Neat PDMC (8)	66.9 ± 4.1	36.4 ± 0.6
15% GT-SSZ-13/PDMC (4)	136 ± 28	32.5 ± 2.1
15% Maxwell Prediction	78.8	51.1
25% GT-SSZ-13/PDMC (3)	146 ± 31	33.8 ± 1.7
25% Maxwell Prediction	87.8	64.7

Inspecting the above data, carbon dioxide permeability was enhanced in GT-SSZ-13/PDMC hybrid membranes by 103% and 118% for 15% and 25% loadings, respectively. The Maxwell model predicts enhancements of only 18% and 31% for these membranes. Considering only permeabilities, these results suggest that the membranes

containing modified and as-received SSZ-13 were similarly defective. The membranes with untreated SSZ-13 (see Section 4.2.4), however, appear to have maintained selectivities closer to that of neat PDMC than the membranes examined here. As discussed, a reduction in membrane selectivity—such as observed in Table 5.2—is indicative of Knudsen diffusivity through molecular-scale voids. Whereas the analysis in Chapter 4 suggested that voids having the dimensions necessary for Knudsen diffusivity may exist at the polymer/sieve interface, such voids are not expected to remain in membranes composed of Grignard-treated sieves [2]. Unfortunately, due to the resolution limits for SEM imaging of these materials, and due to the potential for defect formation during TEM sample preparation, direct imaging of these apparent interfacial voids does not appear feasible. As such, probing the interface with gas molecules (e.g., permeation analysis) seems to be the most viable and high-resolution characterization method available.

Further analysis of the Grignard-treated SSZ-13 suggests an alternative mechanism that could result in the observed transport properties reported in Table 5.2. In the pore size distributions presented in Figure 5.2, meso- and macropores between ~10-100 nm are apparent in Grignard-treated SSZ-13. Shu and Husain showed that the thionyl chloride step of the Grignard procedure can lead to dealumination and loss of crystallinity in treated sieves, which could result in such defects [5]. However, considering the relatively low aluminum content of the present sieve (Si:Al > 25 in SSZ-13 versus ~1 in 4A), and the consistent pre- and post-treatment BET data given in Table 5.1, formation of such defects within the sieve itself is unlikely.

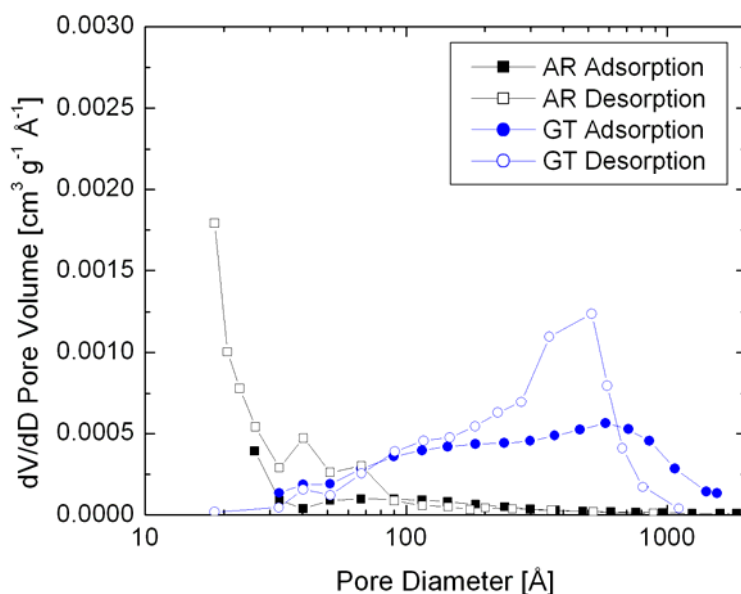


Figure 5.2: Pore size distributions (BJH model applied to both adsorption and desorption isotherm branches) for as-received (AR) and Grignard-treated (GT) SSZ-13.

More likely is the creation of voids within the surface-deposited magnesium hydroxide formations that result from the Grignard procedure. Whereas whisker-like crystalline growths were observed in Grignard-treated zeolite 4A samples [3], only amorphous, non-whiskered deposits were possible after numerous attempts to reproduce the whiskered morphology in SSZ-13 samples. The comparison of pre- and post-treated SSZ-13 samples in Figure 5.3 illustrates the structure of the magnesium hydroxide that is deposited during the procedure.

It is hypothesized that interconnected voids may form within these surface deposits, into which PDMC—having a high molecular weight, rigid backbone—cannot easily percolate. These voids could have dimensions that allow gas transport via Knudsen diffusivity, creating a low resistance pathway through which gases would

bypass the sieve. Moreover, Knudsen diffusion in these voids could result in the reduced membrane selectivity noted in Table 5.2. Such a situation is illustrated in Figure 5.4.

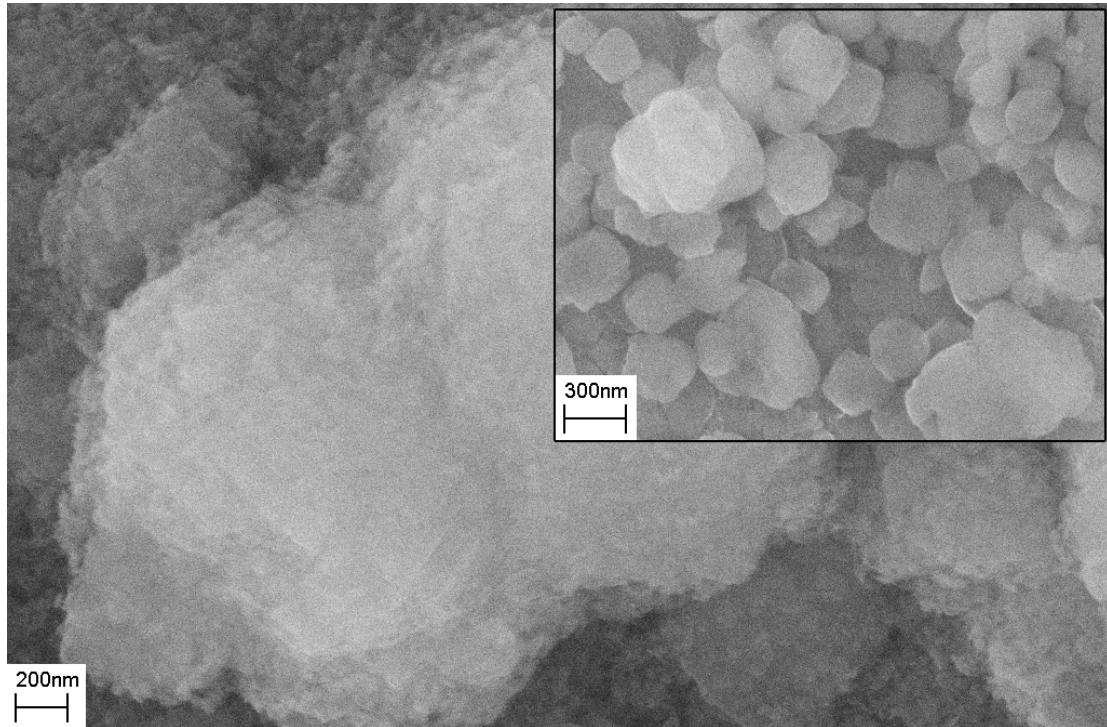


Figure 5.3: Representative SEM image of Grignard-treated and as-received SSZ-13 (inset).

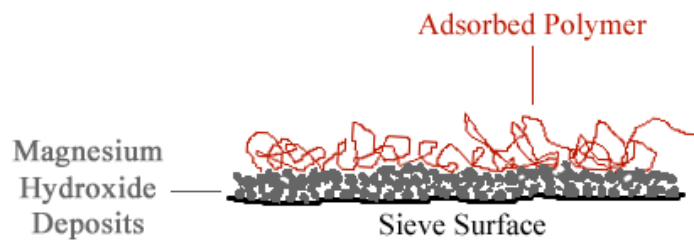


Figure 5.4: Hypothesized structure of interconnected voids within the Grignard-deposited magnesium hydroxide surface layer on modified sieves.

To further support this hypothesis, consider the radius of gyration (R_g) of a solvated polymer chain. While the R_g of PDMC has not been explicitly determined, Kwan et al. have reported the results of a light scattering study involving a similarly structured fluorinated polyimide: 6FDA-PFMB (where PFMB is 2,2'-(trifluoromethyl)-4,4'-biphenyldiamine). They reported the R_g of several fractions of 6FDA-PFMB dissolved in THF, noting that a molecular weight (M_w) of $\sim 134,000 \text{ g mol}^{-1}$ corresponded to an R_g of 32.4 nm, while a M_w of $\sim 203,000 \text{ g mol}^{-1}$ corresponded to an R_g of 41.9 nm. Based solely on their structures, PDMC and 6FDA-PFMB are expected to have similar backbone stiffness due to steric hindrance. Moreover, THF is a good solvent for both polymers and was used for casting membranes throughout this work. It is anticipated, therefore, that PDMC and 6FDA-PFMB have similar enough solvated chain dimensions to support the current hypothesis.

Considering the preceding data, it is reasonable to assume that the PDMC used in this research ($M_w \sim 148,000 \text{ g mol}^{-1}$) had an R_g on the order of $\sim 30 \text{ nm}$. Again referring to the pore size distributions in Figure 5.2, it is clear that a substantial fraction of the voids present in Grignard-treated SSZ-13 have pore diameters $< 30 \text{ nm}$. This suggests that solvated PDMC chains may indeed be too large to access some of the intra-surface layer voids hypothesized to exist in modified sieves. Even if PDMC could freely percolate into all pores large enough to contain solvated chains, the smaller pores might remain unfilled, maintaining a low resistance pathway for gas molecules to bypass the sieve. These voids must be eliminated in order to obtain better performing membranes. The results of developing a technique to fill—or *caulk*—these voids will be detailed in the following section.

5.3 Reactive-Sized, Grignard-Treated SSZ-13/PDMC Mixed Matrix Membranes

As discussed in the previous section, non-selective voids are apparently formed within the magnesium hydroxide surface deposits that result from the Grignard procedure. As mentioned, these voids must be caulked in order to minimize sieve bypass and improve membrane performance. It was most desirable to caulk these voids with a PDMC-philic material in order to avoid any interfacial adhesion issues due to possible material immiscibility. As such, a caulking—or *reactive-sizing*—technique was developed to essentially perform an in-situ PDMC synthesis. Contrary to bulk PDMC synthesis, little care was taken to ensure high molecular weight material since low molecular weight oligomers are ideal for diffusing into and caulking the voids. The details of this technique can be found in Section 3.3.2.

A total of two membranes were prepared from reactive-sized, Grignard-treated (RS-GT) SSZ-13 in PDMC: one with 15% and the other 25% loading (w/w). The results of permeation analysis are presented and compared with neat PDMC and Maxwell-predicted transport properties in Table 5.3.

Table 5.3: Measured and Maxwell-predicted pure gas carbon dioxide permeabilities and ideal carbon dioxide/methane selectivities for 15% and 25% reactive-sized, Grignard-treated (RS-GT) SSZ-13/PDMC membranes. Numbers in parentheses are total membranes tested; errors represent one standard deviation. All membranes tested at 35 °C and ~65 psia.

Membrane	P_{CO2} [barrer]	$\alpha_{\text{CO}_2/\text{CH}_4}$
Neat PDMC (8)	66.9 ± 4.1	36.4 ± 0.6
15% RS-GT-SSZ-13/PDMC (1)	83.9	39.1
15% Maxwell Prediction	78.8	51.1
25% RS-GT-SSZ-13/PDMC (1)	104	38.6
25% Maxwell Prediction	87.8	64.7

As evidenced by the data in Table 5.3, transport in membranes containing reactive-sized, Grignard-treated sieves is improved compared to both neat PDMC and Grignard-treated only SSZ-13/PDMC membranes. While the improvement in selectivities is small, a definite enhancement over previously tested membranes was observed. Moreover, the permeability enhancement in these membranes is much closer to predicted values than previously observed. These data suggest that the reactive-sizing technique is able to at least partially caulk the non-selective voids in Grignard-treated sieves, allowing the sieve to contribute to gas transport. This conclusion is further supported by the comparisons of Grignard-treated (GT) and reactive-sized, Grignard-treated (RS-GT) SSZ-13 pore size distributions and surface area data presented in Figure 5.5 and Table 5.4, respectively.

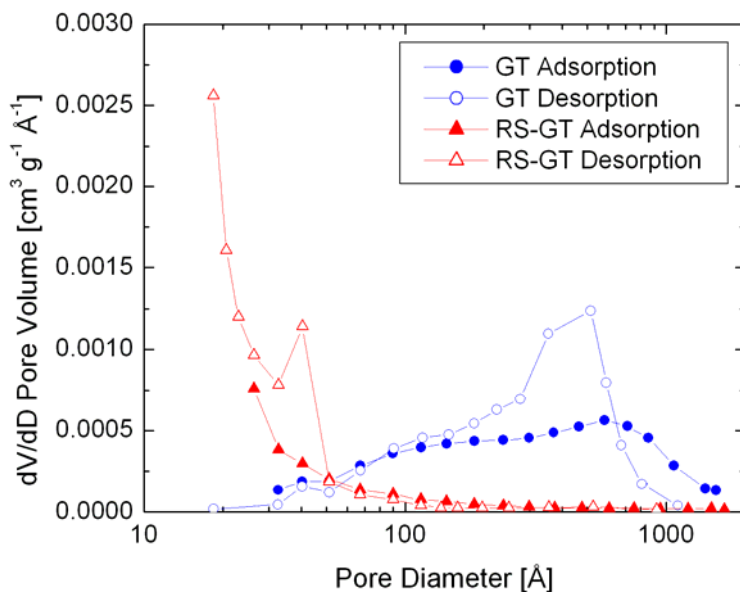


Figure 5.5: Pore size distributions (BJH model applied to both adsorption and desorption isotherm branches) for Grignard-treated (GT) and reactive-sized, Grignard-treated (RS-GT) SSZ-13.

Table 5.4: Nitrogen physisorption data for as-received (AR), Grignard-treated (GT), and reactive-sized, Grignard-treated (RS-GT) SSZ-13. Pore volume determined using the Horvath-Kawazoe method (cylindrical pores).

Sample	BET Surface Area [m² g⁻¹]	Pore Volume [cm³ g⁻¹]
AR-SSZ-13	686 ± 19	0.310 ± 0.040
GT-SSZ-13	687 ± 19	0.299 ± 0.039
RS-GT-SSZ-13	386 ± 11	0.174 ± 0.023

The mesopore volume reduction for reactive-sized GT-SSZ-13—evident in the pore size distributions presented in Figure 5.5—clearly suggests that the voids have been largely caulked. This is also reflected in the reduction in BET surface area and pore volume reported in Table 5.4. Since micropores contribute the bulk of the surface area and pore volume, the area and volume reductions can be primarily attributed to the additional mass resulting from the sizing.

To ensure that the enhancement in ideal selectivity reported in Table 5.3 was not an artifact of pure gas permeation testing, membranes were also tested with a gas mixture (10 mol% carbon dioxide/90 mol% methane). Mixed gas carbon dioxide permeabilities for neat PDMC, 25% Grignard-treated (GT) SSZ-13/PDMC, and 25% reactive-sized, Grignard-treated (RS-GT) SSZ-13/PDMC membranes are compared in Figure 5.6. Carbon dioxide/methane selectivities for these membranes are compared in Figure 5.7. The membranes were tested at 35 °C.

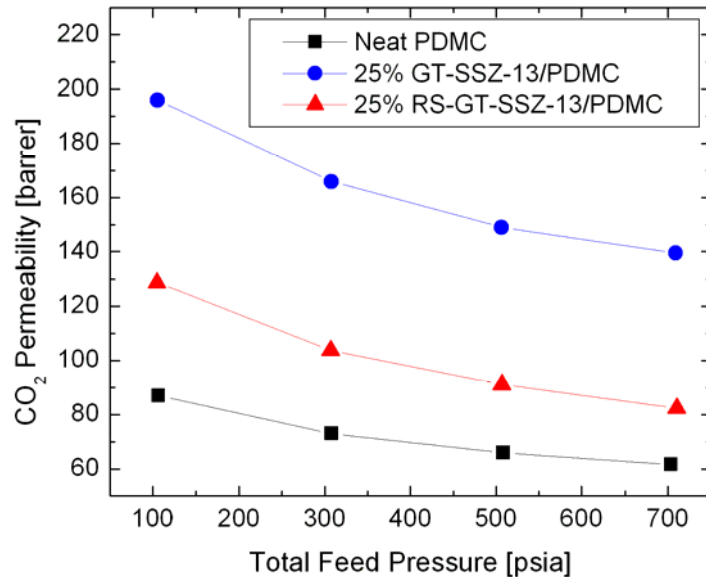


Figure 5.6: Mixed gas carbon dioxide permeabilities for 25% Grignard-treated (GT) and 25% reactive-sized, Grignard-treated (RS-GT) SSZ-13/PDMC membranes.

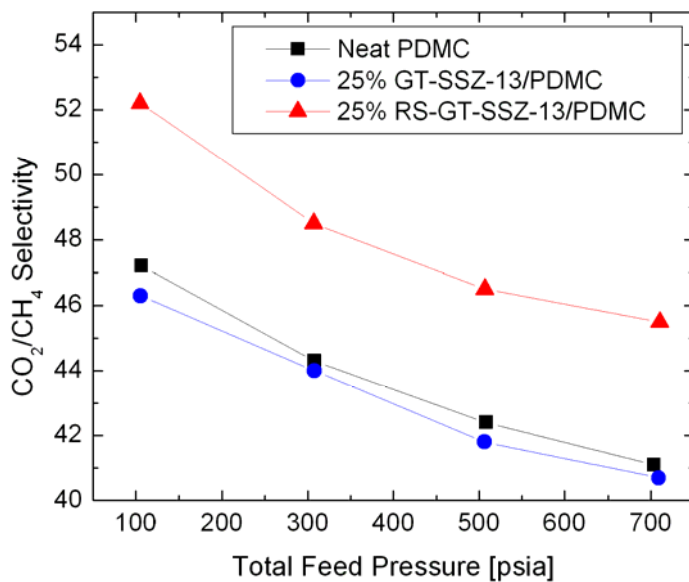


Figure 5.7: Mixed gas carbon dioxide/methane selectivities for 25% Grignard-treated (GT) and 25% reactive-sized, Grignard-treated (RS-GT) SSZ-13/PDMC membranes.

The downward trends in permeability and selectivity in the above figures result from well-known dual-mode sorption phenomena (see Section 2.1.2). Increasing feed pressure results in increasing Langmuir saturation, reducing the sorption coefficient and, consequently, lowering the permeability. Langmuir saturation also reduces the ability of carbon dioxide to out-compete methane for sorption, leading to a reduction in selectivity with increasing pressure. The ability of carbon dioxide to out-compete methane for sorption also results in a higher neat polymer mixed gas selectivity than pure gas (at comparative carbon dioxide partial pressures). This is evidenced by the ~12% increase in selectivity for neat PDMC when comparing mixed gas selectivity (at 700 psia total pressure, 70 psia carbon dioxide partial pressure) to pure gas selectivity (65 psia carbon dioxide pressure).

Comparing the carbon dioxide permeabilities in Figure 5.6, the trends previously observed with pure gas testing are maintained: the GT-SSZ-13 membrane exhibited a considerably higher permeability than the RS-GT-SSZ-13 membrane, and both hybrid membranes exhibited higher permeabilities than the neat PDMC membrane. The previously observed trends in selectivity are also maintained: the GT-SSZ-13 membrane exhibited slightly reduced selectivity versus neat PDMC, and the RS-GT-SSZ-13 membrane exhibited enhanced selectivity. Interestingly, while the RS-GT-SSZ-13 membrane selectivity was enhanced by ~6% in pure gas testing, an enhancement of ~11% was observed with mixed gas testing.

Dual-mode sorption effects may also explain the additional gains in selectivity under mixed gas conditions. The reactive sizing procedure allows the sieve to contribute more to overall membrane transport. Since the sieve has a higher sorption capacity than

the polymer, it can enhance overall permeability by increasing the effective sorption coefficient of the membrane (it may also change the diffusion coefficient). Methane is not completely excluded from SSZ-13, so methane sorption is enhanced during pure gas permeation (though not as much as for carbon dioxide, hence the ~6% selectivity enhancement over neat PDMC with pure gas testing). During mixed gas permeation, carbon dioxide can out-compete methane for sorption in both the polymer and the sieve. Due to the greater overall sorption capacity of the mixed matrix membrane, sorption competition further favors carbon dioxide, increasing selectivity ~11% over neat PDMC under mixed gas conditions.

5.4 Reactive-Sized, As-Received SSZ-13/PDMC Mixed Matrix Membranes

The enhancements in transport properties obtained with mixed matrix membranes containing reactive-sized, Grignard-treated SSZ-13 mark a significant step forward in developing these materials for commercial natural gas purification. However, comparing the measured properties to Maxwell-predicted values, it appears that considerable room for selectivity improvement remains. A number of explanations exist that can explain the discrepancy between measured and predicted properties: partially defective interfaces; partial sieve blockage due to modification (Grignard and/or sizing); or using incorrect pure sieve properties in the Maxwell model. Since both interfacial defects and sieve properties have been addressed, the possibility of sieve blockage by modification procedures is considered further. Nitrogen physisorption (see Table 5.1) suggested that the sieve remained microporous after Grignard treatment, and the impact of the treatment on membrane transport was investigated (see Table 5.2). This leaves only the impact of reactive sizing on membrane transport to be probed.

Several small batches of as-received SSZ-13 were treated with the reactive sizing procedure previously discussed. A total of three 25% (w/w) mixed matrix membranes were prepared using these treated sieves. The results of pure gas permeation analyses are compared with previous results in Table 5.5.

Table 5.5: Measured and Maxwell-predicted pure gas carbon dioxide permeabilities and ideal carbon dioxide/methane selectivities for 25% reactive-sized, Grignard-treated (RS-GT) and 25% reactive-sized, as-received (RS-AR) SSZ-13/PDMC membranes. Numbers in parentheses are total membranes tested; errors represent one standard deviation. All membranes tested at 35 °C and ~65 psia.

Membrane	P_{CO2} [barrer]	$\alpha_{CO2/CH4}$
Neat PDMC (8)	66.9 ± 4.1	36.4 ± 0.6
25% RS-AR-SSZ-13/PDMC (3)	148 ± 17	38.9 ± 2.0
25% RS-GT-SSZ-13/PDMC (1)	104	38.6
25% Maxwell Prediction	87.8	64.7

As evidenced by the similar transport property enhancements in membranes containing both RS-AR- and RS-GT-SSZ-13, the reactive sizing procedure apparently leads to improved compatibility between the SSZ-13 surface and PDMC. Considering that the reactive sizing procedure is essentially a modified PDMC synthesis, and recalling that the analyses presented in Chapter 4 concluded that SSZ-13 and PDMC are not inherently compatible, the compatibility improvement proposed here is, at first, counterintuitive.

To elucidate the impact of the sizing procedure on the sieve surface, treated sieve samples were analyzed with TGA and X-ray photoelectron spectroscopy (XPS). The TGA analysis presented in Figure 5.8 suggests that even after 10 washes in THF, considerable material remains adhered to the sieve surface (each wash cycle consisted of

adding sufficient THF to sieves to yield a ~1% (w/v) suspension, followed by dispersion in an ultrasonication bath for 10-15 min; particles were then collected via centrifugation).

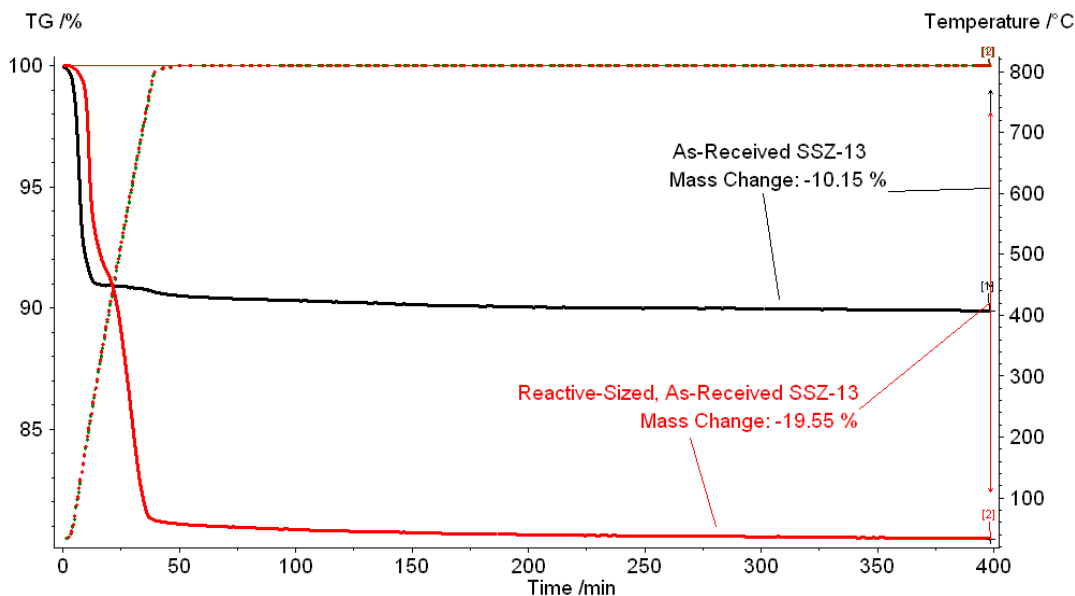


Figure 5.8: TGA analyses for as-received (AR) and reactive-sized, as-received (RS-AR) SSZ-13.

The surface elemental compositions obtained from XPS analyses of pre- and post-sized SSZ-13 are presented in Table 5.6. The carbon, nitrogen, and fluorine content on the RS-AR-SSZ-13 surface suggest that PDMC-like material is deposited on the sieves during sizing. As mentioned, this finding contradicts the conclusion made in Chapter 4 that PDMC and SSZ-13 are inherently incompatible. However, while the presumption of material incompatibility may hold somewhat true for fully synthesized PDMC, it is entirely feasible that both the dianhydride and the diamine monomers used to synthesize PDMC can interact strongly with silanol groups on the surface of SSZ-13. Moreover, it is expected that the polyamic acid precursor to the polyimide would have greater

interaction with the sieve surface than would the imidized polymer. Hypothesized mechanisms for material attachment during the reactive sizing procedure are discussed further in Appendix A.

Table 5.6: Surface elemental atomic percentages for as-received (AR) and reactive-sized, as-received (RS-AR) SSZ-13.

Sample	Atomic %						Total
	Si	Al	O	C	N	F	
AR-SSZ-13	27.6	2.3	68.5	1.6	-	-	100
RS-AR-SSZ-13	23.7	1.3	48.2	22.5	1.2	3.0	99.9

The pure gas permeation data in Table 5.5 suggests that membranes containing reactive-sized, as-received SSZ-13 may perform similarly to those containing reactive-sized, Grignard-treated sieve. To further investigate this possibility, two different 25% RS-AR-SSZ-13/PDMC membranes were prepared and analyzed via mixed gas permeation testing. Figure 5.9 presents the averaged carbon dioxide permeabilities of these membranes along with those of neat PDMC and the 25% RS-GT-SSZ-13/PDMC membrane discussed in the previous section. The carbon dioxide/methane selectivities for these membranes are presented in Figure 5.10. The error bars in these figures represent one standard deviation. The membranes were tested at 35 °C.

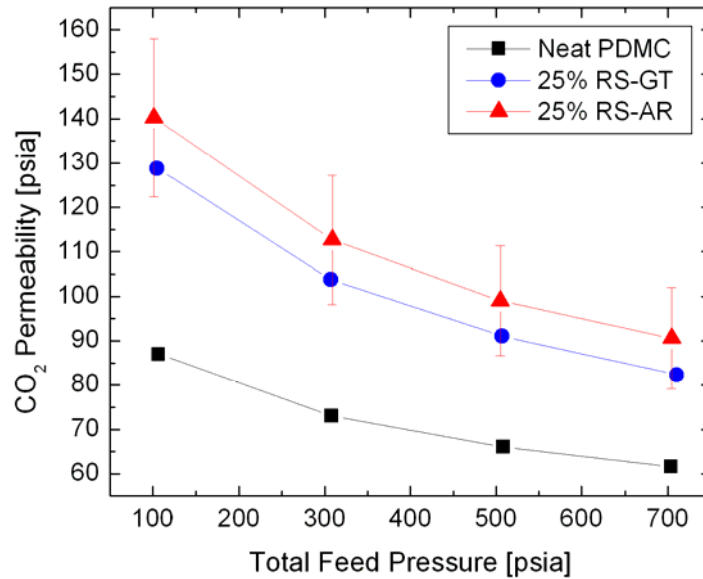


Figure 5.9: Mixed gas carbon dioxide permeabilities for 25% reactive-sized, Grignard-treated (RS-GT) and 25% reactive-sized, as-received (RS-AR) SSZ-13/PDMC membranes.

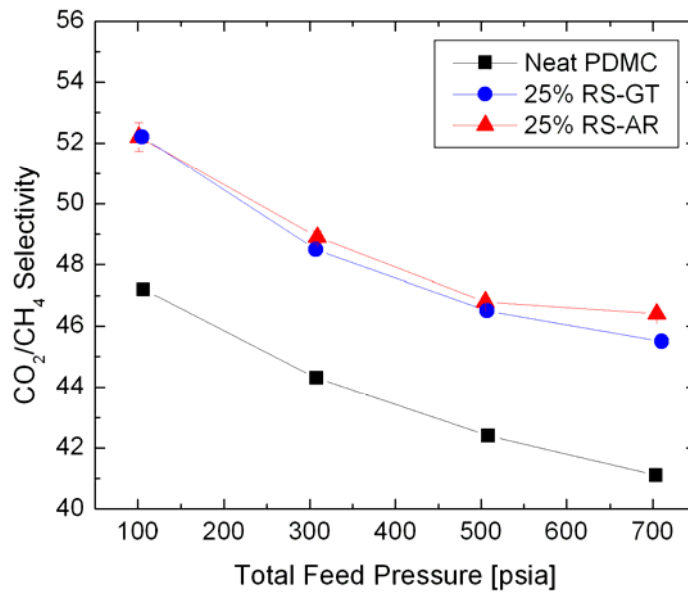


Figure 5.10: Mixed gas carbon dioxide/methane selectivities for 25% reactive-sized, Grignard-treated (RS-GT) and 25% reactive-sized, as-received (RS-AR) SSZ-13/PDMC membranes.

Interestingly, the membranes containing RS-GT- and RS-AR-SSZ-13 appear to have quite similar mixed gas permeabilities (within error). Since the error bars for selectivity data are so small, membranes containing RS-AR-SSZ-13 appear to have slightly higher selectivity than membranes with RS-GT-SSZ-13, especially at higher feed pressures. However, additional testing is needed to verify this observation.

These results suggest that as-received SSZ-13 treated with only the reactive sizing procedure is at least as effective as reactive-sized, Grignard-treated sieves in PDMC membranes. This is an important point to consider since any additional material processing will increase the cost of mixed matrix membranes and lead to reduced commercial interest. Still, the roughened surface produced during the Grignard procedure may be necessary to maintain good polymer/sieve interfaces during hollow fiber spinning [6]. Investigation of this claim, however, was outside the scope of the present research.

5.4.1 Mixed Matrix Membranes with Reactive-Sized, Uncalcined SSZ-13

A similar study to that discussed in Chapter 4 in which the polymer/sieve interface was probed by testing mixed matrix membranes prepared with uncalcined SSZ-13 was repeated here. In the present study, however, uncalcined sieve was modified with the reactive sizing procedure and mixed gas permeation was used instead of pure gas. Considering the improvement in membrane transport reported above, it was presumed that ideal interfaces were formed in membranes prepared with reactive-sized SSZ-13. However, inspecting the permeabilities and selectivities presented in Figures 5.11 and 5.12, respectively, it appears that ideal interfaces may not have actually been formed.

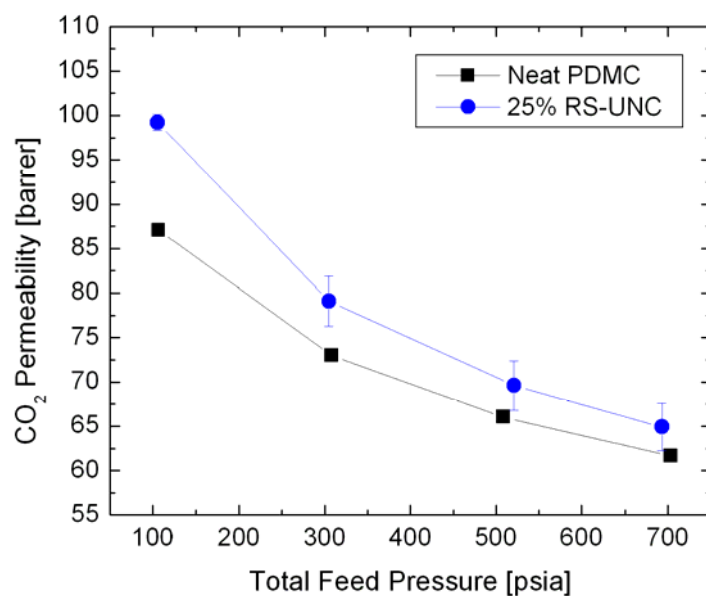


Figure 5.11: Mixed gas carbon dioxide permeabilities for neat PDMC and 25% reactive-sized, uncalcined (RS-UNC) SSZ-13/PDMC membranes. Error bars represent one standard deviation.

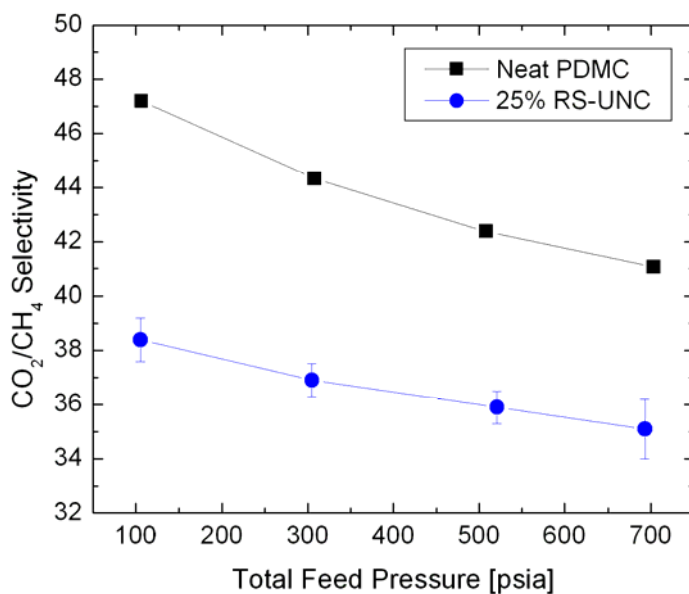


Figure 5.12: Mixed gas carbon dioxide/methane selectivities for neat PDMC and 25% reactive-sized, uncalcined (RS-UNC) SSZ-13/PDMC membranes. Error bars represent one standard deviation.

In the above figures, the averaged permeabilities and selectivities for two separate 25% reactive-sized, uncalcined SSZ-13/PDMC membranes are compared to the respective data for neat PDMC. As mentioned in Chapter 4, the permeability of an ideal mixed matrix membrane prepared with a non-porous dispersed phase is expected to be lower than that for neat polymer; the selectivity is expected to equal that of the neat polymer. However, the mixed matrix membrane permeabilities presented in Figure 5.11 are higher than neat PDMC, and the selectivities presented in Figure 5.12 are lower than neat PDMC. Similar to the findings reported in Section 4.3.2, these permeation data again suggest leaky interface defects, contrary to the good interfaces suggested by the data in the previous section.

5.5 Analysis of a Non-Ideal Mixed Matrix Membrane Transport Mechanism

5.5.1 Background and Mechanism Development

The recurring contradiction in transport data between membranes with calcined and uncalcined SSZ-13 further emphasizes the complexities of studying and developing mixed matrix membranes. Defects in these materials are often easily identified, such as by the appearance of gross sieve-in-a-cage voids in SEM images or the tell-tale reduction in selectivity due to leaky interfaces. Less common, it seems, are situations in which multiple defect types appear to affect a system virtually simultaneously. Needless to say, such a perplexing situation could be frustrating. In the present study, however, the inconsistent permeation analyses have led to the consideration of a complex transport mechanism that combines several distinct, but loosely related phenomena that have been reported for hybrid materials.

To establish the framework of the transport mechanism proposed here, first consider the work reported by Merkel and coworkers in which reverse-selective gas separation membranes were developed by dispersing nanoscale nonporous silica throughout a rigid, high T_g polymer [7]. They showed that enhanced permeability and reverse-selectivity were obtained from enhanced polymer free volume resulting from disruptions in chain packing. These disruptions were caused simply by the presence of the nanoparticles. Such free volume enhancement due to chain packing disruptions has also been attributed to anomalous polymer melt behavior [8] and condensable gas sorption enhancement in hybrid membranes [9].

Next, consider work reported by Priestley et al. in which it was shown that a glassy polymer (PMMA in this case), when strongly adsorbed onto a rigid substrate (such as silica), will experience a significant reduction in the rate of aging dynamics [10]. They also showed that the hindered chain mobility responsible for the reduced rate of aging can extend to over 100 nm from the rigid surface [11]. Recall from the discussion in Chapter 2 that physical aging in polymers leads to more consolidated chain packing, resulting in lower gas permeability and higher selectivity. With this in mind, it is quite conceivable that the regions near a strongly interacting polymer/substrate interface may have considerably different transport properties than exhibited by the bulk polymer. Such chain immobilization—or rigidification—has been noted as the cause of lower-than-expected permeabilities in mixed matrix gas separation membranes [12, 13], lower-than-expected water permeation rates in reinforced epoxy systems [14], and greater-than-expected mechanical properties in reinforced polymers [15].

Now consider the hypothetical structure of a simple solvated polymer chain and its change in structure upon removal of a relatively good solvent. An example of this situation is illustrated in Figure 5.13.

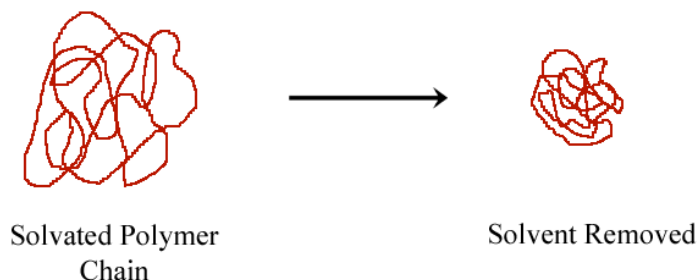


Figure 5.13: Hypothetical polymer chain in solution and after solvent removal.

If the solvated polymer chain interacts strongly with a surface prior to solvent removal, the configuration of chains near the interface might become essentially locked in after solvent removal. This would be especially true for rigid, high- T_g polymers since their intrinsic stiffness—further increased by surface immobilization—hinders chain relaxation. Figure 5.14 illustrates how the structure of an adsorbed solvated polymer chain may change upon solvent removal.

With the above concepts in mind, it is reasonably straightforward to envision a situation in which particles (either porous or nonporous) dispersed throughout a strongly interacting, relatively rigid polymer would result in dilated regions near particle surfaces. These dilated regions—resulting from a combination of solvated chain configurations and chain packing disruption due to the presence of the particles—could exhibit considerable resistance to physical aging due to intrinsic polymer rigidity and strong polymer/surface interactions. The resulting enhanced free volume near particle surfaces would surely

alter gas transport properties from bulk polymer values. In fact, a number of researchers have described a correlation between polymer free volume and gas permeation [16-20]. Moreover, higher sieve loadings would eventually lead to overlap of these dilated regions, resulting in a membrane with transport properties essentially equal to that of the dilated region.

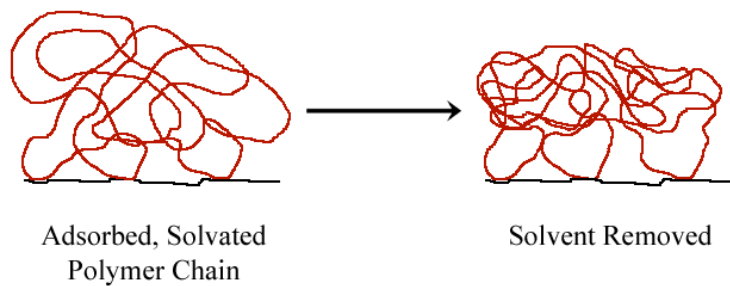


Figure 5.14: Hypothetical adsorbed polymer chain before and after solvent removal.

The above transport mechanism discussion fundamentally echoes similar developments by Hill [21, 22] and Khounlavong and Ganesan [23]. In their respective work, they attempt to describe the unexpected high permeability and reverse-selectivity for the membranes reported by Merkel and coworkers [7]. Hill suggested a model that qualitatively describes both the enhanced permeability and reverse-selectivity reported by Merkel et al. Khounlavong and Ganesan extended Hill's theory with a numerical approach that predicts nanocomposite membrane properties based on polymer rigidity, particle size, and sieve loading. Consistent with the above discussion, both of these models assume regions of lower polymer density near particle surfaces.

5.5.2 Application to Present Research

The permeation data presented in Chapters 4 and 5 have thus far been interpreted to suggest that sieve-in-a-cage defects exist in membranes with calcined SSZ-13, while leaky interface defects exist in membranes with uncalcined SSZ-13. No reasonable explanation for this discrepancy has been identified beyond presuming that SSZ-13 and PDMC are intrinsically incompatible. This conclusion is problematic, though, considering that reactive sizing leads to enhanced performance in membranes with as-received SSZ-13. This paradox can be explained, however, by applying the foregoing transport mechanism framework to SSZ-13/PDMC mixed matrix membranes.

First, it can be reasonably argued that PDMC can, in fact, strongly interact with SSZ-13. This is supported by TGA and XPS analyses which show that considerable PDMC-like material remains on the sieve surface, even after rigorous washing in THF. Instead of assuming nanoscale interfacial voids to explain the transport properties observed for membranes with uncalcined SSZ-13, a dilated interphase, as described above, can be assumed to extend from the particle surface to some distance, ℓ_I , into the polymer matrix. It is also assumed that interphase dilation linearly decreases from its maximum at the sieve surface to zero at ℓ_I , where bulk polymer transport properties resume.

Owing to the dilated nature of this hypothesized interphase, gas flux through this region is expected to be greater than in the bulk polymer; selectivity is expected to be lower. High flux, low selectivity transport through the interphase can easily account for both the higher-than-neat polymer permeabilities and lower-than-neat polymer selectivities observed for uncalcined SSZ-13/PDMC membranes. In fact, such membrane

transport can be modeled using the 3-phase Maxwell model provided that the approximate thickness of the interphase and its transport properties are known.

In a similar application of the present mechanism, the observed performance of calcined SSZ-13/PDMC membranes can also be explained by high flux, low selectivity transport through dilated interphase regions. In this case, however, gas transport is complicated by having access to the calcined sieve, creating an additional path through which molecules can pass. Though the sieve will ideally also provide high flux transport, its selectivity should be considerably greater than that of the interphase. In the present case, a situation can be envisioned in which the combined transport of carbon dioxide through the bulk polymer, interphase, and sieve would yield a significantly higher overall permeability (with respect to neat PDMC). Owing to the high flux, low selectivity in the interphase, the combined methane transport through these phases could result in overall membrane selectivity nearly equal to that of the neat polymer. Again, the 3-phase Maxwell model can describe such transport provided that the interphase properties are known.

While the above discussion reasonably describes the transport trends observed for as-received SSZ-13/PDMC membranes in terms of the hypothesized interphases proposed in this section, the similar behaviors of membranes with reactive-sized, Grignard-treated (RS-GT) and reactive-sized, as-received (RS-AR) SSZ-13 have not been addressed from the perspective of this mechanism. In the case of membranes with RS-GT sieves, it is believed that voids within the surface magnesium hydroxide layer are truly caulked by the sizing procedure. This is supported by nitrogen physisorption and permeation analyses. It is anticipated that material resulting from the sizing procedure

will interact (most likely hydrogen bond) with the magnesium hydroxide surface on GT-SSZ-13, similar to how the sizing material is hypothesized to interact with silanol groups on the as-received sieve surface. As a result, the surfaces of AR- and GT-SSZ-13 would appear similar after the sizing procedure. The interaction of material bound to these sized surfaces with bulk polymer is hypothesized to occur as illustrated in Figure 5.15.

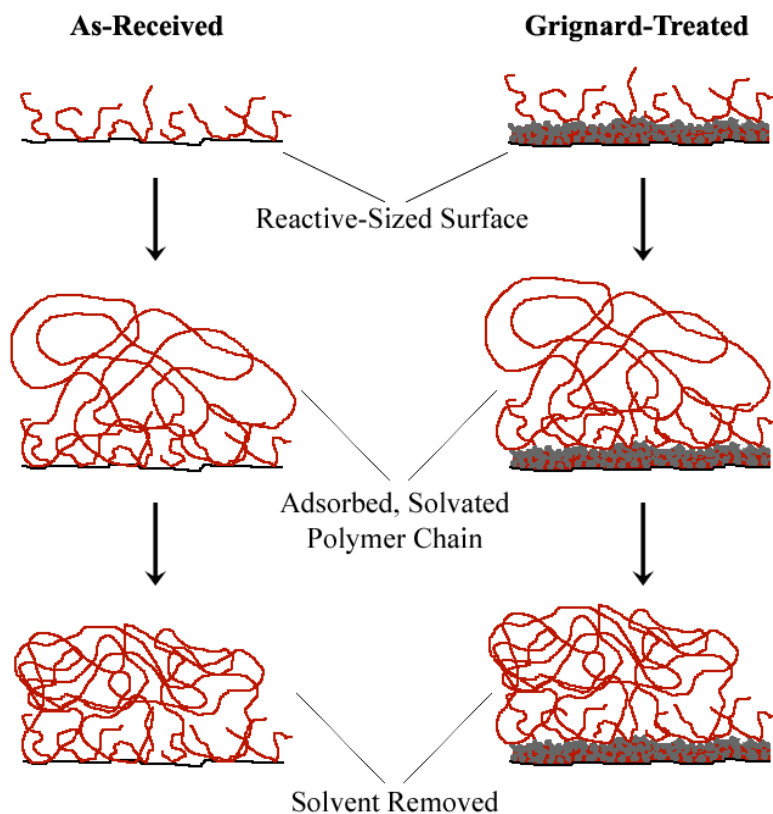


Figure 5.15: Hypothesized interaction of material on the surface of sized sieves with bulk polymer chains.

In the above figure, monomers and/or low molecular weight oligomers are attached to the sieve surface during the sizing procedure (see Appendix A for possible attachment mechanisms). Solvated bulk polymer could interact with this surface-bound

material as the chains adsorb onto the treated surface. Any material extending from the surface of the sieve would entangle the adsorbed polymer chains, filling a fraction of the free volume that would remain at the surface of un-sized sieves. After solvent removal, the polymer interphase may be effectively less dilated due to the entangled surface material, leading to interphase transport properties closer to those of the bulk polymer. Since this hypothesis predicts similar interfaces and interphases for membranes containing both RS-GT and RS-AR SSZ-13, it explains quite well the nearly identical transport properties observed for these membranes.

5.5.3 Prediction of Interphase Parameters

It was found in the present research that the 3-phase Maxwell model can be used to predict interphase properties from mixed matrix membrane permeation data. By simultaneously solving the model as applied to both uncalcined and calcined sieve-containing membranes, a reasonable estimate of both the interphase thickness and its transport properties were determined. Such a solution was feasible by assuming identical interphase properties in membranes with uncalcined and calcined SSZ-13. This assumption was valid since identical sieve loading and particle sizes were used for each of the membranes. The results of this modeling are discussed below; the details of the calculations are included in Appendix B.

Using the above method, the interphase thickness, ℓ_i , was estimated to be ~50 nm. Carbon dioxide permeability in the interphase was estimated to be ~540 barrer, with selectivity over methane of ~19. These values are quite reasonable and, when considered within the above transport mechanism framework, provide a consistent explanation for the observed permeation results for the various hybrid membranes studied.

5.6 Summary and Conclusions

Modified SSZ-13 was investigated in an attempt to eliminate nanoscale interfacial defects presumed to exist in membranes with as-received sieve. The magnesium hydroxide deposits resulting from the sieve modification procedure apparently form voids within the deposited surface layer into which high molecular weight polymer chains can not percolate. These voids serve as non-selective pathways which allow gas molecules to bypass sieve particles, resulting in membrane performance lower than that observed for membranes with untreated sieves. A sizing technique was developed to caulk these voids in order to eliminate sieve bypass; nitrogen physisorption and permeation analyses suggested that this technique was largely successful. However, the sizing procedure also resulted in considerable transport property improvement in membranes with as-received SSZ-13. Moreover, contrary to the conclusion drawn in Chapter 4 that SSZ-13 and PDMC are intrinsically incompatible, TGA and XPS analyses of sized sieve suggested that PDMC—or PDMC-like material—in fact strongly adheres to the untreated sieve surface. This realization led to the development of a novel, non-ideal transport mechanism that may occur in mixed matrix membranes. This mechanism provides an elegant solution that simultaneously describes the behavior of all the membranes analyzed in this research.

5.7 References

1. Husain, S. and W.J. Koros, *Mixed matrix hollow fiber membranes made with modified HSSZ-13 zeolite in polyetherimide polymer matrix for gas separation*. Journal of Membrane Science, 2007. **288**(1-2): p. 195-207.
2. Shu, S., S. Husain, and W.J. Koros, *A general strategy for adhesion enhancement in polymeric composites by formation of nanostructured particle surfaces*. Journal of Physical Chemistry C, 2007. **111**(2): p. 652-657.

3. Shu, S., S. Husain, and W.J. Koros, *Formation of nanostructured zeolite particle surfaces via a halide/Grignard route*. *Chemistry of Materials*, 2007. **19**(16): p. 4000-4006.
4. Husain, S., *Mixed Matrix Dual Layer Hollow Fiber Membranes for Natural Gas Separation*, in *School of Chemical & Biomolecular Engineering*. 2006, Georgia Institute of Technology: Atlanta, GA.
5. Shu, S., S. Husain, and W.J. Koros, *Sonication-assisted dealumination of zeolite A with thionyl chloride*. *Industrial & Engineering Chemistry Research*, 2007. **46**(3): p. 767-772.
6. Koros, W.J., *Personal Communication*. 2009.
7. Merkel, T.C., et al., *Ultraporous, reverse-selective nanocomposite membranes*. *Science*, 2002. **296**(5567): p. 519-522.
8. Mackay, M.E., et al., *Nanoscale effects leading to non-Einstein-like decrease in viscosity*. *Nature Materials*, 2003. **2**(11): p. 762-766.
9. Sadeghi, M., M.A. Semsarzadeh, and H. Moadel, *Enhancement of the gas separation properties of polybenzimidazole (PBI) membrane by incorporation of silica nano particles*. *Journal of Membrane Science*, 2009. **331**(1-2): p. 21-30.
10. Priestley, R.D., et al. *Evidence for the molecular-scale origin of the suppression of physical ageing in confined polymer: fluorescence and dielectric spectroscopy studies of polymer-silica nanocomposites*. 2007: Iop Publishing Ltd.
11. Priestley, R.D., et al., *Structural relaxation of polymer glasses at surfaces, interfaces and in between*. *Science*, 2005. **309**(5733): p. 456-459.
12. Mahajan, R. and W.J. Koros, *Factors controlling successful formation of mixed-matrix gas separation materials*. *Industrial & Engineering Chemistry Research*, 2000. **39**(8): p. 2692-2696.
13. Mahajan, R. and W.J. Koros, *Mixed matrix membrane materials with glassy polymers. Part 2*. *Polymer Engineering and Science*, 2002. **42**(7): p. 1432-1441.
14. Manson, J.A. and E.H. Chiu, *PERMEATION OF LIQUID WATER IN A FILLED EPOXY RESIN*. *Journal of Polymer Science Part C-Polymer Symposium*, 1973(41): p. 95-108.
15. Galperin, I. and T.K. Kwei, *DYNAMIC MECHANICAL PROPERTIES OF TITANIUM DIOXIDE-FILLED POLY(VINYL ACETATE) AT 0-40 DEGREES C*. *Journal of Applied Polymer Science*, 1966. **10**(5): p. 673-&.

16. Kim, T.H., et al., *RELATIONSHIP BETWEEN GAS SEPARATION PROPERTIES AND CHEMICAL-STRUCTURE IN A SERIES OF AROMATIC POLYIMIDES*. Journal of Membrane Science, 1988. **37**(1): p. 45-62.
17. Miyata, S., et al., *Relationship between gas transport properties and fractional free volume determined from dielectric constant in polyimide films containing the hexafluoroisopropylidene group*. Journal of Applied Polymer Science, 2008. **107**(6): p. 3933-3944.
18. Park, J.Y. and D.R. Paul, *Correlation and prediction of gas permeability in glassy polymer membrane materials via a modified free volume based group contribution method*. Journal of Membrane Science, 1997. **125**(1): p. 23-39.
19. Recio, R., et al., *Effect of fractional free volume and T-g on gas separation through membranes made with different glassy polymers*. Journal of Applied Polymer Science, 2008. **107**(2): p. 1039-1046.
20. Xiao, Y.C., et al., *The strategies of molecular architecture and modification of polyimide-based membranes for CO₂ removal from natural gas-A review*. Progress in Polymer Science, 2009. **34**(6): p. 561-580.
21. Hill, R.J., *Diffusive permeability and selectivity of nanocomposite membranes*. Industrial & Engineering Chemistry Research, 2006. **45**(21): p. 6890-6898.
22. Hill, R.J., *Reverse-selective diffusion in nanocomposite membranes*. Physical Review Letters, 2006. **96**(21): p. 4.
23. Khounlavong, L. and V. Ganesan, *Influence of interfacial layers upon the barrier properties of polymer nanocomposites*. Journal of Chemical Physics, 2009. **130**(10): p. 12.

CHAPTER 6

MEMBRANE PERFORMANCE IN THE PRESENCE OF TOLUENE- CONTAMINATED FEEDS

6.1 Introduction

In Chapter 5, the impact of sieve modification on mixed matrix membrane performance was discussed. The significant performance gains achieved illustrate that functional hybrid membranes with crosslinkable polyimides are indeed feasible. However, these membranes were tested with an ideal mixture of only carbon dioxide and methane. Most natural gas deposits contain a variety of hydrocarbon impurities. While feed streams are often treated to reduce the concentration of these materials, it is impractical to fully remove all contaminants. Moreover, system upsets must be anticipated, and purification operations must be able to withstand these events. Prior work has shown that heavy hydrocarbon impurities in natural gas feeds can lead to substantial membrane performance loss. Toluene has proven especially problematic, inducing plasticization in several polyimides [1-3] and causing significant permeability reduction in PDMC hollow fibers [4].

In addition to the benefits of crosslinkable mixed matrix membranes already established, these materials may also provide a means to prevent the deleterious impact of highly sorbing contaminants on membrane performance. Omole has shown that PDMC is resistant to plasticization, even in the presence of high concentrations of toluene. However, at these concentrations, PDMC membranes appear to suffer from substantially lower gas permeabilities due to both competition and antiplasticization effects [4]. Owing to the inability of relatively large contaminants, such as toluene, to enter the pore

network of SSZ-13, crosslinked mixed matrix membranes with this sieve may be able to simultaneously prevent plasticization and minimize the permeability crash previously observed in neat PDMC membranes. It is therefore desirable to determine the response of these hybrid membranes under contaminated feed conditions.

Following the lead of previous researchers, toluene was chosen as the impurity with which to probe membrane response under contaminated feed conditions. In the remainder of this chapter, neat PDMC dense film membrane response to toluene-contaminated feeds will first be analyzed and compared to that of asymmetric hollow fibers. Following this will be the analysis and performance comparison of various crosslinkable mixed matrix membranes with both as-received and modified sieves.

6.2 Neat PDMC Dense Film Membranes

Neat PDMC dense film membranes were first characterized with clean and toluene-contaminated feeds in order to establish a baseline for comparison to mixed matrix membrane results. Clean feeds were composed of 10% (molar basis) carbon dioxide with methane as the balance. Contaminated feeds were composed of either 500 ppm or 1000 ppm toluene with 10% carbon dioxide and methane as the balance. Omole showed that hollow fiber membrane transport was severely impaired at these concentrations [4]. Since the aim of the present study is to investigate mixed matrix membrane efficacy in the presence of contaminated feeds, the same concentrations were used in this work. These gas mixtures were used for all analyses reported in this chapter.

Figure 6.1 presents mixed gas carbon dioxide permeabilities for two membranes first tested with clean feeds and then exposed to either 500 ppm or 1000 ppm toluene-contaminated feeds. Figure 6.2 presents the carbon dioxide/methane selectivities for

these membranes. The two membranes, though prepared separately, exhibited virtually identical transport properties prior to toluene exposure as evidenced by the overlapping permeabilities and selectivities reported in the figures. The downward trends in transport properties prior to toluene exposure can be explained by dual-mode sorption effects, as previously discussed. However, the decline in permeability and the slight selectivity enhancement in the presence of toluene can not be explained by sorption effects alone.

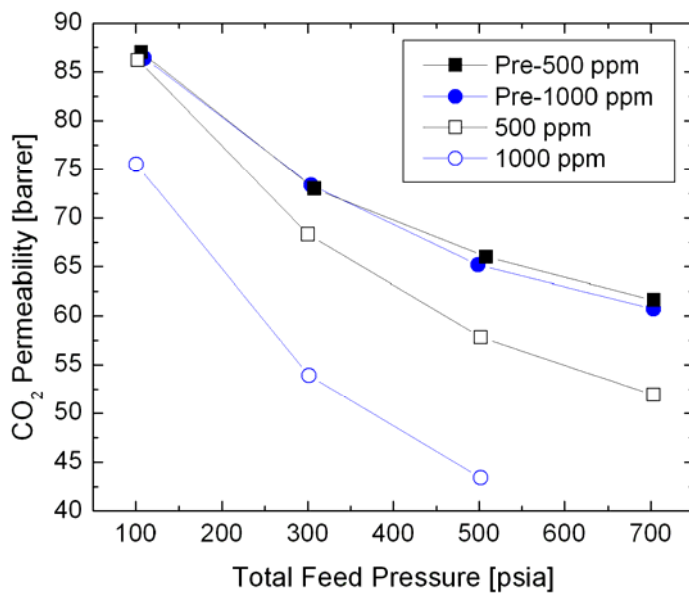


Figure 6.1: Mixed gas carbon dioxide permeabilities for neat PDMC dense film membranes.

The membrane behavior in this case is likely attributable to a combination of both sorption competition and antiplasticization effects. The observations here are similar to those reported by Maeda and Paul in which the addition of low concentrations of various diluents to glassy polymer membranes resulted in substantial permeability losses [5, 6]. In some cases, it was noted that selectivities were enhanced with increasing diluent

concentration. However, increasing concentrations beyond certain levels led to reduced selectivities as antiplasticization was replaced by a conventional plasticization response. Maeda and Paul [7], and Madden, in later work [8], correlated the impact of antiplasticization on membrane transport with changes in polymer free volume. This relationship will be discussed further in the following comparison of PDMC dense film and hollow fiber membrane response to toluene-contaminated feeds.

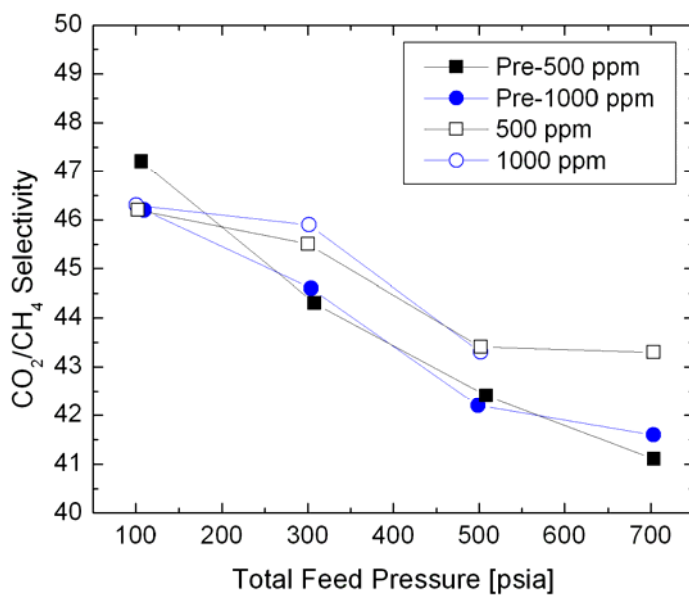


Figure 6.2: Mixed gas carbon dioxide/methane selectivities for neat PDMC dense film membranes.

6.2.1 Comparison of Dense Film and Hollow Fiber Membrane Performance

In order to compare the above dense film responses to those of hollow fibers, it is most convenient to consider normalized transport properties. This is due to the convention of reporting dense film and hollow fiber data in different units. Without an accurate measure of the skin thickness, transport data for hollow fiber membranes are

reported as permeances with units of gas permeation units (GPU). Normalizing data allows for direct comparison of dense film and hollow fiber trends on a single graph.

Normalized carbon dioxide permeability/permeance data for dense film and hollow fiber membranes (taken from [4]) are presented in Figure 6.3. Figure 6.4 presents normalized carbon dioxide/methane selectivities for the same membranes. These membranes were tested with identical clean and contaminated feeds under similar conditions; only the permeate pressures varied for these measurements (vacuum for dense films and atmospheric for hollow fibers). For each of the membranes, transport data were normalized by the lowest pressure point prior to toluene exposure: 100 psia for dense films and 200 psia for hollow fibers.

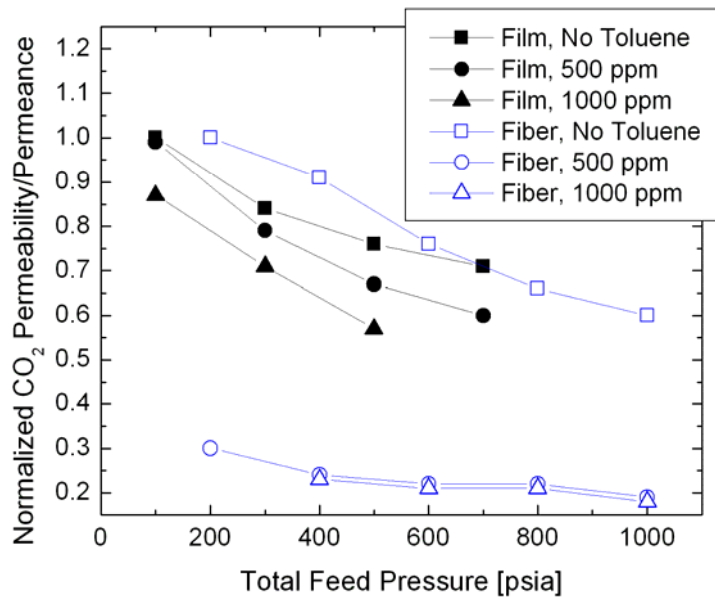


Figure 6.3: Normalized mixed gas carbon dioxide permeabilities/permeances for neat PDMC dense film and hollow fiber membranes. Hollow fiber data from [4].

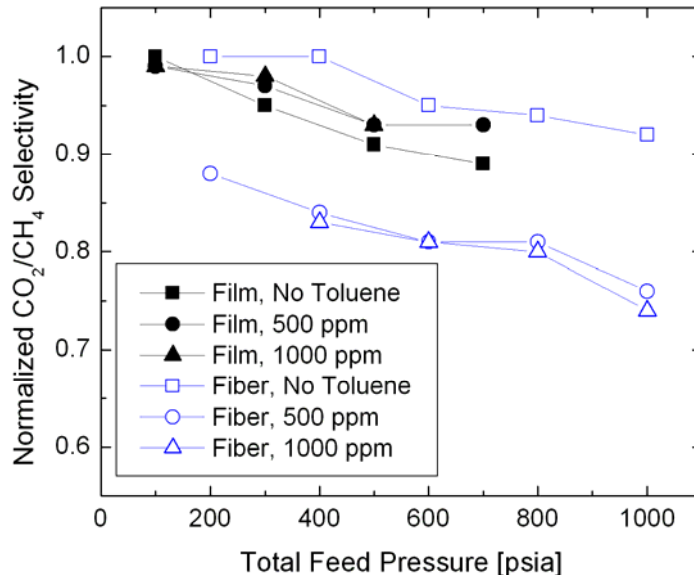


Figure 6.4: Normalized mixed gas carbon dioxide/methane selectivities for neat PDMC dense film and hollow fiber membranes. Hollow fiber data from [4].

It is clear from the trends in Figures 6.3 and 6.4 that significant differences exist between dense film and hollow fiber response to toluene-contaminated feeds. Whereas the dense film permeability reduction was proportional to toluene concentration in the feed, hollow fiber permeance immediately plummeted as much as 70% with the introduction of toluene into the feed. Moreover, hollow fiber selectivity decreased roughly 10% in the presence of toluene while dense film selectivity appeared to actually increase slightly.

Omole explained the severe depression in hollow fiber performance as primarily the result of antiplasticization [4]. Madden arrived at an identical conclusion in studying Matrimid[®] hollow fiber membrane response to toluene- and n-heptane-contaminated feeds [8]. Based on his observations, Madden ultimately developed a model to predict

the impact of antiplasticization on transport properties. This model was able to successfully anticipate membrane response to highly sorbing contaminants based on free volume estimates. A summary of this model follows.

Recall from the discussion in Chapter 2 that membrane permeability is the product of penetrant diffusivity and solubility in a given glassy polymer. It is known that both diffusivity and solubility in glassy polymers are dependent upon free volume. Park and Paul have developed the following semi-empirical relation to describe the dependence of permeability on the fractional free volume of a polymer [9]:

$$P_i = A_i \exp\left[-\frac{B_i}{FFV}\right] \quad (6.1)$$

Here the permeability of penetrant i is expressed in terms of two penetrant-dependent parameters— A_i and B_i —and the fractional free volume of a given polymer, FFV . A and B parameters have been determined for several gases from published transport data for various polymers (105 in the case of carbon dioxide). Fractional free volume is defined as:

$$FFV = \frac{\hat{V} - \hat{V}_0}{\hat{V}} \quad (6.2)$$

where \hat{V} is the measured specific volume of the glassy polymer determined under specified conditions, and \hat{V}_0 is the specific volume occupied by the polymer chains, often predicted by group contribution methods such as proposed by Bondi [10]. Madden showed that the permeability reduction upon introduction of a feed contaminant can be estimated by:

$$\frac{(P_i)_{mix}}{P_i} = \exp\left[B_i\left(\frac{1}{FFV} - \frac{1}{FFV_{mix}}\right)\right] \quad (6.3)$$

Here $(P_i)_{mix}$ is the permeability resulting from contaminated feed conditions. FFV_{mix} is the fractional free volume of the polymer/contaminant mixture and is defined as:

$$FFV_{mix} = \frac{\hat{V}_{mix} - (\hat{V}_0)_{mix}}{\hat{V}_{mix}} \quad (6.4)$$

where \hat{V}_{mix} is the measured specific volume of the glassy polymer/contaminant mixture, and $(\hat{V}_0)_{mix}$ is the calculated specific volume occupied by the polymer and contaminant molecules. An antiplasticization response ($(P_i)_{mix}/P_i < 1$) is observed when $FFV_{mix} < FFV$; a plasticization response ($(P_i)_{mix}/P_i > 1$) is observed when $FFV_{mix} > FFV$. The implication of Equation 6.3 is that relatively minor differences/changes in free volume can have a considerable effect on permeability. The dependence of permeability on free volume provides a reasonable explanation for the differences in membrane behaviors depicted in Figures 6.3 and 6.4—this is discussed below.

Unrelaxed free volume in a polymer is defined by space between adjacent polymer chain segments. It has been suggested that the selective skin layer of hollow fiber membranes may contain varying amounts of such free volume due to fiber formation methods [11, 12]. Owing to the rapid vitrification of hollow fibers, polymer chains have little time to relax into more efficiently packed configurations. As such, it is conceivable that a relatively large amount of volume may be trapped in rapidly quenched systems. Conversely, dense film membrane formation is deliberately slow. In this case, chains have considerably more time to relax into tightly packed configurations, thus eliminating volume from the matrix that would otherwise become trapped upon membrane vitrification. Since the production of hollow fibers is in such stark contrast to

that of dense films, it is quite conceivable that the free volume content in a hollow fiber may differ from that in a dense film.

These hypothesized free volume differences, coupled with the above model, may explain the inconsistent toluene response in PDMC membranes noted. An illustration of the potential free volume differences, before and during toluene exposure, is presented in Figure 6.5.

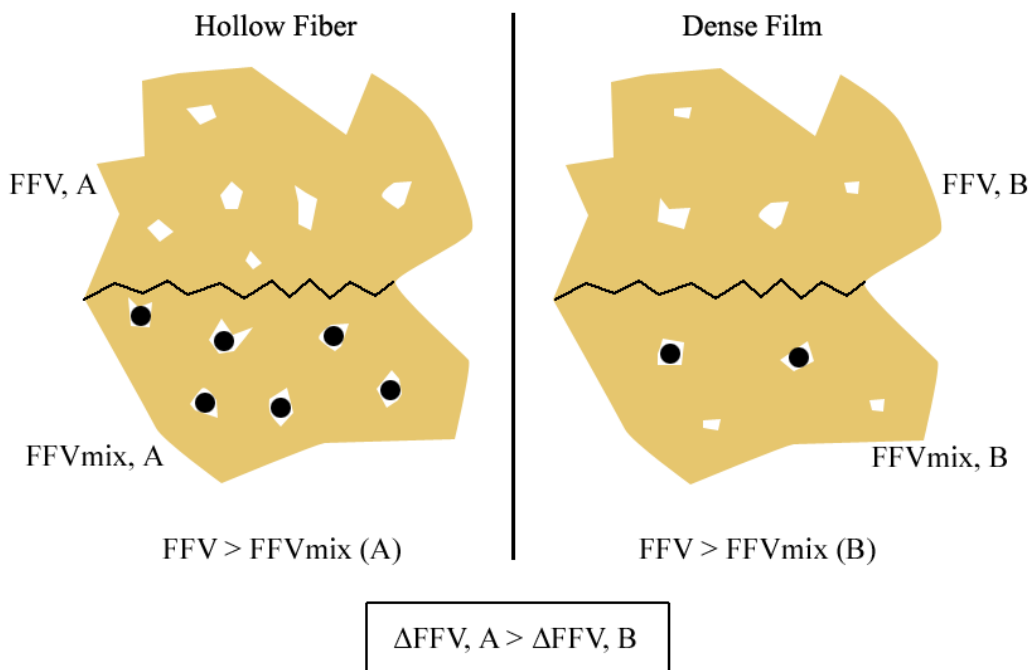


Figure 6.5: Representation of possible free volume differences between hollow fiber and dense film membranes. FFV refers to membrane state prior to toluene exposure; FFVmix refers to state during toluene exposure. (A) refers to hollow fiber membrane; (B) refers to dense film. Black spheres represent sorbed toluene molecules.

Excess free volume is represented in Figure 6.5 as white, empty space dispersed within the polymer matrix. For each membrane, this volume is depicted under clean (*FFV*) and contaminated (*FFV_{mix}*) conditions. The total amount of excess volume in the

hollow fiber has been drawn to be greater than that in the dense film; this reflects the potential free volume differences discussed above. The sorption of toluene in these free volume voids is represented by the black spheres. It is suggested in the figure that for both the hollow fiber and dense film cases, toluene fills the available volume such that the fractional free volume is reduced as compared to clean feed conditions ($FFV > FFV_{mix}$). It is also indicated in Figure 6.5 that the relative free volume change upon toluene sorption (ΔFFV) is greater for the hollow fiber case. According to Equation 6.3, a larger reduction in FFV for hollow fibers as compared to dense films would result in a larger depression in permeability. As discussed, the permeability reduction in hollow fibers is indeed greater than that in dense films upon toluene exposure.

While this hypothesis is certainly speculative and was not directly probed here, it does provide a reasonable argument for the present observations based on prior reports of similar behavior. A detailed study of free volume in these membranes using high resolution gas sorption and/or positron annihilation lifetime spectroscopy (PALS) would facilitate a better understanding of the fundamental mechanism behind the inconsistent toluene responses. Such a study, however, was beyond the scope of this research.

6.2.2 Physical Aging in PDMC Dense Film Membranes

As discussed in Section 2.1.3.4, the relaxation of excess volume in glassy polymers is known as *physical aging*. The resulting densification of the polymer matrix leads to lower membrane permeabilities and higher selectivities in both uncrosslinked and crosslinked polymers [13-18]. Such a response is illustrated by the differences in pre- and post-toluene permeabilities and selectivities presented in Figures 6.6 and 6.7, respectively.

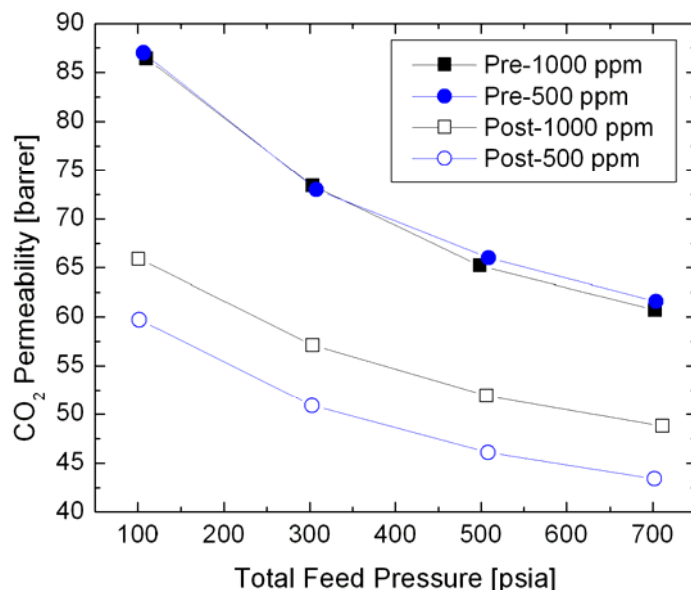


Figure 6.6: Mixed gas carbon dioxide permeabilities for PDMC dense film membranes.

Clearly the membranes were physically aged during testing as evidenced by the lower permeabilities and higher selectivities observed for the post-toluene tested membranes. The differing reductions in permeability and increases in selectivity suggest that the membranes experienced different degrees of aging. These differences cannot be attributed to variations in thermal annealing or other factors since the membranes were identically processed.

While it may initially seem counterintuitive for the membrane exposed to a lower concentration of toluene to be aged more, similar behavior has been reported in the literature [19-22]. It was found that while polymers aged under vacuum showed a predictable decay in sorption capacity for various penetrants, the same polymers, when aged in the presence of low penetrant activities, maintained higher sorption capacities. It

was determined that the sorbed penetrant molecules effectively served as molecular props, hindering the loss of free volume and preventing matrix consolidation.

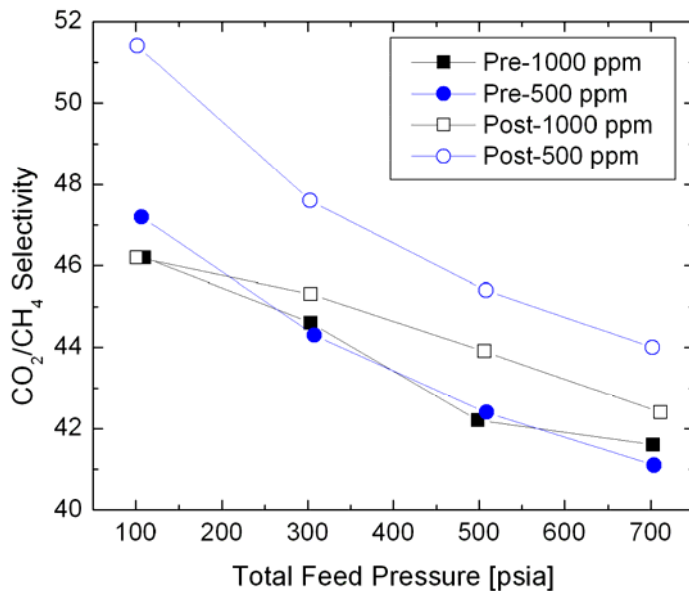


Figure 6.7: Mixed gas carbon dioxide/methane selectivities for PDMC dense film membranes.

According to the above phenomenon, toluene sorbed in a membrane should prevent polymer consolidation. As such, higher concentrations of toluene should be more effective in preventing this consolidation than lower concentrations. Though it was noted that any amount of toluene in the feed appears to accelerate the rate of aging (versus clean feed), the above mechanism can explain quite well the observation that PDMC membranes age less in the presence of higher toluene concentrations.

6.3 As-Received SSZ-13/PDMC Mixed Matrix Membranes

In order to investigate the efficacy of mixed matrix membranes in mitigating performance losses under contaminated feed conditions, a 25% (w/w) as-received (AR) SSZ-13/PDMC hybrid membrane was prepared and tested using mixed gas permeation analysis. The membrane was tested a total of three times: first with clean feed, followed by 500 ppm toluene-contaminated feed, and finally with clean feed again. The 500 ppm toluene-contaminated feed was selected for two reasons: 1) 500 ppm and 1000 ppm resulted in nearly identical performance loss in Omole's hollow fiber testing (Figures 6.3 and 6.4); and 2) 500 ppm resulted in more significant aging in PDMC dense films (Figures 6.6 and 6.7). Since the intent of the present study is to probe hybrid membrane performance under contaminated feed conditions, the concentration that led to the greatest loss of performance in neat PDMC membranes was chosen. The resulting carbon dioxide permeabilities are compared with those of neat PDMC in Figure 6.8; carbon dioxide/methane selectivities for these membranes are compared in Figure 6.9.

Comparing the pre-toluene permeation data in the figures below, the considerably higher-than-neat PDMC permeability and slightly lower-than-neat PDMC selectivity suggest that the membrane is defective. This is not surprising considering that similar results were obtained for membranes with as-received sieve in Chapter 4. Interestingly, though, the presence of the sieve apparently affects membrane transport under contaminated feed conditions primarily by reducing the extent of physical aging as compared to neat PDMC (10% permeability reduction for hybrid; 30% for neat at 700 psia). The permeability reduction for the hybrid membrane due to antiplasticization is comparable to that for neat polymer (20% for hybrid; 16% for neat at 700 psia).

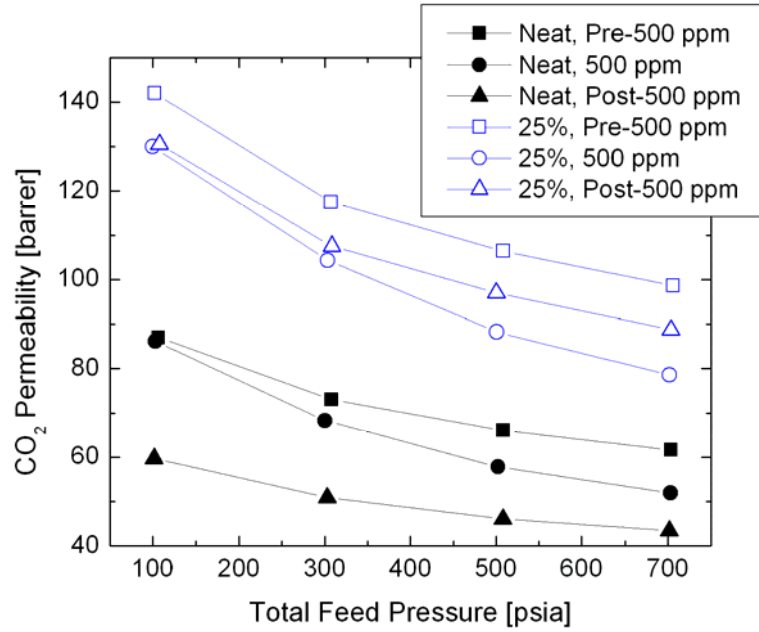


Figure 6.8: Mixed gas carbon dioxide permeabilities for neat PDMC dense film and 25% as-received (AR) SSZ-13/PDMC mixed matrix membranes.

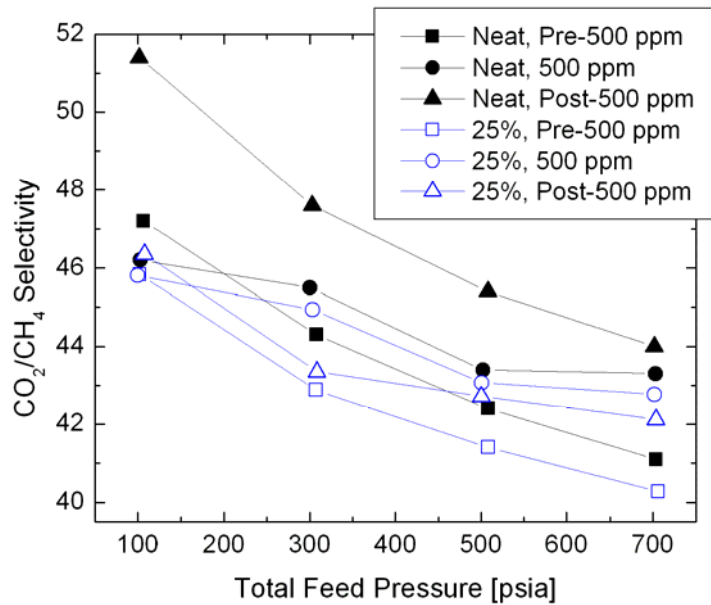


Figure 6.9: Mixed gas carbon dioxide/methane selectivities for neat PDMC dense film and 25% as-received (AR) SSZ-13/PDMC mixed matrix membranes.

These observations somewhat contradict the anticipated behavior of a hybrid membrane with interfacial defects. Since a physical void is presumed to separate the particle surface from the bulk polymer at such a defect, the polymer at the void boundary is expected to behave as a free surface. Polymer chain mobility is not expected to be hindered at free surfaces; in fact, it may be enhanced [23-27]. As such, defective hybrid membranes and neat polymer membranes should age similarly. This was not the case, however, according to the above data. As mentioned, the hybrid membrane lost only 10% of its original permeability (at 700 psia) after toluene exposure versus 30% lost by the neat polymer membrane.

The reduced aging response might be due to chain rigidification stemming from segmental surface adsorption that is adequate to retard large scale segmental packing and motion. As discussed in Chapter 5, Priestley et al. reported drastic reductions in aging rates for polymers that interacted strongly with rigid substrates [28, 29]. While surface adsorption of polymer chains is not expected to cease aging dynamics entirely, aging processes may be impeded such that the tell-tale permeability reduction/selectivity enhancement may not be observed on the time scale of the experiments conducted in this research. Additional work—including long-term permeation studies—is needed to elucidate the mechanism behind the observed differences in aging between hybrid and neat polymer membranes.

6.4 Grignard-Treated SSZ-13/PDMC Mixed Matrix Membranes

As discussed in Chapter 5, the Grignard procedure has been shown to improve membrane transport by enhancing polymer/sieve adhesion [30, 31]. It was initially presumed that similar enhancements would be realized in modified SSZ-13/PDMC

hybrid membranes. However, as shown in Chapter 5, non-selective voids were apparently formed within surface deposits in Grignard-treated SSZ-13, leading to increasingly defective membrane performance. Even so, to continue the study of mixed matrix membrane response to contaminated feeds, two 25% (w/w) Grignard-treated (GT) SSZ-13/PDMC hybrid membranes were prepared and tested as before. Averaged carbon dioxide permeabilities for these membranes are presented in Figure 6.10; averaged carbon dioxide/methane selectivities are presented in Figure 6.11. Error bars were omitted from the figures for clarity (average permeability error of ± 28 barrer). Permeabilities and selectivities for neat PDMC and 25% as-received SSZ-13/PDMC membranes are included in the respective figures for comparative reference.

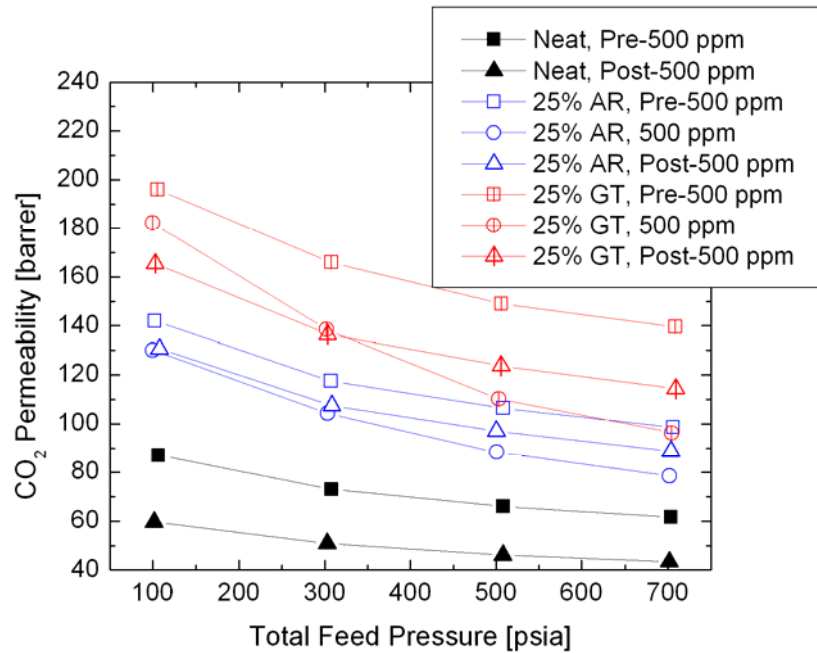


Figure 6.10: Mixed gas carbon dioxide permeabilities for 25% Grignard-treated (GT) and 25% as-received (AR) SSZ-13/PDMC mixed matrix membranes.

It can be seen in the above figure that the membranes with Grignard-treated SSZ-13 exhibited higher permeability than both the membrane with as-received SSZ-13 and the neat PDMC membrane. This permeability enhancement can most likely be attributed to increased flux through the surface layer voids discussed in Section 5.2.2. Additionally, these membranes exhibited a more significant permeability depression in the presence of toluene and showed greater aging as compared to the membrane containing as-received sieve. However, considering the variance in the data for these membranes (± 28 barrer), the apparent differences in these responses may actually be less than is suggested by the figure.

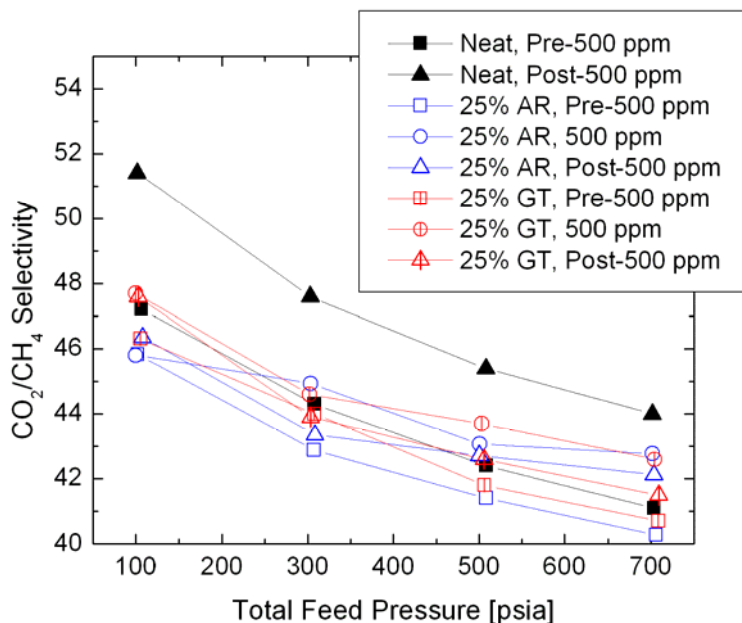


Figure 6.11: Mixed gas carbon dioxide/methane selectivities for 25% Grignard-treated (GT) and 25% as-received (AR) SSZ-13/PDMC mixed matrix membranes.

As discussed in Chapter 5, PDMC is expected to interact with Grignard-treated SSZ-13. Also, it has been suggested that PDMC may interact more significantly than initially thought with as-received SSZ-13. If true, according to the transport mechanism discussed in Chapter 5, hybrid membranes containing as-received and Grignard-treated SSZ-13 can be expected to respond similarly to given feed conditions. As observed, the GT- and AR-SSZ-13/PDMC hybrid membranes do appear to exhibit roughly similar behavior (within error).

The selectivities presented in Figure 6.11 follow anticipated trends. Though slight, the enhancements observed between pre- and post-toluene permeation testing reflect the minor extent of aging in these membranes as compared to neat PDMC membranes (see Figure 6.7). The small selectivity enhancement observed in the presence of toluene can most likely be attributed to antiplasticization effects, as discussed above. The repeatable reduction of physical aging in these hybrid membranes (versus neat polymer) is possible evidence of rigidified interphases. Admittedly, this explanation is speculative. Additional work is needed to probe the nature of the interface/interphase in these hybrid membranes.

6.5 Reactive-Sized SSZ-13/PDMC Mixed Matrix Membranes

6.5.1 Reactive-Sized, Grignard-Treated SSZ-13/PDMC Mixed Matrix Membranes

The preceding study of Grignard-treated SSZ-13/PDMC membranes showed that significant permeability enhancements over neat PDMC are possible with hybrid membranes. Although these membranes were somewhat successful in mitigating performance losses due to contaminated feeds and aging, the desired selectivity enhancements were not achieved. Work described in Chapter 5 with reactive-sized,

Grignard-treated SSZ-13 suggested that modest selectivity gains are possible with additional sieve treatment.

For that reason, a 25% (w/w) reactive-sized, Grignard-treated (RS-GT) SSZ-13/PDMC membrane was prepared and tested as above. Carbon dioxide permeabilities for this membrane are presented in Figure 6.12; carbon dioxide/methane selectivities are presented in Figure 6.13. Permeabilities and selectivities for neat PDMC and 25% Grignard-treated (GT) SSZ-13/PDMC membranes are included in the respective figures for comparative reference.

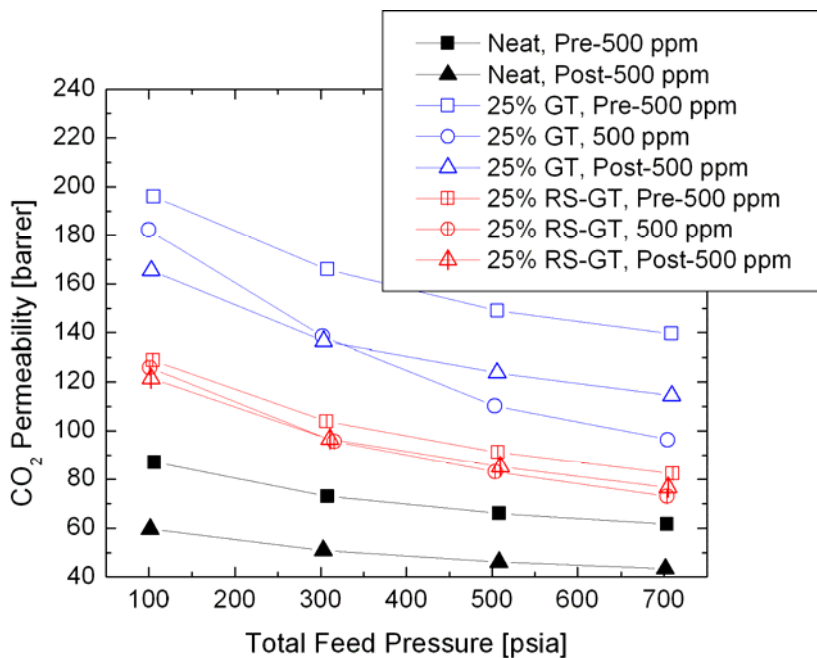


Figure 6.12: Mixed gas carbon dioxide permeabilities for 25% Grignard-treated (GT) and 25% reactive-sized, Grignard-treated (RS-GT) SSZ-13/PDMC mixed matrix membranes.

As illustrated by Figures 6.12 and 6.13, the sizing procedure leads to significant improvements in membrane permeabilities, selectivities, and aging and toluene resistance

over previous membranes. In particular, quite impressive permeability and selectivity enhancements over neat PDMC were observed. For this membrane at 700 psia feed pressure: pre-toluene permeability was enhanced 34% and selectivity was enhanced 11%; permeability in the presence of 500 ppm toluene was enhanced 41% and selectivity was enhanced 9%; and post-toluene permeability was enhanced 77% and selectivity was enhanced 6%.

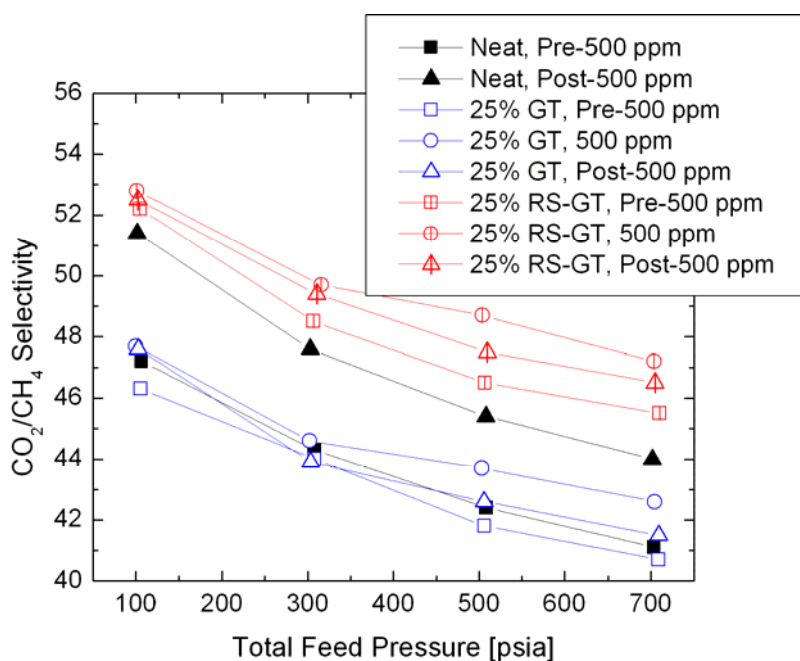


Figure 6.13: Mixed gas carbon dioxide/methane selectivities for 25% Grignard-treated (GT) and 25% reactive-sized, Grignard-treated (RS-GT) SSZ-13/PDMC mixed matrix membranes.

The transport mechanism framework previously described may provide a reasonable explanation of these improvements. First, the sizing procedure is able to effectively caulk non-selective voids within the GT-SSZ-13 surface layer; this was evidenced by nitrogen physisorption and permeation characterization in Chapter 5. Next,

material deposited on the sieve during the sizing procedure is presumed to entangle adsorbed bulk polymer chains. Material extending from the sieve surface—where polymer dilation is expected to be greatest—may reduce excess volume within the interphase. This could lead to lower permeability and higher selectivity (versus membranes with unsized sieves) since increased interphase transport resistance would lead to better utilization of the sieve. Moreover, such a reduction in free volume within the interphase may limit the antiplasticization-induced permeability reduction in the presence of toluene. Finally, the hypothesized polymer chain rigidification on and near the sieve surface—in combination with reduced free volume—could limit the degree to which the membrane can age.

6.5.2 Reactive-Sized, As-Received SSZ-13/PDMC Mixed Matrix Membranes

Work in Chapter 5 suggested that membranes with as-received SSZ-13 may perform at least as well as those with Grignard-treated SSZ-13 when treated with the reactive sizing procedure. To evaluate the performance of these membranes in the presence of toluene, two 25% (w/w) reactive-sized, as-received (RS-AR) SSZ-13/PDMC membranes were prepared and tested as before. Carbon dioxide permeabilities for these membranes are presented in Figure 6.14; carbon dioxide/methane selectivities are presented in Figure 6.15. Permeabilities and selectivities for neat PDMC and 25% reactive-sized, Grignard-treated (RS-GT) SSZ-13/PDMC membranes are included in the respective figures for comparative reference.

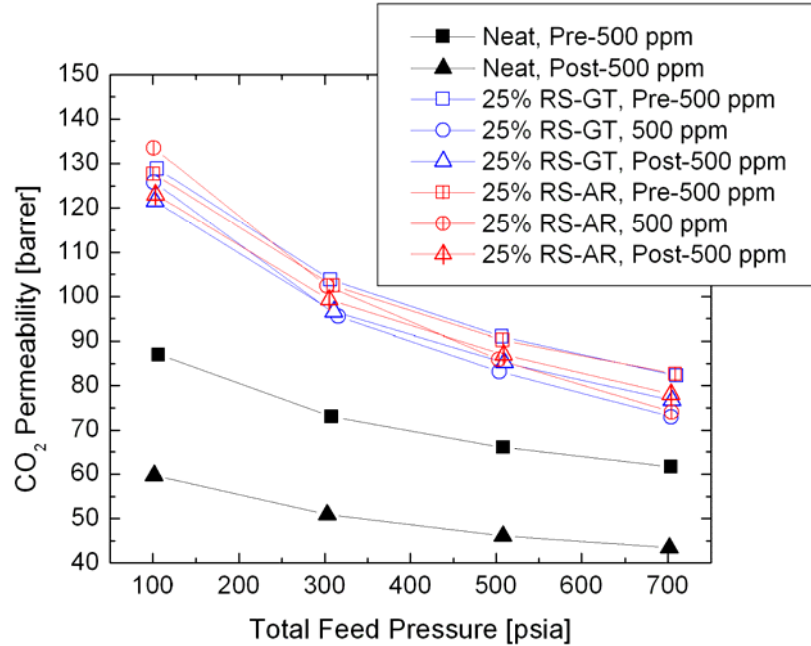


Figure 6.14: Mixed gas carbon dioxide permeabilities for 25% reactive-sized, Grignard-treated (RS-GT) and 25% reactive-sized, as-received (RS-AR) SSZ-13/PDMC mixed matrix membranes.

As evidenced by the above figures, the reactive sizing procedure leads to virtually identical transport properties for membranes with both as-received and Grignard-treated SSZ-13. This outcome may be attributable to similar sieve surface properties and membrane microstructure resulting from the sizing procedure. Once any non-selective voids within the GT-SSZ-13 surface layer are caulked, the treated sieve can interact with the polymer matrix similarly to reactive-sized, as-received sieve. The free volume and surface chain entanglement mechanisms described previously would likely occur similarly in both systems, and thus, the anticipated transport properties would resemble those observed here.

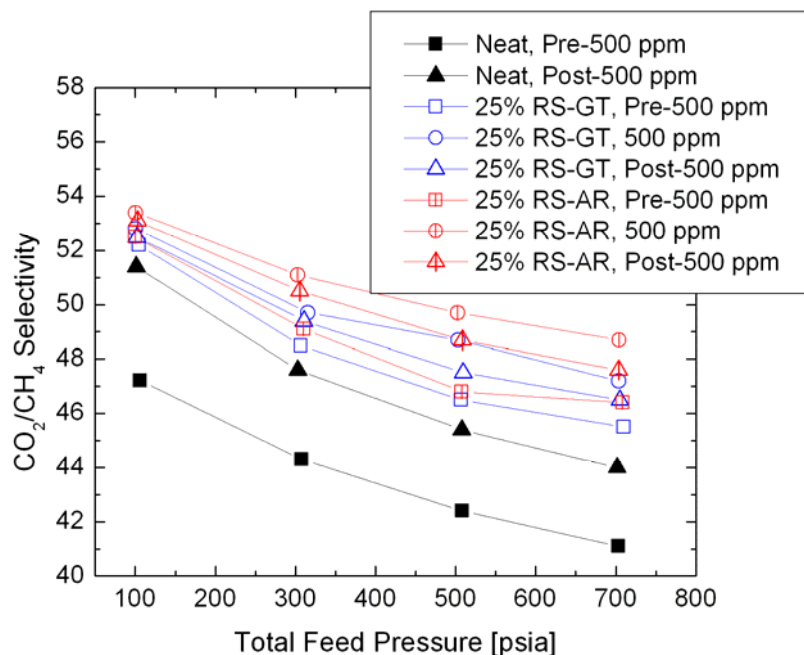


Figure 6.15: Mixed gas of carbon dioxide/methane selectivities for 25% reactive-sized, Grignard-treated (RS-GT) and 25% reactive-sized, as-received (RS-AR) SSZ-13/PDMC mixed matrix membranes.

6.6 Summary and Conclusions

Neat PDMC dense film membrane response to toluene-contaminated feeds was compared to a similar study of hollow fiber membranes. Hollow fibers apparently suffered from a severe antiplasticization response to toluene; dense films exhibited a much less severe response. Physical aging was observed in all membranes tested. However, it was shown that exposure to 1000 ppm toluene resulted in less aging than exposure to 500 ppm. This behavior was most likely due to the prevention of polymer matrix consolidation by sorbed penetrant molecules.

The efficacy of hybrid membranes with as-received and modified SSZ-13 in mitigating the deleterious impact on membrane performance under contaminated feed conditions was evaluated. Membranes with as-received and Grignard-treated sieve

showed modest improvements in aging resistance and permeability preservation in the presence of toluene. Selectivities for these membranes, however, were not enhanced over neat PDMC as desired. However, membranes with reactive-sized, Grignard-treated and reactive-sized, as-received sieve resulted in substantial permeability and selectivity enhancements over neat PDMC. These membranes were also quite resistant to aging and maintained permeability in the presence of toluene. The results reported here represent a significant step forward in developing these materials as a viable alternative for natural gas purification.

6.7 References

1. Al-Juaied, M. and W.J. Koros, *Performance of natural gas membranes in the presence of heavy hydrocarbons*. Journal of Membrane Science, 2006. **274**(1-2): p. 227-243.
2. Vu, D.Q., W.J. Koros, and S.J. Miller, *Effect of condensable impurities in CO₂/CH₄ gas feeds on carbon molecular sieve hollow-fiber membranes*. Industrial & Engineering Chemistry Research, 2003. **42**(5): p. 1064-1075.
3. White, L.S., et al., *PROPERTIES OF A POLYIMIDE GAS SEPARATION MEMBRANE IN NATURAL-GAS STREAMS*. Journal of Membrane Science, 1995. **103**(1-2): p. 73-82.
4. Omole, I.C., *Crosslinked Polyimide Hollow Fiber Membranes for Aggressive Natural Gas Feed Streams*, in *School of Chemical and Biomolecular Engineering*. 2008, Georgia Institute of Technology: Atlanta, GA.
5. Maeda, Y. and D.R. Paul, *EFFECT OF ANTIPLASTICIZATION ON GAS SORPTION AND TRANSPORT .2. POLY(PHENYLENE OXIDE)*. Journal of Polymer Science Part B-Polymer Physics, 1987. **25**(5): p. 981-1003.
6. Maeda, Y. and D.R. Paul, *EFFECT OF ANTIPLASTICIZATION ON SELECTIVITY AND PRODUCTIVITY OF GAS SEPARATION MEMBRANES*. Journal of Membrane Science, 1987. **30**(1): p. 1-9.
7. Maeda, Y. and D.R. Paul, *EFFECT OF ANTIPLASTICIZATION ON GAS SORPTION AND TRANSPORT .3. FREE-VOLUME INTERPRETATION*. Journal of Polymer Science Part B-Polymer Physics, 1987. **25**(5): p. 1005-1016.

8. Madden, W.C., *The Performance of Hollow Fiber Gas Separation Membranes in the Presence of an Aggressive Feed Stream*, in *School of Chemical & Biomolecular Engineering*. 2005, Georgia Institute of Technology: Atlanta, GA.
9. Park, J.Y. and D.R. Paul, *Correlation and prediction of gas permeability in glassy polymer membrane materials via a modified free volume based group contribution method*. *Journal of Membrane Science*, 1997. **125**(1): p. 23-39.
10. Bondi, A., *Properties of Molecular Crystals, Liquids, and Glasses*. 1968, New York: Wiley.
11. Chung, T.S., Z.L. Xu, and W.H. Lin, *Fundamental understanding of the effect of air-gap distance on the fabrication of hollow fiber membranes*. *Journal of Applied Polymer Science*, 1999. **72**(3): p. 379-395.
12. Chung, T.S. and X.D. Hu, *Effect of air-gap distance on the morphology and thermal properties of polyethersulfone hollow fibers*. *Journal of Applied Polymer Science*, 1997. **66**(6): p. 1067-1077.
13. Jordan, S.M., W.J. Koros, and G.K. Fleming, *THE EFFECTS OF CO₂ EXPOSURE ON PURE AND MIXED GAS PERMEATION BEHAVIOR - COMPARISON OF GLASSY POLYCARBONATE AND SILICONE-RUBBER*. *Journal of Membrane Science*, 1987. **30**(2): p. 191-212.
14. Kim, J.H., W.J. Koros, and D.R. Paul, *Effects of CO₂ exposure and physical aging on the gas permeability of thin 6FDA-based polyimide membranes - Part 1. Without crosslinking*. *Journal of Membrane Science*, 2006. **282**(1-2): p. 21-31.
15. Kim, J.H., W.J. Koros, and D.R. Paul, *Effects of CO₂ exposure and physical aging on the gas permeability of thin 6FDA-based polyimide membranes - Part 2. with crosslinking*. *Journal of Membrane Science*, 2006. **282**(1-2): p. 32-43.
16. Kim, J.H., W.J. Koros, and D.R. Paul, *Physical aging of thin 6FDA-based polyimide membranes containing carboxyl acid groups. Part I. Transport properties*. *Polymer*, 2006. **47**(9): p. 3094-3103.
17. Moe, M.B., W.J. Koros, and D.R. Paul, *EFFECTS OF MOLECULAR-STRUCTURE AND THERMAL ANNEALING ON GAS-TRANSPORT IN 2 TETRAMETHYL BISPHENOL-A POLYMERS*. *Journal of Polymer Science Part B-Polymer Physics*, 1988. **26**(9): p. 1931-1945.
18. Kratochvil, A., *Thickness Dependent Physical Aging and Supercritical Carbon Dioxide Condition Effects on Crosslinkable Polyimide Membranes for Natural Gas Purification*, in *School of Chemical & Biomolecular Engineering*. 2008, Georgia Institute of Technology: Atlanta, GA.
19. Connelly, R.W., et al., *THE EFFECT OF SORBED PENETRANTS ON THE AGING OF PREVIOUSLY DILATED GLASSY POLYMER POWDERS .1.*

- LOWER ALCOHOL AND WATER SORPTION IN POLY(METHYL METHACRYLATE)*. Journal of Applied Polymer Science, 1987. **34**(2): p. 703-719.
20. Enscoe, D.J., H.B. Hopfenberg, and V.T. Stannett, *DIFFUSION, SWELLING, AND CONSOLIDATION IN GLASSY POLYSTYRENE MICROSPHERES*. Polymer Engineering and Science, 1980. **20**(1): p. 102-107.
 21. Stewart, M.E., et al., *THE EFFECT OF SORBED PENETRANTS ON THE AGING OF PREVIOUSLY DILATED GLASSY POLYMER POWDERS .2. N-PROPANE SORPTION IN POLYSTYRENE*. Journal of Applied Polymer Science, 1987. **34**(2): p. 721-735.
 22. Stewart, M.E., et al., *THE EFFECT OF SORBED PENETRANTS ON THE AGING OF PREVIOUSLY DILATED GLASSY POLYMER POWDERS .3. THE EFFECT OF EXPOSURE TO LOWER ALCOHOLS ON ENTHALPY RELAXATIONS IN POLY(METHYLMETHACRYLATE)*. Journal of Applied Polymer Science, 1987. **34**(7): p. 2493-2505.
 23. Ash, B.J., L.S. Schadler, and R.W. Siegel, *Glass transition behavior of alumina/polymethylmethacrylate nanocomposites*. Materials Letters, 2002. **55**(1-2): p. 83-87.
 24. Keddie, J.L., R.A.L. Jones, and R.A. Cory, *INTERFACE AND SURFACE EFFECTS ON THE GLASS-TRANSITION TEMPERATURE IN THIN POLYMER-FILMS*. Faraday Discussions, 1994. **98**: p. 219-230.
 25. Keddie, J.L., R.A.L. Jones, and R.A. Cory, *SIZE-DEPENDENT DEPRESSION OF THE GLASS-TRANSITION TEMPERATURE IN POLYMER-FILMS*. Europhysics Letters, 1994. **27**(1): p. 59-64.
 26. Mattsson, J., J.A. Forrest, and L. Borjesson, *Quantifying glass transition behavior in ultrathin free-standing polymer films*. Physical Review E, 2000. **62**(4): p. 5187-5200.
 27. Robertson, C.G. and C.M. Roland, *GLASS TRANSITION AND INTERFACIAL SEGMENTAL DYNAMICS IN POLYMER-PARTICLE COMPOSITES*. Rubber Chemistry and Technology, 2008. **81**(3): p. 506-522.
 28. Priestley, R.D., et al., *Structural relaxation of polymer glasses at surfaces, interfaces and in between*. Science, 2005. **309**(5733): p. 456-459.
 29. Priestley, R.D., et al. *Evidence for the molecular-scale origin of the suppression of physical ageing in confined polymer: fluorescence and dielectric spectroscopy studies of polymer-silica nanocomposites*. 2007: Iop Publishing Ltd.

30. Husain, S. and W.J. Koros, *Mixed matrix hollow fiber membranes made with modified HSSZ-13 zeolite in polyetherimide polymer matrix for gas separation*. Journal of Membrane Science, 2007. **288**(1-2): p. 195-207.
31. Shu, S., S. Husain, and W.J. Koros, *A general strategy for adhesion enhancement in polymeric composites by formation of nanostructured particle surfaces*. Journal of Physical Chemistry C, 2007. **111**(2): p. 652-657.

CHAPTER 7

CONCLUSIONS AND RECOMMENDATIONS

7.1 Summary and Conclusions

The case has been made—here and elsewhere—for developing mixed matrix hybrid membranes for industrial gas separations. These materials offer substantial improvements in separation performance over currently available commercial polymer membranes. Moreover, the paradigm shift from thermally- to non-thermally-driven separations that these materials represent holds promise for significant reductions in both equipment and operational costs as compared to more traditional separations. The development of mixed matrix membrane materials is, however, not without its challenges. Achieving ideal adhesion at the interface between the polymer matrix and dispersed phase is critical to realize the full separation potential of hybrid membranes, yet this remains one of—if not *the*—most challenging hurdles to overcome.

In this research, analyses of hybrid membranes containing as-received SSZ-13 in PDMC initially suggested that poor interfacial adhesion was to blame for the lack of desired performance enhancement over neat PDMC membranes. A surface treatment that has previously been shown to improve polymer/sieve adhesion was used to modify the sieve surface in an attempt to enhance adhesion in SSZ-13/PDMC membranes. Evidence was shown that strongly suggests in the present case, however, that voids exist *within* the surface deposits resulting from the modification procedure for the particular system studied here. Such voids lead to defective membrane performance. An additional modification procedure—a reactive sizing technique—was developed to *caulk* these

voids to prevent non-selective gas bypass around sieve particles. Nitrogen physisorption and permeation analyses suggested that this procedure was largely successful in eliminating the voids. Hybrid membranes containing these reactive-sized, Grignard-treated sieves exhibited marked performance improvement over neat polymer membranes.

In a serendipitous discovery, the reactive sizing procedure was shown to provide virtually equivalent performance enhancement for membranes containing either as-received or Grignard-treated sieves. This observation is believed to result from a complex non-ideal transport mechanism in hybrid membranes enabled by strong interaction of a rigid, packing-inhibited chain such as PDMC. In stark contrast to the initial concern that interfacial voids exist in hybrid membranes containing unmodified sieves, XPS and TGA analyses of sized SSZ-13 suggest that oligomeric PDMC precursor can strongly adhere to the sieve surface. Disruptions in polymer chain packing are known to enhance free volume in polymer composite materials, and the presence of sieve particles in the polymer matrix can disrupt rigid chain packing in the vicinity of particle surfaces. Combining this disruption in chain packing with strong surface adhesion, it is anticipated that a high free volume, dilated polymer interphase that is resistant to matrix consolidation might result. Albeit speculative, the behavior of all membranes tested over the course of this research can be well described in terms of this hypothesized mechanism.

Performance under realistic feed conditions with complex mixtures was also evaluated for the membranes developed in this research. Prior work with PDMC hollow fiber membranes showed that the presence of low feed concentrations of toluene resulted

in a deleterious reduction in permeability due to combined competition and antiplasticization effects. Similar behavior was observed for PDMC dense film membranes; however, the response was much less severe. It was postulated that differences in free volume between the two membrane types could be responsible for the differing responses, though a detailed study of this was beyond the scope of the present work. Dense film hybrid membranes containing as-received and Grignard-treated sieves displayed modest resistance to aging- and antiplasticization-related performance reduction, though desired selectivity enhancements over neat PDMC were not achieved. Membranes containing either reactive-sized, Grignard-treated or reactive-size, as-received SSZ-13, however, displayed significant permeability and selectivity enhancements over neat PDMC. Additionally, these membranes showed exceptional improvements in aging resistance and permeability maintenance in the presence of toluene. These results represent a significant step forward in developing SSZ-13/PDMC hybrid membranes as a viable alternative for natural gas purification.

7.2 Recommendations for Additional Research

7.2.1 In-Depth Investigation of the Proposed Transport Mechanism

The transport mechanism proposed in this work was developed from several previously described phenomena to describe the observed transport properties for the variety of hybrid membranes tested. Although the data acquired over the course of this research supports the hypothesis, additional characterization is needed to provide undeniable evidence that the supposed dilated interphases are indeed responsible for the less-than-desirable performance observed for many of the hybrid membranes investigated

in this work. A rigorous gas sorption and/or PALS study of membranes containing several different loadings of as-received and reactive-sized, as-received SSZ-13 should help elucidate any free volume relationship to the presence of the sieve. Such a study should utilize *uncalcined* sieve so as to prevent sorption in the sieve from complicating the analysis. Additionally, high-resolution DSC analysis may be able to provide insight into the nature of the rigidified interphase versus the bulk polymer.

7.2.2 Surface Material Identification and Attachment Mechanism

The surface material resulting from the reactive sizing procedure was characterized with XPS. Nitrogen and fluorine were clearly present, suggesting that both diamine and dianhydride monomer species are present; specific material structures, however, were not determined from this analysis. An attempt to identify the mechanism of surface attachment was made using Auger electron spectroscopy (AES) depth profile/chemical states analysis on single sieve particles; however, this was unsuccessful due to excessive sample charging.

Further efforts are warranted in determining the specific identity of the surface material and its method of attachment. Hydrogen bonding with surface silanol groups is the most likely method; covalent bonding of dianhydride or diamine species is unlikely, but not impossible. The surface-anchored material is clearly resistant to THF washing (as shown with TGA analysis). However, hydrogen-bound species should be relatively easily removed with water washing. Moreover, many Si-O-R bonds are susceptible to hydrolysis; hot water washing should also be able to facilitate the removal of such material. Careful analysis of the filtrate after water washing may yield significant information regarding the specific identity/structure of the surface material.

Additionally, identification of the surface material and its attachment mechanism may allow the time required for the sizing procedure to be shortened. Since sizing is essentially an in-situ PDMC synthesis, if the surface material results from the first stage of synthesis (polyamic acid formation/imidization), then esterification may not be necessary. This would save considerable time and would lower the cost of sieve treatment—points to consider if this method is scaled for commercial use.

7.2.3 Feasibility of Reactive-Sized SSZ-13 in Hollow Fiber Mixed Matrix Membranes

Although substantial performance gains were achieved in SSZ-13/PDMC membranes once the reactive sizing procedure was developed, these advancements were made only in dense films. Since the preferred membrane format for gas separation membranes is the hollow fiber, the next logical step in developing these materials is to transition the present technology to crosslinkable mixed matrix hollow fiber membranes. The question remains, however, as to whether material interaction at the polymer/sieve interface is sufficient to withstand the various stresses that develop during hollow fiber formation. It is anticipated that overall adhesion will not be an issue with adequate entanglement of bulk polymer chains and surface-anchored material. However, it may be necessary to roughen the sieve surface in order to anchor sufficient material to achieve this entanglement. In this case, reactive-sized, Grignard-treated sieve may be required.

Taking into account the time and effort required to treat sieve with the sizing procedure, and considering the amount of sieve typically required for spinning, it would be wise to probe interfacial adhesion quality by means other than full-scale fiber spinning. Much less material would be initially required by studying asymmetric flat sheet membranes or possibly by using syringe tests.

7.2.4 Applicability of the Reactive Sizing Procedure to Other Materials

While the reactive sizing procedure has been shown to improve SSZ-13/PDMC membrane performance, the efficacy of the procedure was not investigated for treating other materials. A considerable number of polymer and molecular sieve combinations are possible for a variety of separations; many of these combinations are likely to experience non-ideal interactions similar to those observed in this research. It may be of considerable value to investigate the sizing procedure as a generalized approach for improving membrane performance in other polymer/sieve combinations.

Of immediate relevance to the present work would be an extension of the sizing procedure to PDMC hybrid membranes containing CVX-7—a silicoaluminophosphate material having an erionite framework with $\sim 3.6 \times 5.1$ Å pore windows (also SAPO-17). The slightly smaller dimension of the window in this material (as compared to chabazite) is expected to provide higher carbon dioxide/methane selectivity than SSZ-13. This is clearly desirable for natural gas purification.

7.2.5 Mixed Matrix Membrane Aging Studies

Physical aging was observed for both neat and hybrid PDMC membranes during permeation testing with toluene-contaminated feeds. It was noted that hybrid membranes appeared to age less than neat polymer membranes during testing. It was also noted that membranes containing reactive-sized sieves (either as-received or Grignard-treated) appeared to experience less significant aging than membranes containing unsized sieves.

It was hypothesized that rigidified polymer surrounding sieve particles may have reduced the rate of aging in hybrid membranes. In order to probe this hypothesis, long-term permeation studies of neat and hybrid PDMC membranes should be conducted. If it

is shown that hybrid membranes truly age at lower rates than neat polymer membranes, the existence of rigidified interphases may be further supported.

APPENDIX A

POSSIBLE ATTACHMENT MECHANISMS OF SURFACE

MATERIAL ON REACTIVE-SIZED SIEVES

Characterization of the material deposited on the surface of SSZ-13 during the reactive sizing procedure was attempted using TGA, XPS, and AES analyses. Mass loss from TGA suggested that ~9% of the treated sieve mass can be attributed to these surface deposits. This material is considered to be well adhered to the surface considering that these analyses were performed after washing treated sieves in THF a total of 10 times. Each wash cycle consisted of adding sufficient THF to the treated sieves to produce a ~1% (w/v) mixture, dispersing the sieves for 10-15 min in an ultrasonication bath, and then recovering the solids via centrifugation. Depth profile/chemical states analyses of individual treated sieve particles were attempted using AES. However, excessive charging during analysis prevented meaningful data from being acquired. Comparing XPS general surveys for as-received and reactive-sized SSZ-13 suggests significantly more carbon, nitrogen, and fluorine on the surface of reactive-sized sieves. Since only the dianhydride (6FDA) contains fluorine and only the diamines (DAM and DABA) contain nitrogen, the XPS general survey indicates that both types of monomer species are present.

Several possible mechanisms exist by which sizing materials could interact with sieve surfaces. While speculative, it is expected that a number of different attachment mechanisms can be found simultaneously anchoring material to the sieve surface. Nearly all of the most likely mechanisms involve hydrogen bonding with surface silanol groups.

One possibility involved the reaction of 6FDA with surface silanols. These mechanisms are illustrated in Figure A.1.

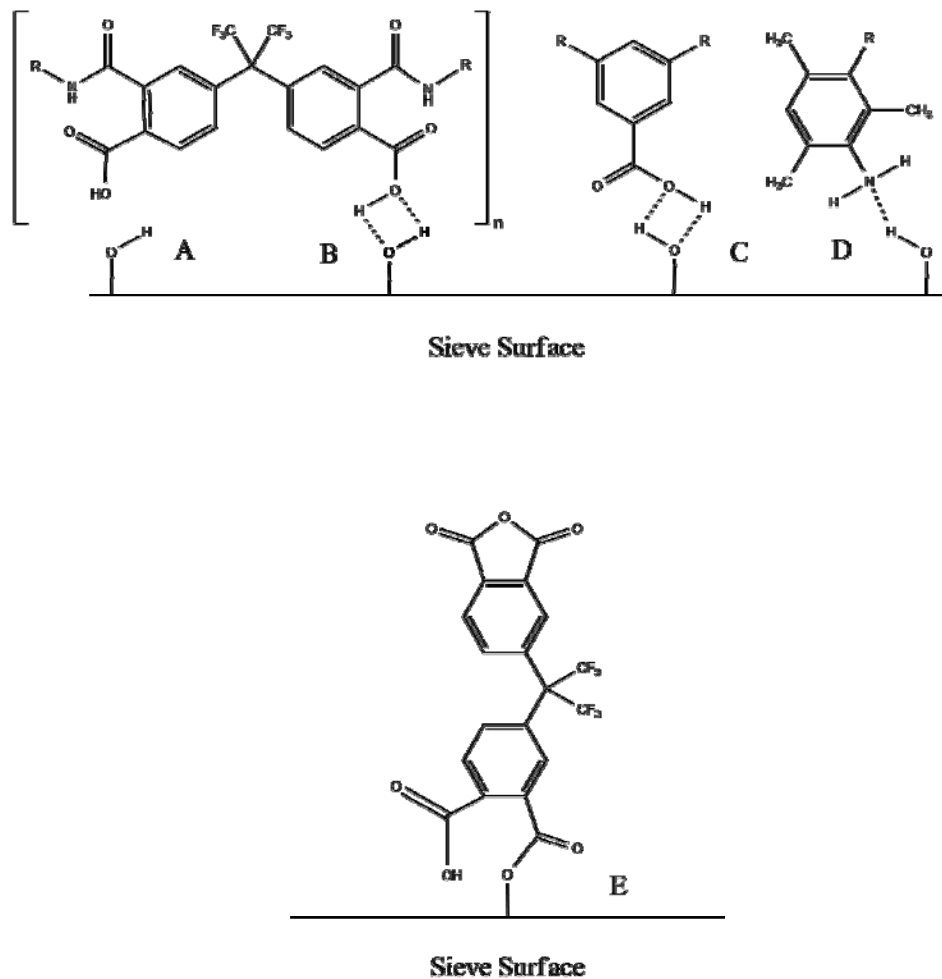


Figure A.1: Proposed attachment mechanisms for material deposited on sieve surfaces during reactive sizing.

Referring to the above figure, case (A) indicates a non-interacting surface silanol group. Case (B) illustrates a polyamic acid oligomer that is hydrogen-bound to a surface silanol. Cases (C) and (D) show the possible interaction of DABA and DAM, respectively, with surface silanols. DABA can hydrogen bond via its carboxylic acid

pendant group. Both DABA and DAM can hydrogen bond via amine groups. Case (E) illustrates an ester that might form between 6FDA and a surface silanol. It is apparent in cases (B)-(E) that polymeric material could extend from the sieve surface via polycondensation reaction with any of these anchored moieties.

APPENDIX B

ESTIMATION OF INTERPHASE PROPERTIES USING THE 3-PHASE MAXWELL MODEL

The steps outlined below describe the use of the 3-phase Maxwell model to estimate the interphase thickness and its transport properties in SSZ-13/PDMC mixed matrix membranes. This method utilizes a trial-and-error technique with experimental transport data for membranes containing uncalcined and calcined molecular sieves. A flowchart describing these steps is presented in Figure B.1.

1. Recall the 3-phase Maxwell model (3MM). We first start with:

$$P_{eff} = P_I \left[\frac{P_d + 2P_I - 2\phi_s(P_I - P_d)}{P_d + 2P_I + \phi_s(P_I - P_d)} \right] \quad (\text{B.1})$$

where P is permeability and the subscripts I and d refer to the interphase and dispersed phase, respectively. P_{eff} is the effective permeability for the combination of the sieve and interphase. The sieve volume fraction in this two-phase *pseudosieve* is defined as:

$$\phi_s = \frac{\phi_d}{\phi_d + \phi_I} \quad (\text{B.2})$$

Equation B.1 is then inserted into the Maxwell model again to arrive at the following:

$$P_{3MM} = P_c \left[\frac{P_{eff} + 2P_c - 2(\phi_d + \phi_I)(P_c - P_{eff})}{P_{eff} + 2P_c + (\phi_d + \phi_I)(P_c - P_{eff})} \right] \quad (\text{B.3})$$

2. We know that $P_d = 0$ for a non-porous dispersed phase (such as uncalcined SSZ-13). Under such conditions, Equation B.1 reduces to:

$$P_{eff} = P_I \frac{2(1 - \phi_s)}{(2 + \phi_s)} \quad (\text{B.4})$$

3. We also know Φ_d from the sieve loading in a given hybrid membrane. We find for a 25% (w/w) uncalcined SSZ-13/PDMS mixed matrix membrane that $\Phi_d = 0.202$. Using this value and Equation B.2, a series of values for Φ_s can be generated by varying Φ_I from 0 to $(1-\Phi_d)$.

4. If P_{eff} in Equation B.4 is set to the experimentally determined permeability for a PDMS hybrid membrane containing *uncalcined* SSZ-13, P_I can be predicted for each of the Φ_s values generated in step 3. These predictions are made for both carbon dioxide and methane.

5. The values for P_I (with respective Φ_s values) determined in the previous step can be used in Equation B.1 to predict a series of P_{eff} values for the case of *calcined* SSZ-13. This is made possible by assuming similar interphase properties for similar volume fractions of uncalcined and calcined SSZ-13 in two separate membranes.

6. The carbon dioxide and methane P_{eff} values (with respective Φ_I values) from step 5 are then used in Equation B.3 to predict a series of 3MM-predicted permeabilities (P_{3MM}).

7. The P_{3MM} values predicted in step 6 are then compared with experimentally measured values for a PDMS hybrid membrane containing *calcined* SSZ-13. The best match between predicted and measured values (CO₂ and CH₄) leads to the best estimate of P_I . Using the respective value for Φ_s , the interphase thickness, ℓ_I , can be estimated from:

$$\phi_s = \frac{\phi_d}{\phi_d + \phi_I} = \frac{r_p^3}{(r_p + \ell_I)^3} \quad (\text{B.5})$$

where r_p is the radius of the sieve particles and ℓ_I is the thickness of the interphase.

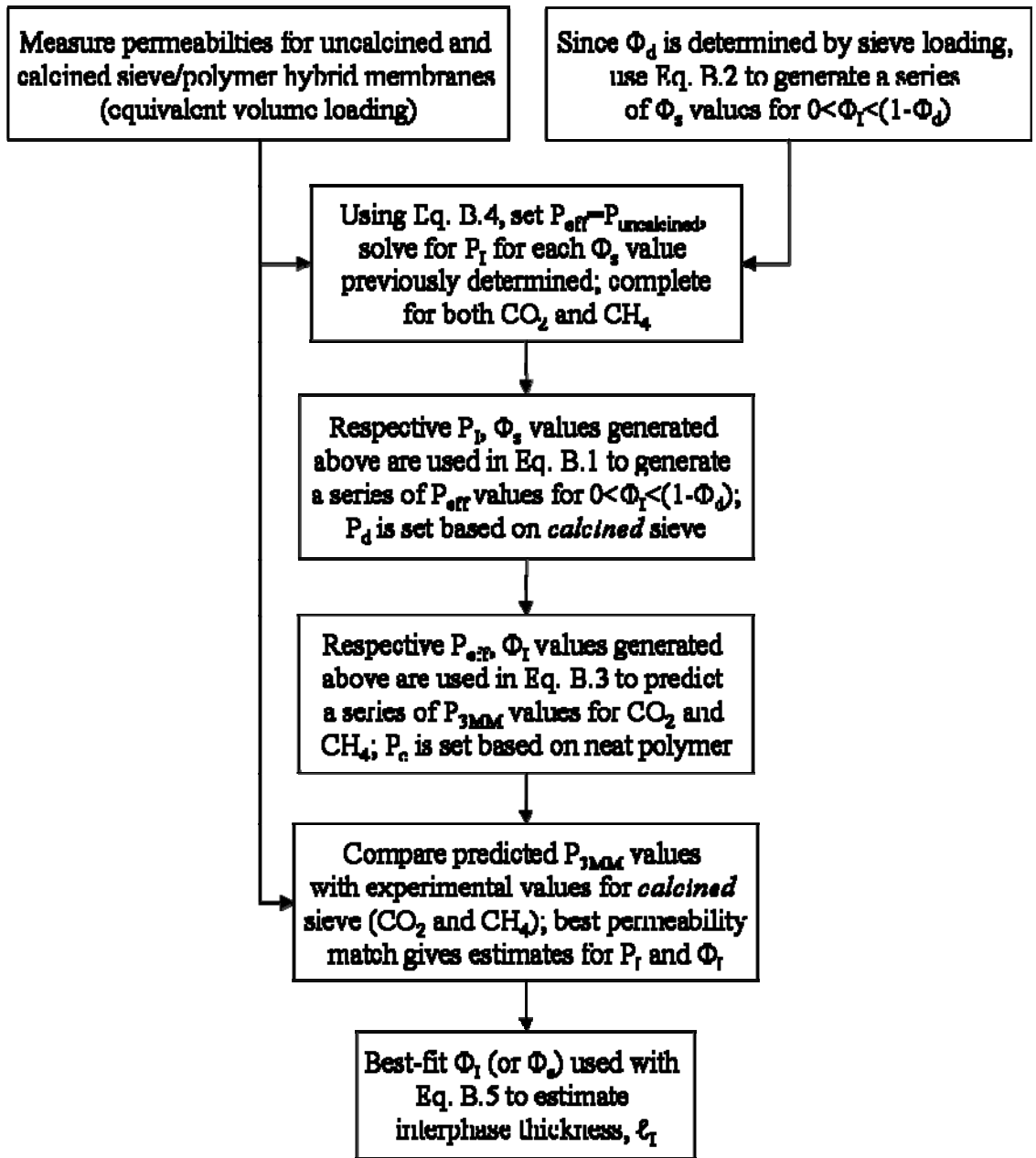


Figure B.1: Flowchart describing the steps necessary to predict interphase properties using the 3-phase Maxwell model.